Chem Soc Rev

REVIEW ARTICLE

View Article Online
View Journal

Cite this: DOI: 10.1039/d5cs00580a

Neuromorphic iontronic devices based on soft ionic conductors

Li Wang, [b] Yide Jiao,[c] Hongjie Zhang,[a] Yaqing Liu, *[d] Yujia Zhang, *[c] Peiyi Wu *[e] and Kai Xiao *[a]

The human brain efficiently processes external information using ions as information carriers, inspiring the development of ionic brain-like intelligence. Central to such systems are neuromorphic iontronic devices (NIDs), including artificial axons, synapses, and neurons, which employ ions as charge carriers. Recently, NIDs based on soft ionic conductors (SICs), such as ionic hydrogels, ionogels, and ionic elastomers, have attracted growing attention due to their ionic compatibility, flexibility, biocompatibility, and facile fabrication and integration, making them promising candidates for next-generation neuromorphic technologies. Despite their potential, research remains in its infancy, with key challenges in elucidating fundamental mechanisms, establishing design principles, and realizing practical applications. To address these issues and guide future research, this review first introduces the functional roles and electrical signalling of axons, synapses, and neurons, thereby defining the performance requirements for NIDs. It then summarizes means for controlling ion transport in SICs and discusses feasible approaches for constructing SIC-based NIDs, including structural and interfacial engineering, device architectures, and dropletronic techniques. Finally, recent advances in SIC-based NIDs are reviewed, and their prospects in human–machine interaction and brain-like computing are discussed along with the remaining challenges.

Received 16th October 2025

DOI: 10.1039/d5cs00580a

rsc.li/chem-soc-rev

[a] *Department of Biomedical Engineering, Guangdong Provincial Key Laboratory of Advanced Biomaterials, Institute of Innovative Materials, Southern University of Science and Technology, Shenzhen 518055, P. R. China. E-mail: zhanghongjiea@163.com, xiaok3@sustech.edu.cn*

[b] *School of Chemistry and Molecular Engineering, Nanjing Tech University, Nanjing 211816, P. R. China. E-mail: wangl_scme@njtech.edu.cn*

[c] *Laboratory for Bio-Iontronics (BION), Institute of Electrical and Micro Engineering (IEM), École Polytechnique Fédérale de Lausanne (EPFL), Lausanne 1015, Switzerland. E-mail: yide.jiao@epfl.ch, yujia.zhang@epfl.ch*

[d] *Key Laboratory of Colloid and Interface Chemistry of the Ministry of Education, School of Chemistry and Chemical Engineering, Shandong University, Jinan 250100, P. R. China. E-mail: liuyaqing@sdu.edu.cn*

[e] *State Key Laboratory of Advanced Fiber Materials, College of Chemistry and Chemical Engineering, Center for Advanced Low-Dimension Materials, Donghua University, Shanghai 201620, P. R. China. E-mail: wupeiyi@dhu.edu.cn*

Li Wang

Dr Li Wang is an Associate Professor at the School of Chemistry and Molecular Engineering, Nanjing Tech University, China. He earned his PhD from East China Normal University in 2022 and conducted postdoctoral research at the Southern University of Science and Technology (2022–2024). His current research focuses on biomedical materials and intelligent soft materials and devices.

Yide Jiao

Yide Jiao is a doctoral student at the EPFL, Switzerland. He received his MSc in Microengineering with a minor in Biomedical Engineering from EPFL, after which he conducted a Master's enhancement project in Professor Yujia Zhang's laboratory on neuromorphic computing based on dropletronics. His current research focuses on advancing micro- and nanofabrication techniques and separation science through microfluidics and dielectrophoresis.

1. Introduction

Artificial intelligence is currently undergoing a critical transition from the conventional von Neumann architecture to more biomimetic neuromorphic architectures, with the ultimate aim of achieving brain-like intelligence.[1–7] Traditional hardware systems based on the von Neumann model operate through a storage-compute separation and serial processing, which results in high energy consumption and low processing speed.[8] In contrast, neuromorphic hardware systems (often referred to as brain-like chips), such as TrueNorth,[9] Loihi,[10] and Tianjic,[11] mimic neural networks by integrating functional units resembling biological synapses and neurons. These systems enable in-memory computation and parallel processing, thus offering significantly improved energy efficiency and computing speed.[12–14] Importantly, the goals of brain-like intelligence extend beyond fast and energy-efficient processing tasks such as classification, recognition, and decision-making. They also aim to simulate biological processes including signal transmission, perception, learning, memory, self-adaptation, and emotion building.[15–19] Achieving these advanced capabilities holds great promise for applications in neuromodulation, disease treatment, prosthetics, brain–machine interfaces, and artificial life.[20–24] However, realizing such goals requires continuous exploration of hardware systems that more closely match the electrical, chemical, and functional characteristics of the human brain.

Artificial axons, neurons, and synapses, collectively known as neuromorphic devices, form the core functional units of brain-like intelligent hardware systems. These devices respectively enable signal transmission,[25] signal integration and encoding,[26] information storage,[27] and computation.[28] Assemblies of neuromorphic devices are expected to process information as efficiently and with minimal energy consumption as the human brain,[29] while enabling seamless communication with biological systems.[30] As of now, the neuromorphic devices that have reached a relatively mature stage in terms of both research and applications are based on solid-state electronics, which use

Yaqing Liu

Dr Yaqing Liu is a professor at Shandong University, China. He received his PhD in 2013 from Institute of Chemistry, Chinese Academy of Sciences, and served as a postdoctoral fellow at Nanyang Technological University, Singapore, from 2014 to 2018. His current research interests include the design of functional soft materials and flexible device technology.

Yujia Zhang

Dr Yujia Zhang is a Tenure Track Assistant Professor at EPFL, Switzerland, and the principal investigator of the Laboratory for Bio-Iontronics. A major interest of his laboratory is the development of iontronic biointerfaces for medicine and hybrid intelligent systems for neuromorphic computing. Recently, his laboratory has pioneered dropletronics, in which networks of microscale, modular, hydrogel droplets function as multifunctional bioiontronic and bioelectronic devices.

Peiyi Wu

Dr Peiyi Wu is a professor at the College of Chemistry and Chemical Engineering, Donghua University, Shanghai, China. His research interests focus on Soft Matter and Spectral Characterization of Polymeric Materials.

Kai Xiao

Dr Kai Xiao is an Associate Professor in the Department of Biomedical Engineering at Southern University of Science and Technology, China. He received his BSc from Jilin University (2012) and PhD from the Institute of Chemistry, Chinese Academy of Sciences (2017), and was an Alexander von Humboldt Fellow at the Max Planck Institute of Colloids and Interfaces. Since 2021, he leads the "Iontronic Materials for Neuromorphic Devices" group at SUSTech. He has authored over 70 papers and two book chapters (H-index 45, >6200 citations). His research focuses on nanofluidics, soft materials, iontronics, and neuromorphic devices.

electrons/holes as charge carriers. In contrast, the human brain, a naturally evolved liquid–electrolyte system, relies on the controlled transport of ions to execute advanced functions such as perception, memory, learning, and computation.[31] Over the past decade, this fundamental distinction has prompted researchers to reconsider the foundational design of neuromorphic devices, driving the development of devices that use ions as charge carriers, namely neuromorphic iontronic devices (NIDs), toward systems that more closely emulate biological characteristics.[32–35] It is widely believed that such ion-based systems offer several advantages, including biosignal compatibility,[36] low energy consumption,[37] and resistance to electromagnetic interference,[38] among others.

NIDs reported to date are mainly composed of two types of materials: nanoscale pores/channels and soft ionic conductors (SICs).[39–41] The former, commonly used in fabricating nanofluidic memristors, has been effective in emulating synaptic plasticity features such as paired-pulse facilitation/depression (PPF/PPD), long-term potentiation/depression (LTP/LTD), and spiking rate/timing-dependent plasticity (SRDP/STDP).[42–52] These devices have also shown potential for implementing pulse-neuron models, such as Hodgkin–Huxley (H–H) circuit.[53–55] Several recent reviews have provided comprehensive summaries of this class of devices.[37,38,40,56,57] Nevertheless, their electrochemical performance depends heavily on the precise manufacturing of nanoscale pores/channels,[58] which would lead to high cost and limited reproducibility. Moreover, the use of liquid electrolytes as ion reservoirs in nanofluidic systems restricts their flexibility, mechanical stability, and scalability.[57] In contrast, SICs, such as ionic hydrogels and ionogels, are stretchable and bendable materials that combine ionic conductivity with properties like flexibility, low toxicity, low cost, and ease of stable fabrication.[59–61] These features make SICs particularly suitable for constructing NIDs that support human–machine interaction,[62–64] flexible wearable electronics,[65–70] long-term semi-implantable/implantable devices,[71–73] and large-scale integrated ionic circuits and artificial neural networks (ANNs).[74–76] Moreover, emerging dropletronic technologies offer a promising platform for device miniaturization, reduced energy consumption, and efficient integration, further accelerating the practical translation of SIC-based NIDs.[77–79] As such, SIC-based NIDs represent a compelling pathway toward the development of next-generation brain-like intelligence.

SICs are a class of soft materials in which ions serve as the primary charge carriers.[76] They typically comprise two or three phases, including ion species, polymers, and solvents.[80] Within these systems, the polymer matrix forms a three-dimensional network that confines the solvent and ions, creating a continuous and stable medium for ion transport.[81] Owing to the mobility of polymer chains, SICs exhibit excellent mechanical flexibility, accommodating stretching, compression, and bending deformations. Representative examples include solvent-containing systems such as ionic hydrogels, ionogels, and ionic organogels, as well as solvent-free systems such as ionic elastomers and polyionic elastomers. By carefully tuning their physical structures, chemical compositions, and interfacial architectures, ion migration behavior within SICs can be precisely controlled, enabling adjustable electrical properties such as capacitance, conductivity, short-circuit current, and open-circuit voltage. These characteristics provide a solid foundation for the development of SIC-based NIDs. It should be emphasized that conventional SICs typically lack electron or hole transport capability, as most polymers do not possess π-conjugated chemical structures capable of long-range electron/hole delocalization. In contrast, conjugated organic semiconductors, such as poly(3,4-ethylenedioxythiophene) (PEDOT),[82] poly(3-hexylthiophene) (P3HT),[83] and poly(benzimidazobenzophenanthroline) (BBL),[84] exhibit both ionic conductivity and tunable electronic/hole transport under ionic (electrochemical) doping, making them widely employed as organic mixed ionic–electronic conductors (OMIECs). Soft organic electrochemical transistors (OECTs) employing these SICs as channel layers have been extensively applied in artificial synapses.[85] Although the source–drain current of these devices mainly originates from electron/hole transport, gate-induced ion doping and dedoping remain essential for signal amplification, conductance modulation, and information storage. Therefore, SICs with coupled ionic and electronic (or hole) conductivity are pivotal for NIDs. A deeper understanding of their synergistic ion–electron transport and coupling is expected to guide the design and optimization of novel NID architectures.[86]

Although SIC-based NIDs have garnered considerable attention in recent years, the field remains in its early stages and faces major challenges, including understanding ion transport mechanisms, establishing robust device design principles, and enabling practical applications. This review aims to provide a theoretical framework and design guidance for the development of SIC-based NIDs, with a particular focus on conventional SICs that lacking electronic or hole conductivity. NID-based OECTs are only briefly discussed, as their design and applications have been extensively reviewed elsewhere.[87–96] Fig. 1 outlines the structure of this review. It begins with an overview of the functional units of the nervous system and their electrochemical characteristics, clarifying the biomimetic objectives and performance requirements for NIDs. Next, we summarize the mechanisms of ion transport in SICs and common strategies to modulate their behavior. Building on this foundation, we highlight both established and prospective design principles for SIC-based NIDs, encompassing artificial axons, synapses, and neurons, which constitute the core content of this work. Finally, recent advances in device development and applications are reviewed, followed by a forward-looking perspective on the challenges and opportunities in this emerging field, particularly regarding human–machine interaction and neuromorphic computing.

2. Neural components and their electrochemical characteristics

The biological nervous system primarily consists of axons, synapses, neuronal cell bodies, and the neural networks they

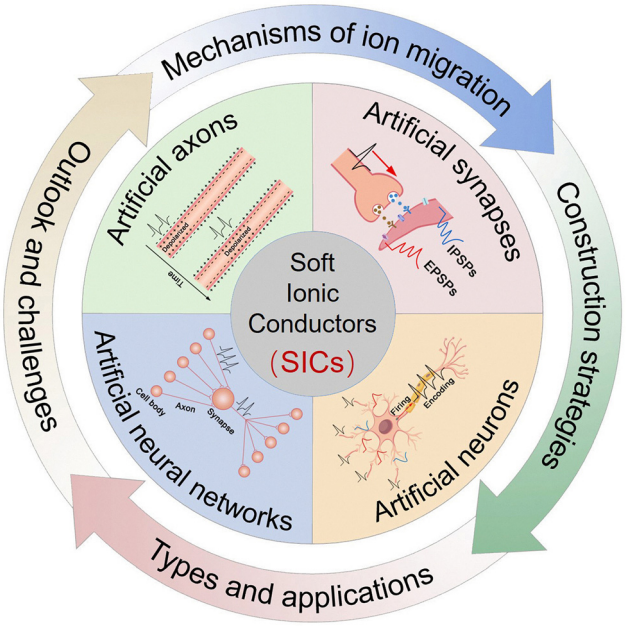

Fig. 1 Schematic outline of this review.

form. Accurately simulating their electrochemical characteristics at the device level is essential for the development of NIDs, which in turn lays the foundation for constructing brain-inspired intelligent systems at the hardware level.

2.1 Axons

Axons serve as transmission pathways for nerve impulses (action potentials), transmitting these signals from the neuronal cell body to the terminal synapses (Fig. 2(a)). This transmission process relies on the coordinated opening and closing of various ion channels, such as voltage-gated Na^+ channels, voltage-gated K^+ channels, K^+ leak channels, and Na^+–K^+ pumps along the axonal membrane (Fig. 2(b)).[97] These mechanisms enable ultra-fast, long-distance, and energy-efficient signal transmission with minimal information loss.[98]

2.2 Synapses

The human brain contains approximately 10^{15} synapses. A typical synapse comprises the axon terminal of a presynaptic neuron, the cell body or dendrite of a postsynaptic neuron, and the synaptic cleft between them (Fig. 2(a)).[99] Beyond merely serving as signal transmission bridges, synapses play a central role in information storage and computation,[100] enabling the brain to operate with ultrahigh speed, ultralow energy consumption, and exceptional fault tolerance.[101] The biological basis for synaptic storage and computational functions lies in the modulability and memory effects of the postsynaptic membrane potentials (PSPs), collectively known as synaptic plasticity.[102] Specifically, upon receiving a nerve impulse, the presynaptic membrane releases excitatory or inhibitory neurotransmitters into the synaptic cleft (Fig. 2(a)). These neurotransmitters bind to specific receptors on the postsynaptic membrane, modulating ion channel activity (*e.g.*, Ca^{2+}, Na^+, K^+, Cl^-), and thereby inducing increases or decreases in PSPs (Fig. 2(a)). The resulting responses are called excitatory/inhibitory postsynaptic potentials (EPSPs/IPSPs) (Fig. 2(c-i)).[103] The timing and frequency of incoming impulses influence changes in PSPs, giving rise to plasticity features such as SRDP[104] and STDP.[105] These changes may be transient or long-lasting, known respectively as short-term plasticity[106] and long-term plasticity.[107] PSP levels directly determine the synaptic weights (SWs) between connected neurons. In simple terms, higher PSPs make it easier for the postsynaptic neuron to be activated, and *vice versa*.[108] Through adaptive regulation of PSPs/SWs at each synapse in neural networks, the brain realizes advanced functions such as perception, memory, learning, and computation.[109]

At the device level, simulating synaptic plasticity involves replicating the PSP signals associated with specific plasticity features. Fig. 2(c) illustrates PSP dynamics for several key behaviors, including PPF/PPD, LTP/LTD, SRDP and STDP. PPF/PPD describes the phenomenon where, under stimulation by two nerve impulses, the PSP amplitude induced by the second impulse is enhanced (PPF)[110] or reduced (PPD)[111] compared to the first (Fig. 2(c-ii)), with the difference diminishing as the inter-pulse interval increases. PSPs induced by a small number of nerve impulses generally decay quickly to the initial level, thus PPF/PPD is a manifestation of short-term plasticity. However, under repetitive stimuli by multiple impulses, the PSP level undergoes significant increases or decreases and requires a long time to recover. This characteristic is known as LTP or LTD, a manifestation of long-term plasticity (Fig. 2(c-iii)).[112] The changes in PSPs induced by nerve impulses at a higher frequency are more pronounced, a characteristic known as SRDP (Fig. 2(c-iv)).[113] Research also suggests that alterations in the PSP level are linked to the timing of presynaptic and postsynaptic nerve impulses. If the presynaptic nerve impulse precedes the postsynaptic one, the PSP level rises, and *vice versa*. This characteristic is termed STDP or Hebbian rule (Fig. 2(c-v)).[114]

2.3 Neuronal cell bodies

Neuronal cell bodies are characterized by numerous dendrites, which provide extensive surface area for synaptic input (Fig. 2(a)). Their primary function is to integrate incoming signals from other neurons and fire nerve impulses.[115] Subsequently, these impulses travel along the axon to synapses, affecting the membrane potential of downstream neurons. A threshold excitation mechanism governs signal integration and impulse generation.[116] Specifically, impulse inputs from all presynaptic neurons modulate the local membrane potential of the cell body, inducing both up- and down-regulation (Fig. 2(d)). When the overall membrane potential exceeds a critical threshold, an action potential is triggered at the axon hillock; otherwise, no signal is fired. Furthermore, neuronal cell bodies encode information through the number and frequency of action potentials.[117] This mechanism has inspired the development of spiking neural network (SNN) architectures.[118] The number and frequency of generated

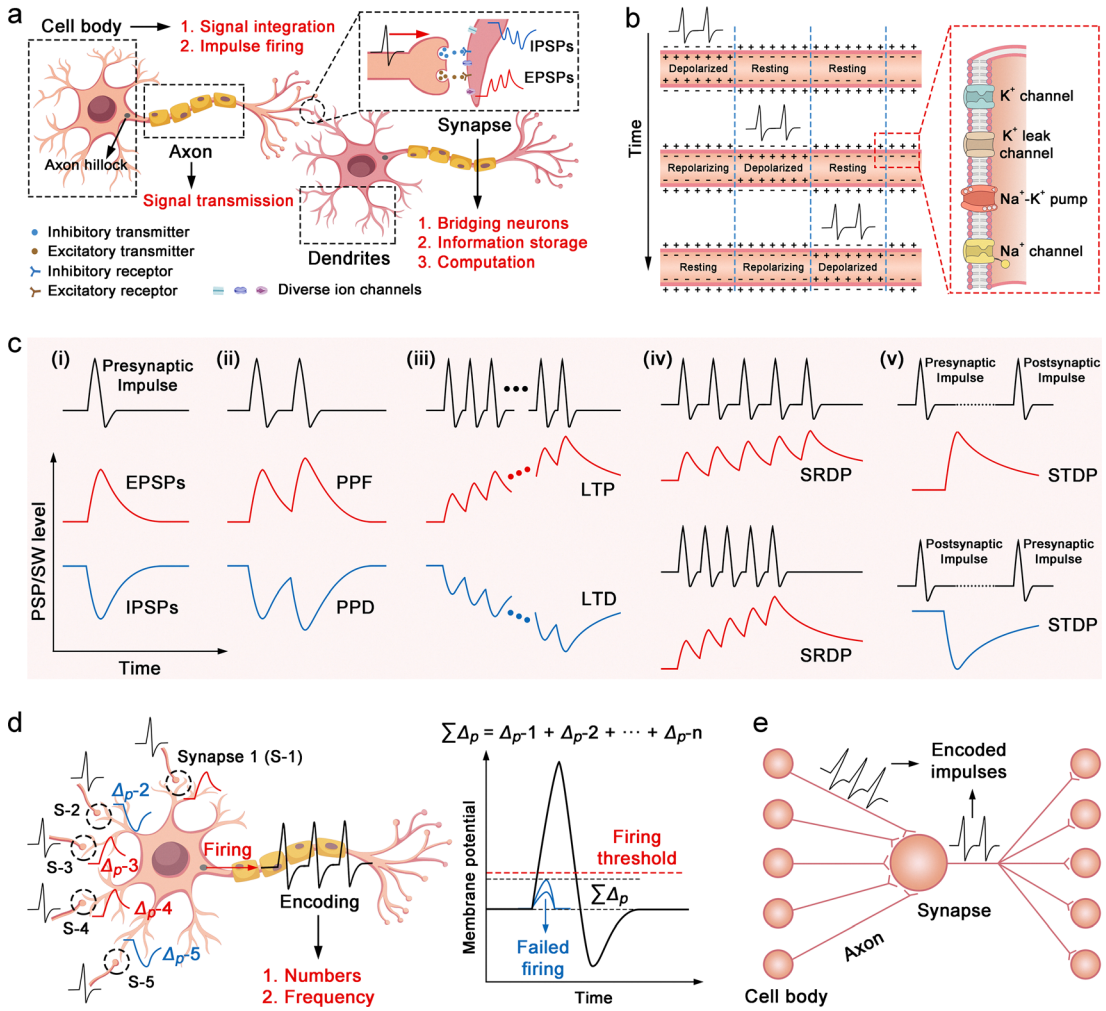

Fig. 2 Neural components and their electrochemical characteristics. (a) Functional schematic of biological axons, synapses, and neurons. (b) Rapid and non-attenuated propagation of ionic action potentials along axons. (c) Synaptic signal characteristics, including EPSPs/IPSPs (c-i), PPF/PPD (c-ii), LTP/LTD (c-iii), SRDP (c-iv), and STDP (c-v). (d) Electrical behavior of neurons, highlighting signal integration, threshold-triggered spiking, and frequency-coded information transmission. (e) Parallel computing paradigm of neural networks, demonstrating how interconnected neurons collaboratively process information.

impulses depend on the cumulative strength of inputs from presynaptic neurons.

2.4 Neural networks

Neural networks are integrated assemblies of axons, neuronal cell bodies, and synapses that enable advanced functions such as cognition, recognition, emotion, decision-making, and associative learning through parallel processing.[119] In this computing paradigm, neuronal cell bodies integrate stimuli from upstream neurons and encode them into action potentials, which are transmitted by axons to downstream synapses (Fig. 2(e)). Synapses serve as dynamic interfaces that connect adjacent neurons and modulate synaptic weights to regulate signal transmission (Fig. 2(e)). In addition to conventional synaptic (hard-wired) connections, signal propagation in neural networks can also occur through ephaptic coupling, a non-synaptic mechanism mediated by local electric field interactions between adjacent neurons.[120] Although ephaptic coupling plays a critical role in biological systems, it remains largely unexplored in current electronic neuromorphic devices. This limitation stems from the fact that electrical crosstalk, which enables ephaptic interactions, is typically considered an undesirable artifact in electronic circuits and is minimized by design. Integrating both synaptic and ephaptic signalling mechanisms into hardware architectures presents a promising direction for developing more biologically realistic and functionally versatile neuromorphic computing systems.

3. Design principles of SIC-based NIDs

SIC-based NIDs combine biocompatibility, flexibility, stretchability, and facile encapsulation and integration. Nevertheless, a systematic theoretical framework for the rational design and construction of such devices remains lacking. In this section, we first summarize the mechanisms of ion transport within SICs, then review common strategies for regulating ion

migration, and finally propose several highly feasible approaches for constructing SIC-based NIDs.

3.1 Migration mechanisms of ions in SICs

Ion transport mechanisms in SICs form the theoretical foundation for designing SIC-based NIDs. These mechanisms are generally categorized into two types: continuous transport and discontinuous transport.[81] Depending on the specific SIC system, one mechanism may dominate, or both may synergistically govern the overall transport behavior.[121–123]

3.1.1 Continuous transport. Continuous transport refers to ion migration within a continuous effective medium (Fig. 3(a)), where ion motion obeys the fundamental continuity

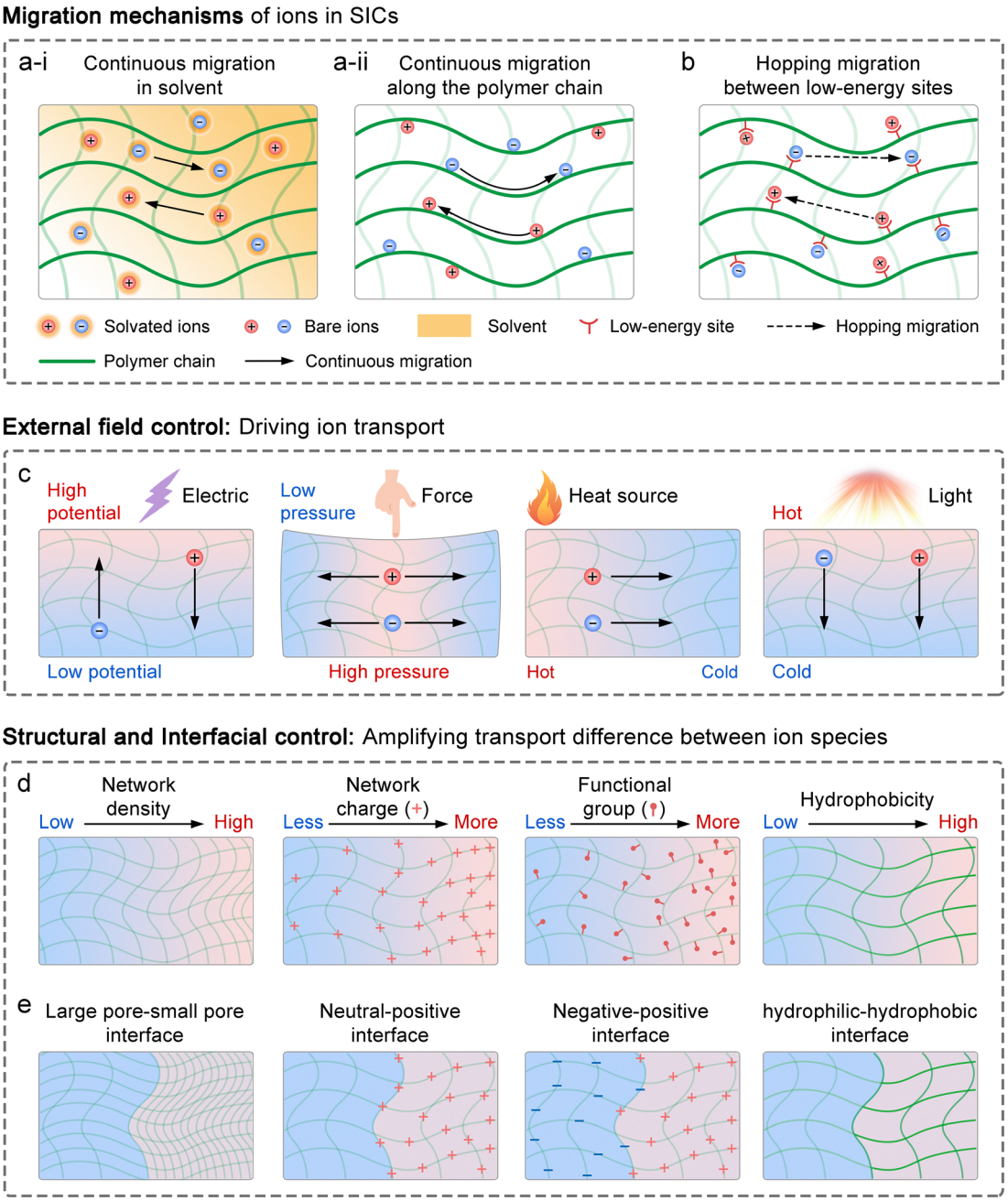

Fig. 3 Theoretical foundation for designing SIC-based NIDs. (a) Continuous ion transport mechanisms, including migration in solvent media (a-i) and along polymer chains (a-ii). (b) Discontinuous ion transport *via* hopping mechanisms. (c) Stimuli-responsive ion transport driven by electrical, mechanical, thermal, and optical inputs. (d) Structural strategies to enhance ion transport rate differences between ion species, including gradients in network density, charge distribution, functional group density, and hydrophilicity/hydrophobicity. (e) Interfacial engineering to modulate ion transport selectivity, such as large pore–small pore network interfaces, neutral-positively/negatively charged network interfaces, negatively–positively charged network interfaces, and hydrophilic–hydrophobic network interfaces.

equation:[124]

$$\frac{\partial c_i}{\partial t} + \nabla \cdot N_i = 0 \quad (1)$$

Here, c_i and N_i represent the concentration and molar flux of ion species i, respectively. The effective medium is a component that has good compatibility with ions, containing solvents and polymer chains. This compatibility arises from van der Waals forces, hydrogen bonding, dipole–dipole interactions, and other non-covalent interactions.[125] It is generally believed that when there is good interaction between the ions and the matrix of SICs, the ions primarily undergo continuous transport, such as in ionic hydrogels, ionic organogels, and ionogels.[81] In SICs with low ion concentrations (covering levels observed in biological systems), continuous ion transport can be accurately described by the Poisson–Nernst–Planck (PNP) theory, governed by the following two key equations:[126]

$$N_i = -D_i \nabla c_i - \frac{z_i c_i D_i F}{RT} \nabla V - \frac{2\alpha_i c_i D_i}{T} \nabla T + u_i c_i \quad (2)$$

$$\nabla \cdot (-\varepsilon_0 \varepsilon_r \nabla V) = F \sum_i z_i c_i \quad (3)$$

where D_i is the diffusion coefficient, z_i is the valence state, F is the Faraday constant, R is the gas constant, T is the absolute temperature, V is the electrostatic potential, α_i is the reduced Soret coefficient, u_i is the convection velocity, ε_0 is the vacuum permittivity, and ε_r is the relative permittivity. This theory suggests that ion fluxes, in both magnitude and direction, arise from multiple contributions, such as free diffusion, electrophoresis, thermophoresis, and solvent convection, but are not limited to these. Although these flux components can be calculated independently, they are inherently interdependent through ion concentration. Meanwhile, the PNP theory indicates that the driving forces behind ion migration originate from controllable factors such as concentration gradients, potential gradients (direction and intensity of the electric field), temperature gradients, and solvent flow. These insights provide a theoretical foundation for manipulating ion transport to modulate the electrochemical properties of SICs. Under identical external conditions, the intrinsic properties of ions, including diffusion coefficients, valence states, and Soret coefficients, govern the differences in their fluxes. Therefore, ionic electrical signals with distinct characteristics can be achieved by selecting the ion species in SICs.

While the conventional PNP theory is well-suited to dilute ionic systems, its accuracy diminishes at high ion concentrations.[127] This is because, in SICs with high ion concentrations, the interactions between ions, as well as between ions and polymer networks, become significant, especially in ionogel and polyionic elastomers. These non-negligible interactions result in non-ideal behaviors, such as deviations in effective ion concentrations (ionic activity) and variations in local permittivity. To extend the applicability of the PNP framework to such complex systems, several modifications have been proposed. These include introducing activity coefficients to correct for non-ideal ion concentrations (ionic activity theory),[128–130] incorporating additional flux terms to account for interaction-induced transport contributions,[131–133] and establishing concentration-dependent permittivity models,[134–136] as reflected in the generalized Poisson–Boltzmann theory.

According to the PNP theory, the diffusion coefficient is a fundamental parameter reflecting the mobility of an ion species: the larger the coefficient, the faster the ion migration, and *vice versa*. The diffusion coefficient of ions in SICs is significantly different from that in pure solvents. In SICs, the diffusion coefficient, besides being negatively correlated with the size of the ion species and the solvent viscosity, and positively correlated with temperature, is also influenced by steric hindrance from the polymer network and by the compatibility between ions and polymer chains.[137–139] Specifically, a denser polymer network imposes greater spatial resistance to ion movement, thereby reducing the diffusion coefficient. Similarly, poor ion–polymer compatibility limits the number of favorable migration pathways, further suppressing ion mobility. Therefore, compared to nanofluidic systems based on nanopores or nanochannels, which use electrolyte solutions as ion reservoirs, SIC systems offer more abundant design possibilities and flexibility for tailoring electrochemical properties.

3.1.2 Discontinuous transport. Discontinuous transport refers to the fact that ions no longer move along a continuous smooth path, but exhibit a hopping behavior,[140] *e.g.* the Grotthuss mechanism[141] (Fig. 3(b)). In SICs, this type of transport typically occurs when ions have poor compatibility with the polymer network and the solvent. In such cases, ions need to jump between energetically favorable sites to achieve long-distance migration.[142] These energetically favorable sites often include hydrogen bonding sites, ionic bonding sites, and defect sites. However, ion hopping requires overcoming the energy of these physical interactions (the activation energy), resulting in a very slow ion transport rate (diffusion coefficient). This behavior can be captured by Arrhenius-type kinetics:[143]

$$k = A \cdot \exp\left(-\frac{E_a}{RT}\right) \quad (4)$$

where k denotes the diffusion coefficient (or ionic conductivity), A is the reference diffusion coefficient (or ionic conductivity) at temperature T, and E_a is the activation energy. This equation can be converted to a linear form:

$$\ln(k) = \ln(A) - \frac{E_a}{R} \cdot \frac{1}{T} \quad (5)$$

By plotting $\ln(k)$ *versus* $1/T$, the activation energy E_a can be experimentally estimated. In addition, molecular dynamics simulations provide a microscopic view of this hopping process and help calculate the associated energy barriers.

A recent study demonstrated that when hydrated ions migrate from hydrophilic hydrogels into hydrophobic organogels, they undergo dehydration, a process that requires sufficient energy to overcome the dehydration energy barrier.[144] Owing to the distinct dehydration energy barriers associated with different ion species, the resulting ion flux under varying

voltage inputs differs, offering a new strategy for generating complex ionic electrical signals in SICs. Once inside the organogel, the migration kinetics of dehydrated (bare) ions resemble those observed in sub-nanopore/channel.[144] In such an extremely confined condition, strong ion–ion pairing interactions (fractional Wien effect[53]), along with ion–polymer interactions like frictional forces, electrostatic attraction, van der Waals forces, and hydrogen bonding, play a crucial role in determining ion transport pathways and rates. Some researchers further suggest that bare ions may exhibit quantum transport behavior under sub-nanometer confinement, characterized by ultrafast, stochastic motion.[145–147]

3.2 Means of controlling ion transport

As previously discussed, ion transport in SICs is strongly influenced by factors including ion concentration, temperature, electric field, solvent flow, and interactions between ions and the polymer network. This indicates that ion transport can be controlled through external fields, structural modifications to SICs, and the introduction of specialized interfaces.

3.2.1 External field control. External stimuli, such as electricity, force, heat, and light, can all drive ion transport in SICs (Fig. 3(c)). This principle underlies many intelligent SIC-based devices, including actuators,[148–150] transistors,[151–153] diodes,[154–156] energy harvesters,[157–160] and ionic skins.[161–164] Electrical stimulation drives ion migration by creating a directional electric field. Force-driven ion migration typically arises from the piezoionic effect.[165] When an external force deforms the SIC, it generates a pore pressure difference within the material. This difference induces solvent flow, which, through Stokes resistance, drives ion migration, as described in the fourth term of eqn (2). In solvent-free ionic and polyionic elastomers, deformation can drive ion transport by generating a chemical potential gradient.[160] Thermal stimuli, both cold and hot, induce temperature gradients within SICs, leveraging the thermodiffusion effect of ions (described by the third term in eqn (2)).[166] Light, when absorbed, can convert into heat through the photothermal effect, driving further ion migration.[167] The ability to respond to external stimuli is essential for SIC-based NIDs, enabling them to perform tasks such as sensing, information transmission, storage, and neuromorphic computing.

3.2.2 Structural control. To ensure that SICs generate detectable ionic electrical signals under external stimuli, it is vital to create a differential transport rate between anions and cations. In addition to the inherent properties of ion species, such as charge, size, and Soret coefficient, the structural features of the polymer network, including density, charge, functional groups, and hydrophilic or hydrophobic nature, can also significantly influence ion transport. These structural features interact with ions in different ways, modulating their transport behavior. Consequently, incorporating structural gradients within SICs can amplify differences in migration rates among ion species, resulting in stronger ionic electrical signals and more complex ion transport behaviors (Fig. 3(d)). This design approach would allow SIC-based devices to better mimic diverse neural electrical signals with greater accuracy.

3.2.3 Interfacial control. Heterogeneous interfaces in SICs, such as hydrophilic–hydrophobic interfaces, large pore–small pore interfaces, and neutral polymer network-positive/negative polymer network interfaces, serve as selective barriers that can significantly amplify the transport differences between ion species (Fig. 3(e)). For example, larger ions often face obstruction at large pore–small pore interfaces, while smaller ions can pass through unimpeded.[168] When ions traverse a hydrophilic–hydrophobic interface, hydrophilic ions (such as metal cations and halide anions) are repelled,[144] sometimes requiring the removal of their hydration shells, while ions with hydrophobic functional groups (*e.g.*, alkyl chain-bearing quaternary ammonium ions and ionic liquids) may pass through more easily. At the neutral polymer network–positive (negative) polymer network interface, cations (anions) are repelled by electrostatic forces, while anions (cations) can pass through.[158] Additionally, at the negative polymer network–positive polymer network interface (ionic p–n junction), dual electrostatic repulsion allows ions to pass in only one direction, creating a unique ion rectification effect.[155] These interface characteristics can be strategically designed and combined within SICs to enable more precise ion selectivity.

3.3 Construction strategies for SIC-based NIDs

The electrical signalling properties of biological axons, neuronal cell bodies, and synapses form the fundamental basis for designing artificial axons, neurons, and synapses. Building on the ion transport mechanisms and modulation methods discussed earlier for SICs, we outline several viable strategies for constructing SIC-based NIDs. While some of these approaches have been preliminarily reported, many still require further experimental validation.

3.3.1 Construction strategies for artificial axons. Artificial axons are designed to transmit electrical pulse signals. In principle, traditional linear SICs, such as ionic hydrogel fibers, ionic organogel fibers, and ionogel fibers, can perform this function *via* long-distance ion migration.[170] However, due to the inherently high resistance and low ion mobility of SICs, these devices may suffer from signal distortion, including diminished signal intensity and frequency. Therefore, enhancing conductivity and ion mobility is crucial. This can be achieved by utilizing ions with high diffusion coefficients, increasing ion concentration, introducing multiple ion transport mechanisms,[122] and constructing axially aligned ion pathways[171] (Fig. 4(a)). Suo *et al.* proposed an SIC-based artificial axon structure, which is highly effective for transmitting pulse signals.[169] This structure relies on the fast charging and discharging of ion capacitors rather than long-distance ion migration, providing advantages such as ultrafast signal transmission and minimal signal distortion (Fig. 4(b)). This strategy is further discussed in Section 4.1.1.

3.3.2 Construction strategies for artificial synapses by two-terminal devices. Using SICs to simulate the characteristic signals of PSPs (Fig. 2(c)) lays the groundwork for constructing

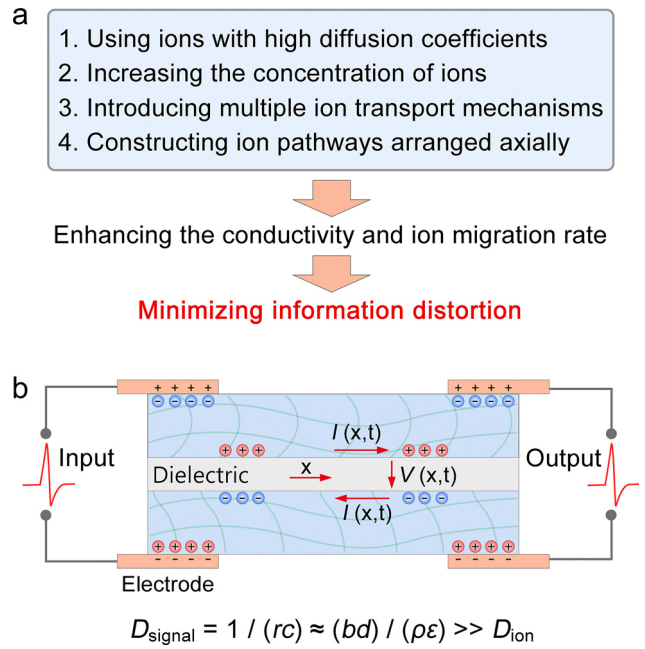

Fig. 4 Construction strategies for artificial axons. (a) Methods to enhance conductivity and ion mobility in SICs. (b) Architecture of SIC-based artificial axons, in which the signal diffusivity (D_{signal}), characterizing the signal transmission speed along the ionic cable (unit: $m^2\ s^{-1}$), greatly exceeds the ion diffusivity (D_{ion}) in SICs. Reproduced with permission from ref. 169. Copyright@2015, Elsevier.

SIC-based artificial synapses with distinctive, tunable intensity and memory characteristics, including IPSPs/EPSPs, PPF/PPD, LTP/LTD, SRDP, STDP, *etc.* Therefore, a promising approach to reproduce such behaviors in SIC-based devices involves the controllable modulation and retention of electrical parameters, including resistance, conductance, short-circuit current (the current generated by the device itself with no connected load), and open-circuit voltage (electrostatic potential) (Fig. 5(a)). Specifically, resistance and conductance reflect the device's electrical conductivity, short-circuit current represents ion flow triggered by external stimuli, and open-circuit voltage corresponds to the internal ion distribution. However, conventional SIC-based sensors, such as strain-resistive, piezoelectric, and thermoelectric types, typically fail to exhibit memory behavior because their electrical signals decay rapidly after stimulus removal. This limitation arises from the absence of specialized structures or interfaces that can regulate ion transport, which is essential for mimicking synaptic functions. In the following sections, we discuss potential strategies to enable controlled modulation and memory of electrical parameters in SIC-based two-terminal devices.

3.3.2.1 For resistance and conductance. The electrical conductivity of SICs is influenced by several factors, including the concentration of charge carriers, the ion migration rate, the size of the effective ion migration paths, the ion flux at heterogeneous interfaces, interactions between ions, and interactions between ions and the polymer network (Fig. 5(b)). Based on this, the following strategies are proposed:

(1) Utilizing ion species with reversible self-assembly/disassembly capabilities: ion species that can reversibly self-assemble and disassemble in response to external stimuli (*e.g.*, light, sound, heat, electricity, or magnetic fields) can serve as dynamic charge carriers. Upon assembly, these ion aggregates exhibit significantly increased volume and consequently lose their mobility, rendering them inactive as charge carriers. This strategy enables precise, stimulus-responsive regulation of charge carrier concentration (Fig. 5(b-i)).

(2) Incorporating ion-adsorbing/releasing functional components: functional components capable of reversibly adsorbing and releasing ions in response to external stimuli can be integrated into the system. Once adsorbed, the ions become immobilized and no longer serve as charge carriers. These components can include micro/nanoparticles, ion-trapping groups such as spiropyran,[172] or host functional groups such as cyclodextrins and cucurbiturils.[173] This strategy provides a reversible and controllable means to regulate charge carrier concentration (Fig. 5(b-ii)).

(3) Using ion species with molecular configurations tunable by external stimuli: ion species whose molecular configurations can be reversibly tuned by external stimuli, such as photoresponsive charged derivatives of spiropyrans and azobenzenes, can be employed. Configuration changes modulate their interactions with the solvent and polymer matrix, including spatial hindrance, hydrogen bonding, electrostatic interactions, and van der Waals forces, thereby altering their diffusion coefficients. This strategy enables precise regulation of ion migration rates (Fig. 5(b-iii)).

(4) Incorporating phase-changeable polymer networks: polymer networks capable of undergoing phase transitions in response to external stimuli, such as thermoresponsive poly(*N*-isopropylacrylamide)[174] as well as its derivatives and analogues, can be introduced. Phase changes such as precipitation or crystallization restrict ion transport by narrowing or blocking migration pathways, enabling precise control over the size of effective ion migration paths (Fig. 5(b-iv)).

(5) Integrating stimuli-responsive polymer networks for contraction/expansion: stimuli-responsive polymer networks capable of reversible contraction or expansion, such as photoresponsive azobenzene- and spiropyran-based polymers,[175] can be incorporated into the system. This strategy allows precise modulation of the effective ion migration pathways by controlling the network's structural changes (Fig. 5(b-v)).

(6) Controlling ion migration paths *via* precipitation formation and dissolution: research has shown that the size of effective ion migration paths can be precisely controlled by regulating the formation and dissolution of local precipitates within SICs.[176] This study reports an anomalous hydrogel ionic p–n junction, where anion and cation enrichment at the heterogeneous interface leads to precipitate formation (detailed in Section 4.1.2.2) (Fig. 5(b-vi)).

(7) Introducing heterogeneous interfaces: heterogeneous interfaces, such as hydrophilic–hydrophobic interfaces, large

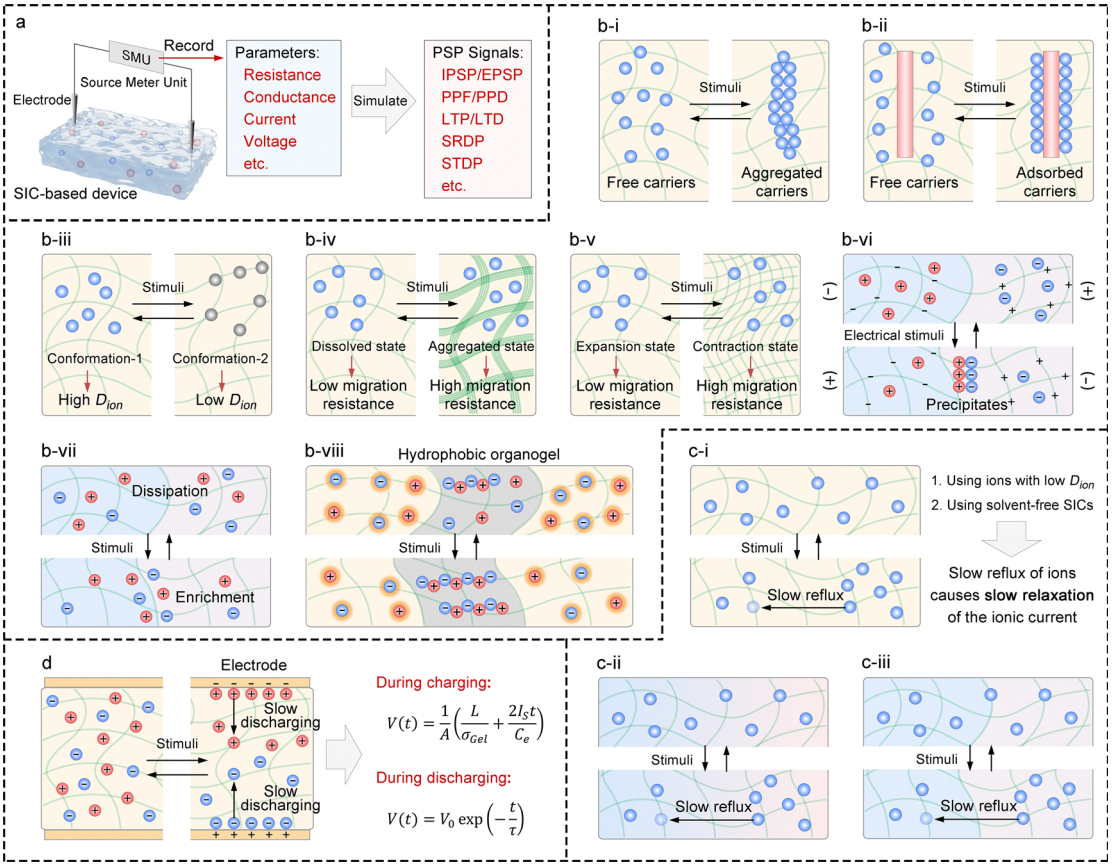

Fig. 5 Construction strategies for two-terminal artificial synaptic devices. (a) Overall design principle, illustrating the use of electrical parameters of SICs to emulate PSP signals. (b-i)–(b-viii) Strategies for achieving controllable modulation and memory effects in the resistance or conductance of SICs. (c-i)–(c-iii) Strategies for achieving controllable modulation and memory effects of short-circuit current and open-circuit voltage in SICs. (d) Exploiting slow ionic EDL discharge to enable controllable modulation and memory effects of open-circuit voltage in SIC-based devices.

pore–small pore interfaces, neutral polymer network-positive/negative polymer network interfaces, and negative polymer network–positive polymer network interfaces, can be introduced. These interfaces promote ion enrichment and dissipation near the interface due to their selective ion permeability. Small changes in ion concentration (induced by external stimuli) within these regions can significantly affect the net ion flux across the interface, thereby modulating the device's conductivity. The combined effect of multiple interfaces may further enhance control (Fig. 5(b-vii)).

(8) Using hydrophobic organogel to confine hydrated ions: a recent study demonstrated that thin-layer hydrophobic organic gels are equivalent to sub-nanoporous membranes for hydrated ions (strong hydrophilic ions).[144] As a result, within the polymer network of organogels, dehydrated (bare) ions exhibit unconventional transport behaviors, such as tightly bound Bjerrum pair formation,[53] ion Coulomb blockade,[177] and quantum transport.[145] These phenomena arise from strong ion–ion and ion–polymer interactions in sub-nanometer confined environments. Leveraging this property, devices with a hydrogel/organogel/hydrogel architecture may exhibit memristive behavior reminiscent of that observed in nanofluidic memristors (Fig. 5(b-viii)).

3.3.2.2 For short-circuit current. To achieve ionic current with memory (*i.e.*, relaxation) behavior in SIC-based devices, the key is to reduce the migration rate of ion species. When external stimuli induce asynchronous transport of cations and anions, a transient ionic current is generated. Upon removal of the stimulus, ions undergo back-diffusion driven by the chemical potential, leading to a gradual decay of the current. By slowing ion migration, the relaxation time of the ionic current is prolonged, enabling memory-like behavior (Fig. 5(c)). Based on this, some general strategies are listed below:

(1) Employing ion species with low diffusion coefficients: ion species with inherently low diffusion coefficients, such as bulky ions or those poorly compatible with the polymer matrix, can effectively slow down ion migration (Fig. 5(c-i)).

(2) Utilizing solvent-free SICs: in solvent-free SICs, such as ionic elastomers or polyionic elastomers, ion mobility is inherently low due to the absence of free solvents (Fig. 5(c-i)).

(3) Introducing structural gradients to impede ion reflux: structural gradients, such as variations in polymer density, charge distribution, functional groups, or hydrophilicity/hydrophobicity, can hinder ion backflow by creating asymmetric migration pathways within the polymer network (Fig. 5(c-ii)).

(4) Introducing heterogeneous interfaces to restrict ion reflux: heterogeneous interfaces act as energy barriers to ion backflow. While external stimuli facilitate ion movement across these interfaces during stimulation, their absence during relaxation impedes backflow, thereby slowing the decay of the ionic current (Fig. 5(c-iii)).

3.3.2.3 For open-circuit voltage. When external stimuli drive the asynchronous transport of cations and anions, an electrostatic potential can be generated due to the uneven ion distribution. To sustain this potential, it is essential to prevent the ion distribution from returning to equilibrium, *i.e.*, to impede ion reflux. Consequently, the strategies for controlling open-circuit voltage closely mirror those for controlling short-circuit current (Fig. 5(c)). Moreover, when inert conductive materials (such as gold, platinum, or indium tin oxide) are used as electrodes, the open-circuit voltage generated by the ionic electric double layer (EDL) on the electrode surface can naturally exhibit controllability and memory behavior. This is because the EDL's charging process is governed by the input charge (electrons and holes), and its discharging process has a long half-life.[178] As a result, SIC-based ionic capacitors hold potential for use in artificial synaptic devices (Fig. 5(d)).

3.3.3 Construction strategies for artificial synapses by three-terminal devices. OECTs based on OMIECs represent a prototypical class of three-terminal NIDs that can function directly as artificial synapses.[179] A typical OECT comprises source, drain, and gate electrodes; an organic semiconductor film serving as the charge transport channel; and an electrolyte layer that facilitates ionic transport and electrochemical coupling at the interface (Fig. 6(a)).[180] The electrolyte may be liquid (*e.g.*, electrolyte solution, ionic liquids), gel-based (*e.g.*, ionic hydrogels, ionogels), or solid-state. The source and drain electrodes inject and collect charge carriers, while the gate electrode regulates ionic migration and tunes the channel conductance through the applied electric field. The fundamental operating mechanism of synaptic OECTs is governed by the gate–voltage-driven ion–electron coupling process (Fig. 6(a)). Specifically, upon applying a voltage to the gate, free ions in the electrolyte migrate across the electrolyte/organic semiconductor interface, analogous to neurotransmitter release; the subsequent ion insertion or extraction modulates the channel's chemical doping and local charge density, mimicking the functional action of neurotransmitters, which in turn induces reversible changes in the source–drain current that emulate the EPSPs and IPSPs of biological synapses.[14] The carrier mobility, ion–channel interaction, and volumetric capacitance of the channel layer collectively determine the transconductance, dynamic response, and memory characteristics of the device. Meanwhile, the ion species, concentration, and viscosity of the electrolyte govern the kinetics and stability of ionic transport. Therefore, the coordinated design of both material parameters (channel and electrolyte) and geometric factors (channel thickness, volume, and electrode overlap area) directly dictates the amplitude, response speed, and retention time of synaptic behavior. Comprehensive reviews of OECT-based devices are available in the literature[87–92,181] and will not be repeated here.

Regarding the channel materials, OECTs are broadly categorized into hole-dominated p-type and electron-dominated n-type devices, each presenting distinct operating mechanisms and design considerations. Representative p-type materials include PEDOT,[182–185] P3HT,[186–189] and alcohol- or polyether-functionalized thiophene-based conjugated polymers (*e.g.*, p(g2T-T), p(g2T-TT)),[190–192] which generally offer high hole mobility, excellent ionic compatibility, and large volumetric capacitance. By modulating the gate voltage to drive ion injection, the hole concentration within the channel can be precisely controlled, enabling reversible doping and dedoping (Fig. 6(b)). N-Type materials, in contrast, have historically been challenged by limited electronic stability and side reactions under aqueous conditions, but notable advances have been achieved recently.[193] Typical examples include BBL,[194–196] naphthalene diimide (NDI)-based conjugated polymers,[197–199] and various donor–acceptor polymers.[88] Incorporating strong electron-accepting units such as bithiophene imide (BTI), diketopyrrolopyrrole (DPP), and azaisoindigo (AIID) can lower the LUMO level, enhancing electron affinity and environmental stability.[200] In n-type devices, a negative gate voltage drives cations into the channel, forming electrostatically neutral pairs with reduced high-electron–density states, thereby increasing electronic conductivity (Fig. 6(b)). Overall, p-type OECTs are particularly advantageous for high transconductance, signal amplification, and mechanical stretchability, whereas the advancement of n-type OECTs is critical for enabling complementary logic circuits,[201] signal amplification,[202] ambipolar synaptic networks,[203] and more complex brain-inspired circuitry.[117] In terms of operation, OECTs are typically categorized into depletion and enhancement (accumulation) modes. Depletion-mode devices exhibit a high-conductivity (ON) state at zero gate bias, and the applied gate voltage triggers dedoping or an opposite chemical transition, leading to a decrease in conductance (OFF) (Fig. 6(c-i)).[204] In contrast, enhancement-mode devices exhibit a low-conductivity (OFF) state at zero gate bias, where the application of a gate voltage with an appropriate polarity drives ion injection into the channel layer, induces electrochemical doping, and consequently increases the channel conductance (ON) (Fig. 6(c-ii)).[205] It should be emphasized that the volatile (short-term memory) or non-volatile (long-term memory) characteristics of OECTs are not determined by the operation mode itself.

Moreover, the physical architecture of OECTs plays a critical role in shaping ionic transport pathways, the distribution of interfacial capacitance, and parasitic impedance, thereby governing the temporal dynamics and amplitude of synaptic function.[85] Top-gate configurations enhance gate–channel coupling and shorten ion penetration paths, improving both response speed and transconductance (Fig. 6(d-i)). Coplanar-gate designs are facile to fabricate and well-suited for flexible integration, but their relatively long lateral ion diffusion limits the device response speed (Fig. 6(d-ii)). Vertical architectures reduce the channel length to the nanometer scale while

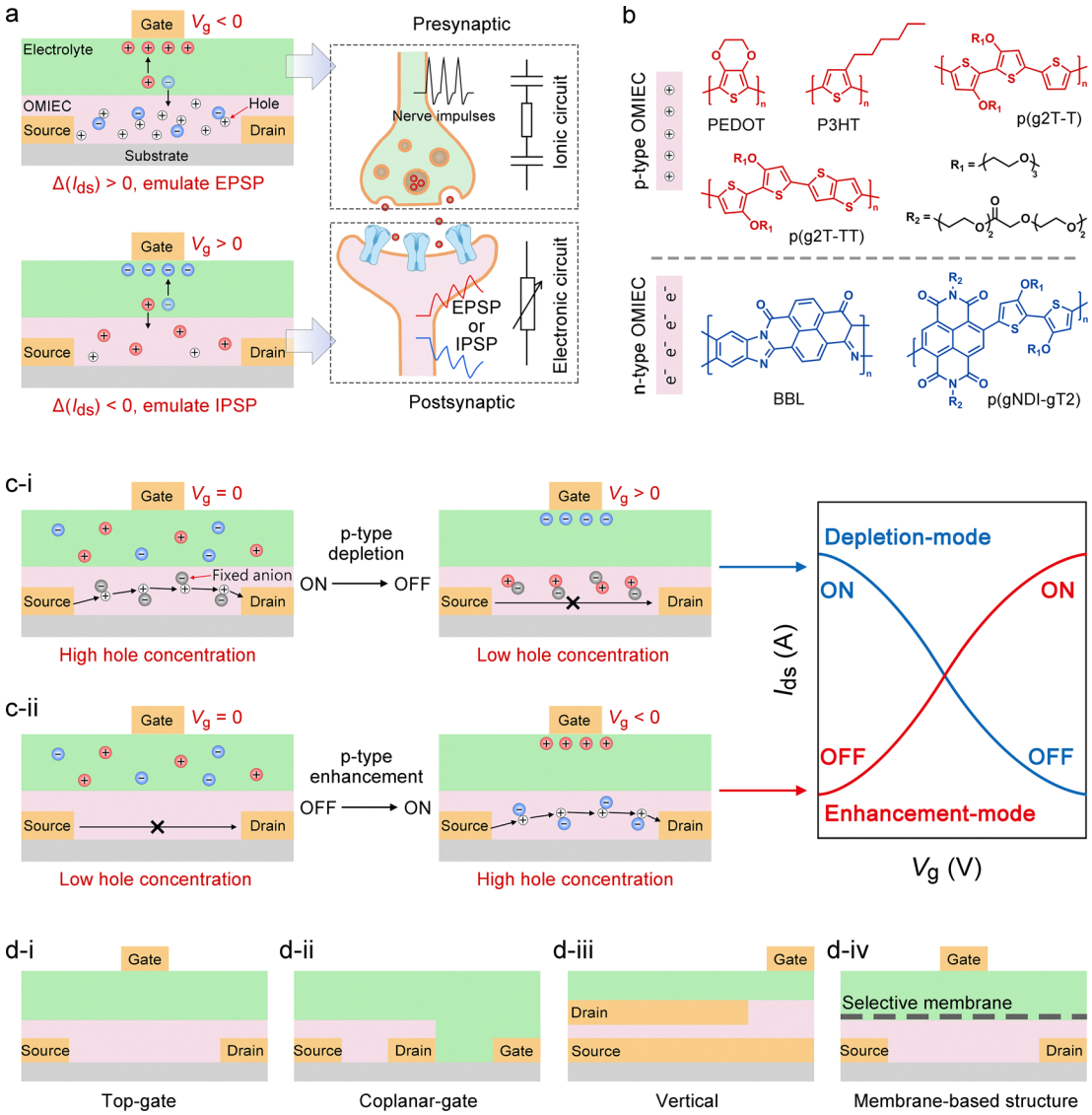

Fig. 6 Working principles and construction strategies of OECT-based artificial synaptic devices. (a) Device composition and the mechanism of synaptic emulation, including the equivalent circuit. A p-type OECT is illustrated as an example, with I_{ds} and V_g denoting the source–drain current and gate voltage, respectively. (b) Representative chemical structures of typical p-type and n-type OMIECs. (c) Operating mechanisms and electrical characteristics of depletion-mode (c-i) and enhancement-mode (c-ii) OECTs, exemplified by a p-type OECT. (d) Physical configurations of OECTs, including top-gate (d-i), coplanar (d-ii), vertical (d-iii), and membrane-based (d-iv) architectures.

maintaining a large cross-sectional area, minimizing ion migration time without compromising transconductance and enabling high-frequency operation (Fig. 6(d-iii)). Membrane-based structures between the channel and electrolyte can localize ion or charge retention and enable selective transport (Fig. 6(d-iv)).[206–210] For example, Nafion[208] and polyethylene oxide layers[211] can extend SW retention time, thereby achieving non-volatile memory behavior.

In summary, the development of high-performance OECT-based artificial synapses relies on the integrated optimization of material chemistry, channel structure, electrolyte properties, and device geometry to precisely regulate the kinetics and reversibility of ion–electron interactions. Employing these strategies enables targeted enhancement and functional tailoring of device performance for diverse applications, including transient information processing, long-term memory, low-power sensing, and high-frequency neuromorphic computing. Inspired by the ion–electron coupling mechanism in OECTs, Yan *et al.* further demonstrated a two-terminal device based on an ionic elastomer/P3HT heterojunction, in which electric-field-induced ion doping and dedoping in P3HT allow precise modulation of channel conductance, leading to a non-volatile synaptic memristor.[86] The conductance of this device arises from the synergistic contributions of ion migration and hole transport. This innovative approach not only expands the conceptual framework of OECT-inspired iontronic systems but also provides valuable guidance for the design of novel SIC-based NIDs.

3.3.4 Construction strategies for artificial synapses by dropletronics. From the perspective of macroscopic device architecture and material interfaces, SICs exhibit excellent processability, enabling not only conventional stacked device configurations but also bioinspired designs that mimic cellular structures. In particular, designing devices as microscale droplets, an approach now referred to as dropletronics,[77] offers a novel route for constructing artificial synapses. Soft microemulsion droplets employed as SICs have been widely utilized to fabricate diverse iontronic devices.[77–79,212] Their intrinsic modularity and facile miniaturization facilitate high-density integration and low-power operation, highlighting their considerable potential for cost-effective neuromorphic computing.[213–215] Moreover, energy consumption analyses[42,46,50,93,110,184,213,216–236] indicate that several dropletronic artificial synapses can achieve per-spike energy efficiencies comparable to, or even lower than, those of biological synapses (Fig. 7).[237]

Building on these advantages, Najem *et al.* demonstrated a two-terminal dropletronic device featuring a droplet interface bilayer (DIB) that exhibited key artificial synapse functionalities.[213] The device comprised two aqueous droplets suspended in a transparent reservoir filled with hexadecane oil, with the aqueous solution containing 1,2-diphytanoyl-*sn*-glycero-3-phosphocholine (DPhPC) lipids, alamethicin peptides, and an electrolyte. In their experiments, each 200 nL droplet was pipetted onto the ball-end of Ag/AgCl electrodes coated with agarose hydrogel and submerged in oil. Within minutes, lipid monomers self-assembled at the droplet surface between the aqueous and oil phases, and when the droplets were brought adjacent to one another, a lipid DIB formed spontaneously. The setup was enclosed in a grounded Faraday cage to minimize electrical noise during measurement. Upon application of a voltage exceeding a threshold, alamethicin peptides inserted into the DIB region, forming conductive ion channels (Fig. 8(a)). A defining characteristic of artificial synapses is the ability to retain temporal information from prior electrical states, which is essential for temporal signal processing. The dropletronic device exhibited such memristive behavior, as evidenced by the pinched, symmetric hysteresis in the *I–V* characteristics under voltage sweeps (Fig. 8(b)). In addition, Najem, Collier, and collaborators reported memcapacitive effects in similar dropletronic devices.[214] Two adjacent droplets suspended in oil formed a DIB at their interface. In the absence of ion channels spanning the DIB, the hydrophobic acyl chains of DPhPC lipids prevented ion transport across the bilayer, producing an ionic capacitor structure. Under zero transmembrane potential, the measured specific capacitance was 0.46 μF cm^{-2} in decane and 0.68 μF cm^{-2} in hexadecane. Upon voltage application, two primary geometric effects were

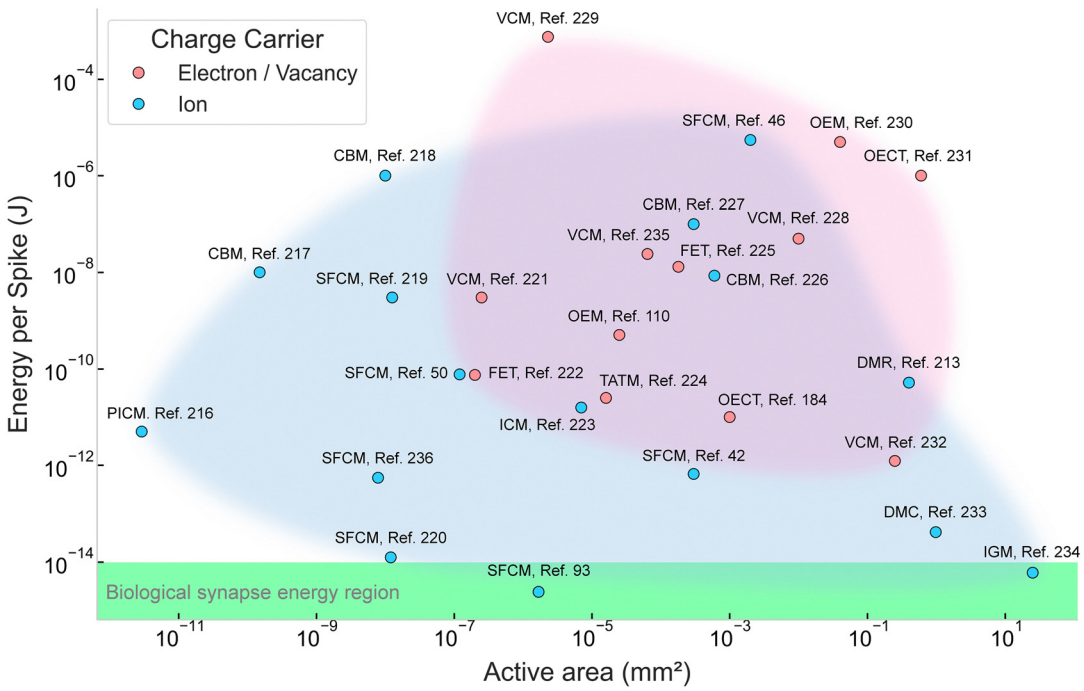

Fig. 7 Comparison of the energy consumption per spike of investigated artificial synapses and reservoir computing based on different charge carriers.[42,46,50,93,110,184,213,216–236] OECT, organic electrochemical transistor; OEM, Optoelectronic memristor; FET, field effect transistor; TATM, trap-assisted tunneling memristor; IGRT, ion-gating reservoir transistor; VCM, valence changing memristor; CBM, conductive bridge memristor; SFCM, solid-state fluidic channel memristor; ICM, ion carrier memristor; PICM, protein ion channel memristor; DMR, droplet memristor; DMC, droplet memcapacitor. The "active area" refers to the functional region of each device where primary physical or chemical phenomena occur. For instance, Paulo *et al.* designed a cylindrical hydrophobic nanopore activated for ion transport, in which the axial cross-section of the pore was defined as the active area.[216] Hossain *et al.* utilized droplet-based memcapacitors for their work, with DIB formed between two droplets.[233] The DIB area constituted the active region. In the case of photonic memristors developed by Yamazaki *et al.*, the junction area served as the active area.[230]

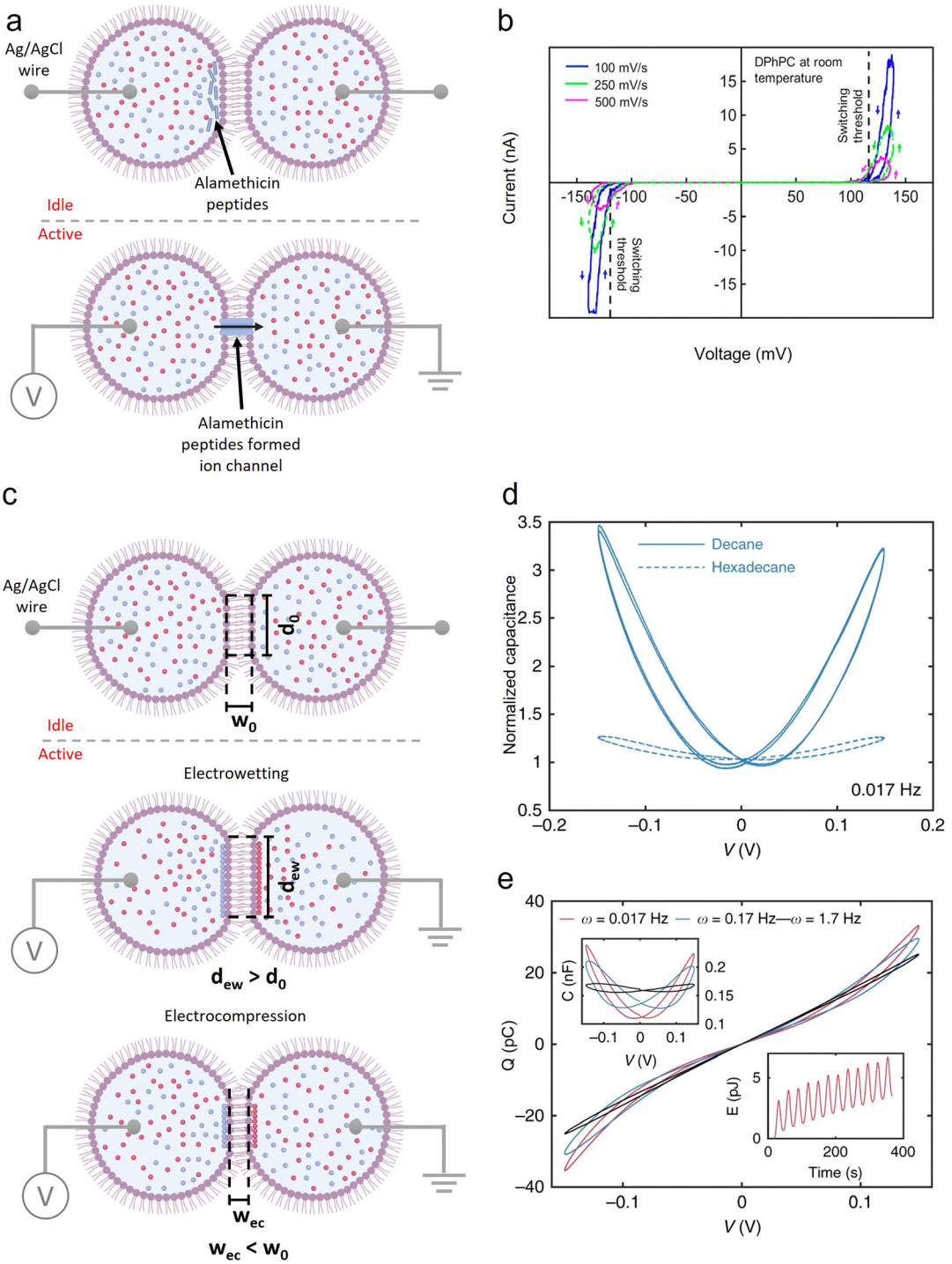

Fig. 8 Dropletronic devices exhibiting memristive and memcapacitive effects. (a) A two-terminal droplet assembly mimicking the biological structure and switching mechanism of neuron synapses, indicating a memristor effect. The assembly was activated when the imposed voltage exceeded the threshold voltage. (b) A dropletronic memristor under voltage sweeps at room temperature. Reproduced with permission from ref. 213. Copyright@2018, American Chemical Society. (c) A two-terminal droplet assembly without ion channels across the DIB (Idle), having a diameter of d_0 and a width of w_0 at the DIB area, underwent two main geometric changes (Active) in response to voltage: (1) electrowetting increased DIB diameter ($d_{ew} > d_0$); (2) electrocompression reduced the DIB thickness ($w_{ec} < w_0$). (d) Dynamic capacitance of a dropletronic memcapacitor as a function of voltage. (e) The Q–V and C–V characteristics (shown as upper insets) obtained in response to a sinusoidal voltage applied to the memcapacitors formed in decane. The lower inset represents the energy dissipated at an excitation frequency of 0.017 Hz. Reproduced with permission from ref. 214. Copyright@2019, Springer Nature.

observed (Fig. 8(c)): (1) electrowetting (EW), which increased the DIB area due to charge-induced reductions in bilayer tension;[238] (2) electrocompression (EC), resulting from expulsion of trapped oil between the DIBs, reducing DIB thickness while maintaining the area.[213] Both EW and EC contributed to the non-linear capacitance–voltage (*C*–*V*) response (Fig. 8(d)) and the pinched hysteresis in charge–voltage (*Q*–*V*) loops, indicative of memcapacitive behavior. Furthermore, owing to the lower viscosity of decane, the non-linear capacitive response was more pronounced and faster than in hexadecane (Fig. 8(e)), highlighting the role of oil viscosity in modulating the memcapacitance bandwidth.

These experimental results demonstrate that dropletronic devices can emulate key synaptic behaviors—both memristive and memcapacitive—while providing tunable electrochemical properties. By integrating microscale droplets with precise interfacial control, dropletronic devices exemplify the practical potential of SIC-based NIDs to achieve energy-efficient, high-density, and functionally versatile neuromorphic computing components. Moreover, despite the limited number of studies to date, dropletronic technology is expected to be broadly compatible with most SIC-based NID fabrication strategies discussed above, further supporting its promise as a scalable platform for future neuromorphic systems.

3.3.5 Construction strategies for artificial neurons. Artificial neuron devices are commonly implemented using electrical components such as memristors, resistors, and capacitors, which are configured into neuronal circuit models like the H–H model (Fig. 9(a)) and the Leaky integrate-and-fire (LIF) model (Fig. 9(b)). The H–H model, regarded as the most biologically accurate representation of neuronal dynamics, captures the complex interplay between Na^+ and K^+ channels, including their voltage-dependent activation and directional transport.[36] Recent theoretical studies have suggested that analog nanofluidic memristive devices could be integrated into such models to mimic neuronal spiking and signal encoding.[53–55] However, the H–H model's complexity and reliance on multiple power supplies pose challenges for system miniaturization and integration. To address these limitations, the simplified LIF model has been widely adopted. This model focuses on the opening and closing of voltage-gated ion channels, which can be abstracted as a threshold-switching digital memristor.[227] A representative *I*–*V* curve of such a device is shown in Fig. 9(c) (red curve), featuring two threshold voltages corresponding to the set (turn-on) and reset (turn-off) transitions. To date, however, no digital-type memristors based on ionic charge carriers have been experimentally demonstrated. Here, we propose a conceptual design for an ionic threshold-switching memristor by introducing an energy barrier at a heterogeneous interface (green curve in Fig. 9(c)). In this design, when the input voltage exceeds a certain threshold (set voltage), ions gain sufficient energy to overcome the interfacial barrier, triggering a transition from a low-conductance to a high-conductance state. Conversely, when the voltage drops below another threshold (reset voltage), the ions are no longer able to cross the barrier, and the device reverts to a low-conductance state. This

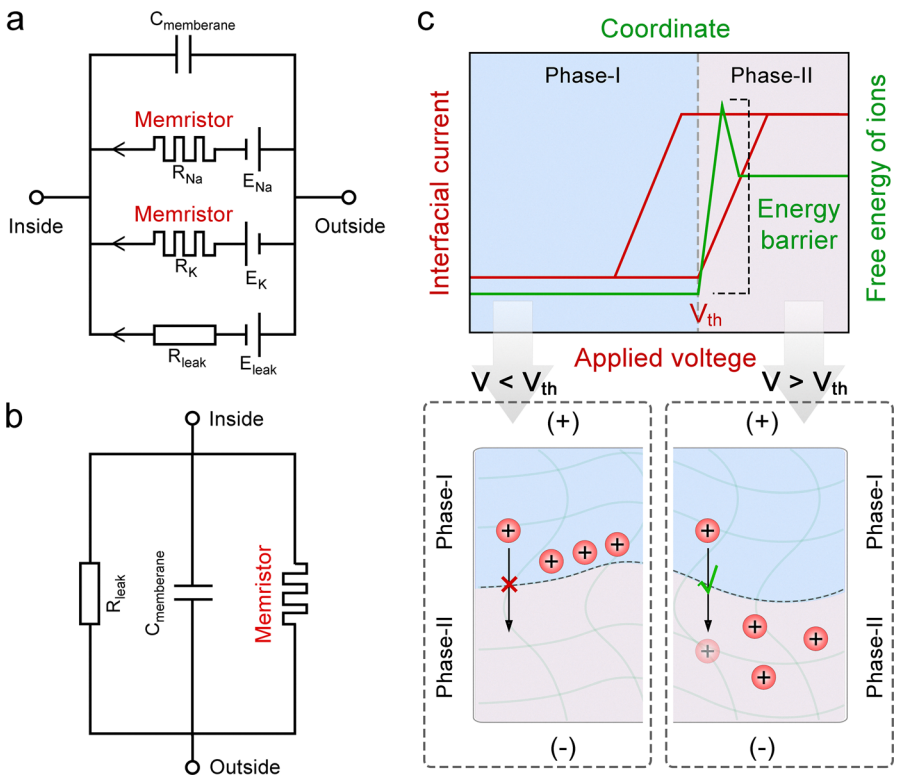

Fig. 9 Construction strategies for artificial neurons. (a) Typical H–H neuron circuit. (b) Typical LIF neuron circuit. (c) Characteristic *I*–*V* curve of digital memristors and a potential implementation approach that utilizes interfacial energy barriers to enable threshold switching of ionic conductivity.

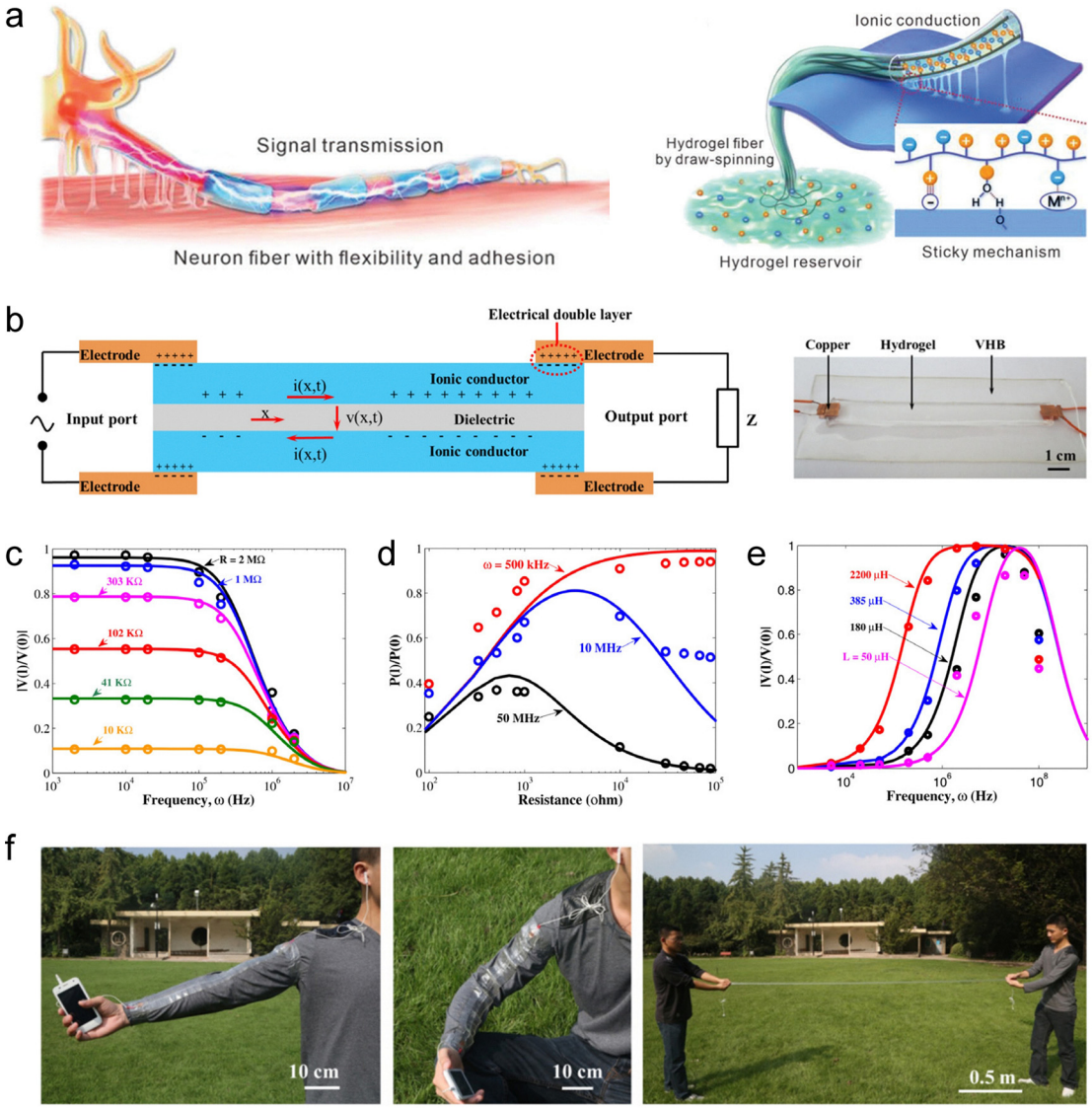

Fig. 10 SIC-based artificial axons. (a) Linear signal transmission system based on long-distance ion migration. Reproduced with permission from ref. 240. Copyright@2023, Wiley-VCH. (b) Sandwich-structured hydrogel-based ionic cable. (c) Theoretical results (solid curves) and experimental results (open circles) of $|V(l)/V(0)|$ vary with frequency for several fixed resistors, in which $V(l)$ and $V(0)$ represent the maximum amplitudes of the output and input AC voltage signals, respectively. (d) The ratio $P(l)/P(0)$ varies with resistance for several fixed frequencies, in which $P(l)$ and $P(0)$ represent the average power at the output and input ends, respectively. (e) The ratio $|V(l)/V(0)|$ varies with frequency for several fixed inductors. (f) Demonstration of the flexibility of the ionic cable. Reproduced with permission from ref. 169. Copyright@2015, Elsevier.

approach offers a promising pathway toward the realization of compact, ion-based artificial neurons.

All discussions regarding design principles above focus on how to achieve the analog of neural electrical signals. Besides this, practical application scenarios also need to be considered. For instance, NIDs intended for wearable electronics require flexible, stretchable electrodes and packaging materials. In contrast, implantable or semi-implantable NIDs necessitate the use of highly biocompatible ionic hydrogels. For integration into iontronic chips, NIDs should be constructed using SICs that are compatible with high-precision processing and scalable fabrication. In addition, NIDs based on ionic or polyionic elastomers offer enhanced durability and operational stability, as they are free of issues such as solvent leakage and evaporation.[239]

4. Research progress of SIC-based NIDs

Currently, the development of SIC-based NIDs is still in its early stages, primarily focusing on the fabrication and performance evaluation of individual devices, with system-level integration yet to be achieved. This section provides an overview of the research progress on SIC-based NIDs, including device classification and applications. It should be noted that

well-established studies on OECT-based NIDs are not repeated here, as their developments have already been comprehensively reviewed in the existing literature.[87–96]

4.1 Classification

4.1.1 Artificial axons. The conventional artificial ionic signalling transmission system typically relies on linear SICs, which transmit electrical signals through the long-distance migration of ion species (Fig. 10(a)).[240–242] However, compared to electronic conductors, such as gold, copper, silver, and aluminum, SICs have much higher resistance, leading to significant energy and signal intensity losses. Additionally, since the signal pattern of artificial neural systems typically consists of pulse trains, slower ion migration in SICs would lead to the loss of frequency information within the pulse trains, and limit signal transmission.

To address the above issues, Suo *et al.* pioneered a sandwich-structured hydrogel-based ionic cable.[169] This device uses ions as charge carriers to achieve high-speed, long-distance, and ultra-low-decay transmission of pulsed signals, and is therefore also referred to as an artificial axon. Fig. 10(b) shows the structure and working principle of this ionic cable. The device consists of two parallel wires of ionic hydrogels, insulated from each other by a sheet of dielectric. One end of the ionic cable serves as the input port, connecting to a pulse source *via* two copper electrodes, and the other end serves as the output port, connecting to an external load through two copper electrodes. When an electrical signal is applied, an EDL forms at the hydrogel/electrode interface, which in turn induces ion capacitance within the cable. Each small segment of the cable behaves like a capacitor, charging and discharging as current flows through the wires, enabling signals to transmit from one side to the other. The authors conducted theoretical modeling of this phenomenon. The theory shows that the potential difference $v(x, t)$ between the two sides of the dielectric layer in the ionic cable obeys the a diffusion equation, $\partial v/\partial t = D\partial^2 v/\partial x^2$, with the diffusion coefficient (reflecting the transmission speed of the signal) of the signal being $D \approx (bd)/(\rho\varepsilon)$, where b and d respectively are the thickness and resistivity of the ionic hydrogel, ρ and ε respectively are the thickness and permittivity of the dielectric. In a typical device, D can reach 10^7 m^2 s^{-1}, which is much higher than the diffusion coefficient of ions in water and hydrogels (10^{-10} to 10^{-8} m^2 s^{-1}).[137] Based on this mechanism, the ionic cable can transmit pulsed signals remotely and efficiently retain information such as frequency, amplitude and energy of the signals (Fig. 10(c)–(e)). Interestingly, the hydrogel's flexibility allows the ionic cable to exhibit excellent stretchability (Fig. 10(f)). Additionally, this device paradigm could be extended to other SICs, such as organogels and ionogels, which can effectively prevent problems such as short lifetimes and device instability caused by water evaporation and bacterial contamination. This study not only lays the foundation for the construction of circuits in brain-like intelligent systems using ions as charge carriers (for connecting artificial neurons and synapses), but also provides the means to create brain–computer interfaces.

4.1.2 Artificial synapses. In recent years, artificial synaptic devices based on SICs have witnessed rapid development, driven by strategies to precisely regulate ionic dynamics. These approaches primarily focus on four aspects: control of carrier concentration, regulation of ion migration path dimensions, design of systems with intrinsically low ionic mobility, and construction of heterogeneous interfaces. The following sections present representative studies exemplifying each of these approaches.

4.1.2.1 Based on controlling the concentration of carriers. Liu *et al.* designed a supramolecular hydrogel whose electrical conductivity can be modulated by near-infrared light, successfully realizing a photosynaptic device.[243] The polymer network of this hydrogel consists of polyacrylamide and supramolecular nanofibers self-assembled from azo-benzene functionalized imidazole (AZIM) salt, with its interior also filled with triiron tetraoxide (Fe_3O_4) nanoparticles which possess photothermal effects (light-to-heat conversion) (Fig. 11(a)). When the hydrogel is irradiated with near-infrared light, the converted heat drives the disassembly of the supramolecular nanofibers, generating a large number of mobile ion carriers and thereby increasing the hydrogel's conductance (Fig. 11(a)). This enhanced conductance gradually diminishes after the near-infrared light is removed due to the spontaneous reassembly of AZIM (Fig. 11(a)). Based on this mechanism, the hydrogel device can simulate synaptic PSP signalling patterns such as PPF and LTP under pulsed light stimulation (Fig. 11(b) and (c)). To further improve the mechanical durability of the hydrogel device, the team introduced a dynamic covalent polymer network, building on their previous work. This modification endowed the device with enhanced stretchability and self-healing capabilities.[244] Unfortunately, controlling the self-assembly behavior of ions through the photothermal effect is a unidirectional process, and thus cannot achieve reversible regulation of carrier concentrations. Therefore, the synaptic device cannot regulate SWs in either direction.

4.1.2.2 Based on controlling the size of effective ion migration paths. Chung *et al.* developed a hydrogel heterojunction with a size-tunable ionic conductive path, which successfully mimicked the short-term and long-term plasticity of synapses.[176] As shown in Fig. 11(d) and (e), the heterojunction is composed of p-type polyanionic and n-type polycationic hydrogels, with a precipitable pair of reservoir solutions on each gel side, *e.g.*, barium chloride ($BaCl_2$) aqueous solution on the p-type hydrogel side and sodium sulfate (Na_2SO_4) aqueous solution on the n-type hydrogel side. In this case, Ba^{2+} and SO_4^{2-} accumulate at the junction under a forward-bias voltage to form $BaSO_4$ precipitates, which act as physical barriers to narrow the ionic conductive path (Fig. 11(d)). Under a reverse-bias voltage, the precipitates dissolve to expand the conductive pathway (Fig. 11(d)). Thus, the conductivity of the device can be reversibly controlled by applying external electric fields in different directions. Building on this principle, the device simulated PSP signalling patterns

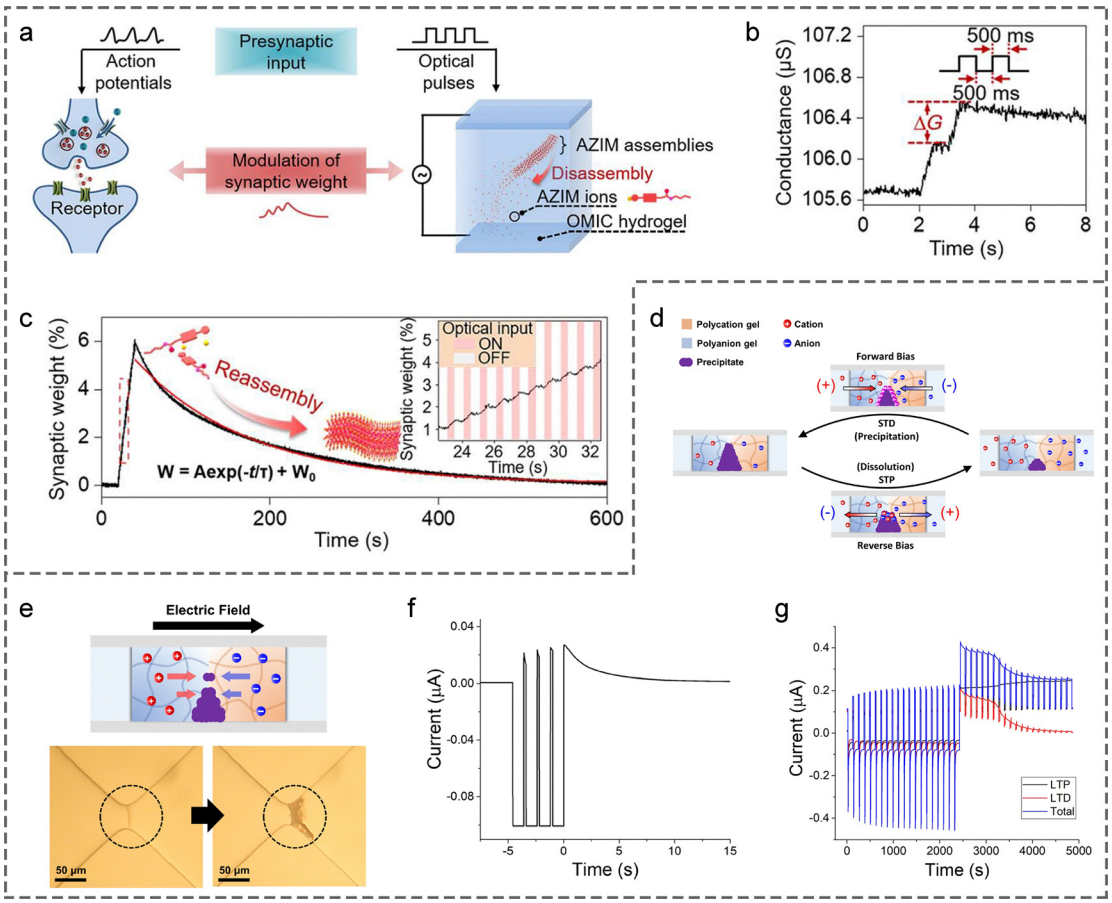

Fig. 11 (a) An optically modulated ion-conductive (OMIC) hydrogel for synaptic function emulation. (b) Conductance response of OMIC hydrogel to two successive optical pulses, demonstrating PPF. (c) Modulation of SWs in OMIC hydrogel under 20 optical pulses; inset shows magnified data in the red dashed box. Reproduced with permission from ref. 243. Copyright@2023, American Association for the Advancement of Science. (d) Schematic of ionic conductive path regulation in a hydrogel precipitation heterojunction. (e) Mechanism of precipitate formation with corresponding optical images. (f) Ionic currents measured under train of four reverse-bias pulses, mimicking short-term plasticity. (g) Mimicking LTP and LTD effects. Reproduced with permission from ref. 176. Copyright@2022, National Academy of Sciences.

corresponding to different synaptic plasticity characteristics under pulsed voltage stimulation, including short-term plasticity, LTP, and LTD (Fig. 11(f) and (g)). Excitingly, this artificial synapse has been demonstrated to be adaptable to aqueous environments, laying a solid foundation for the construction of implantable brain-like intelligent devices and human–computer interfaces.

4.1.2.3 Based on the low migration rate of ions. Leveraging the principle of slow ion migration, several studies have explored SIC-based devices that can emulate synaptic behaviors. Lee *et al.* first reported an ionic organogel heterojunction capable of mimicking EPSPs.[245] This device comprises two organogel layers with distinct polymer networks and ion species (Fig. 12(a)). Due to differences in ion diffusivity and solubility across the layers, an ionic EDL forms at the heterogeneous interface under equilibrium, resulting in pronounced ionic rectification (Fig. 12(b)). Upon application of a pulsed voltage, the device generates a current spike followed by slow relaxation, resembling the typical PSP memory profile (Fig. 12(c)). This relaxation process is attributed to the slow ion reflux. However, the specific role of the heterogeneous interface in this relaxation behavior remains unclear. Wu *et al.* conducted a similar study and developed a stretchable sandwich-structured device composed of a low-salt-concentration neutral hydrogel, a polyanionic hydrogel, and a high-salt-concentration neutral hydrogel (Fig. 12(d)).[246] This work reported the first hydrogel-based synaptic device, representing a major breakthrough in the field of smart hydrogels. Beyond exhibiting pronounced ionic rectification, the device can also emulate synaptic plasticity, such as PPD, when subjected to pulsed voltage stimulation (Fig. 12(e)). Although their introduction of heterogeneous interfaces endowed the hydrogel device with rectification properties, these interfaces did not play a decisive role in the relaxation behavior of the current. Instead, it was still primarily due to the inherently slow rate of ion reflux. Zhang *et al.* provided additional evidence for this conclusion.[247] They designed a synaptic device based on ionic elastomers without incorporating any heterogeneous interfaces. The device adopts a sandwich structure in which an ion-containing poly(ureaurethane) (PUU) layer

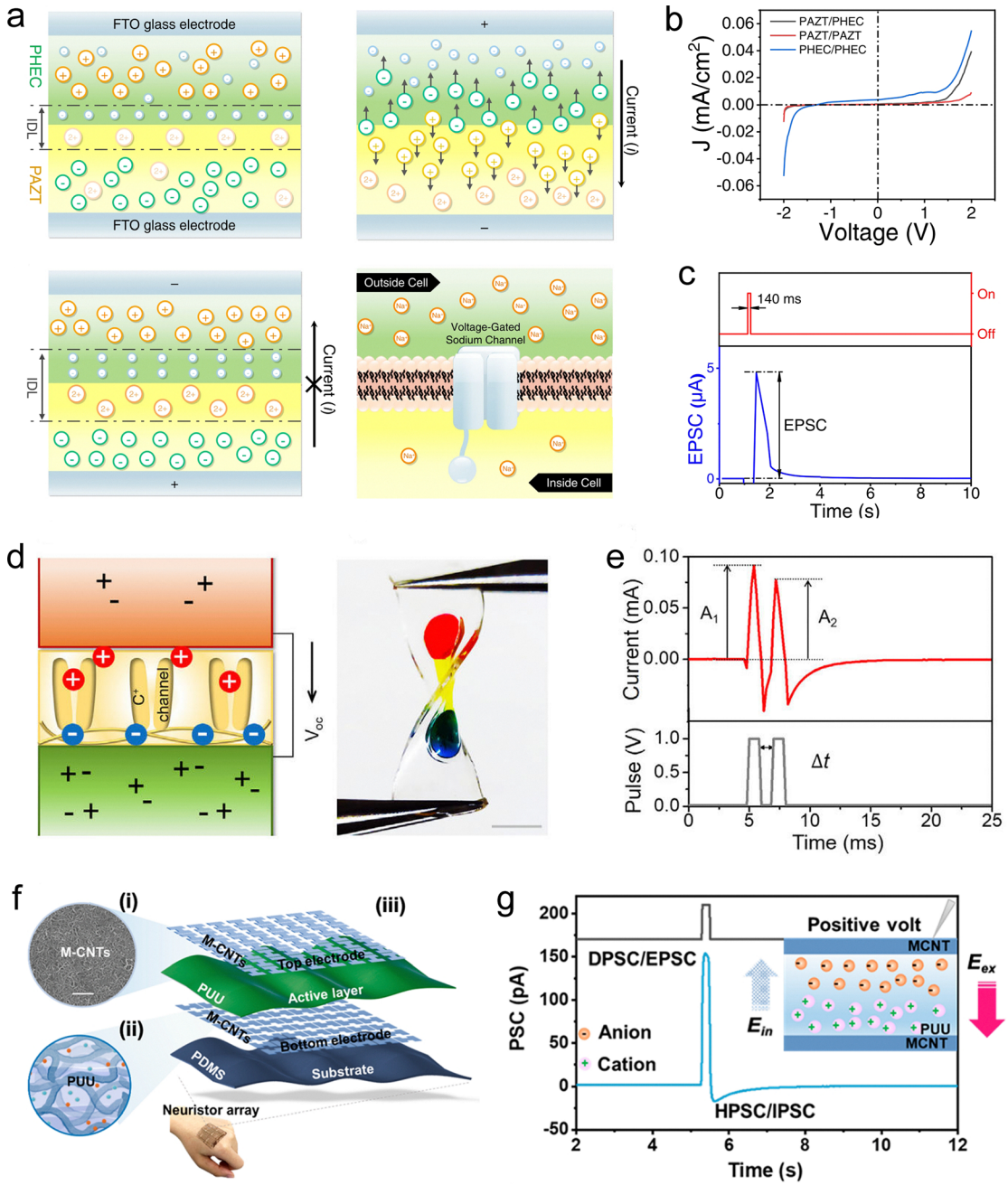

Fig. 12 (a) Schematic illustration and rectification mechanism of the bilayer ionic organogel diode. (b) *I*–*V* curves of the device, demonstrating rectifying behavior. (c) EPSP triggered by electrical stimulation. Reproduced with permission from ref. 245. Copyright@2022, Springer Nature. (d) Schematic design and optical image of the first hydrogel-based synaptic device, composed of a low-salt-concentration neutral hydrogel, a polyanionic hydrogel, and a high-salt-concentration neutral hydrogel. (e) PPF response induced by two successive voltage pulses. Reproduced with permission from ref. 246. Copyright@2023, Elsevier. (f) Structural design of the sandwich-type ionic elastomer-based synaptic device. (g) Simulated PSPs and corresponding mechanism. Reproduced with permission from ref. 247. Copyright@2023, American Chemical Society.

is placed between two metallic carbon nanotube (CNT) film electrodes on PDMS substrates (Fig. 12(f)). When a positive pulsed voltage is applied, cations and anions migrate within the PUU layer toward opposite directions, generating a positive current. After stimulus removal, the ions gradually reflux, producing a negative current accompanied by a relaxation response (Fig. 12(g)). The slow ion reflux suppresses subsequent current spikes, enabling the emulation of PPD and LTD. Moreover, the SWs (current level) of the device can be reversibly adjusted by applying pulsed voltages of opposite polarities. Building on this principle, Chen *et al.* designed the devices with a fiber-based architecture, enabling seamless integration with textiles and establishing a paradigm for smart wearable electronics.[248]

To impart light-responsiveness, Huang *et al.* developed a bilayer ionic elastomer synaptic device with asymmetrical incorporation of photothermal nanoparticles.[249] The device consists of two elastomer layers, each containing lithium bis(trifluoromethanesulfonyl)imide (LiTFSI), with one layer additionally doped with polypyrrole nanoparticles (PPy-NPs) that exhibit strong photothermal effects (Fig. 13(a)). Upon exposure to light, the PPy-NPs convert optical energy into heat, generating a temperature gradient across the bilayer structure. This gradient drives the directional migration of $TFSI^-$ and Li^+ ions from the PPy-NP-doped layer to the undoped layer. Owing to the differences in ion size, Soret coefficient, and effective diffusivity, the cation and anion migration rates diverge, resulting in a net ionic current. When the light stimulus is removed, the temperature gradient decays gradually due to slow heat dissipation, leading to a progressive relaxation of the current, a behavior analogous to synaptic memory (Fig. 13(b)). This light-gated ion transport mechanism enables the device to emulate synaptic plasticity features such as PPF and LTP under pulsed light stimulation (Fig. 13(c) and (d)). In a similar study, Liu *et al.* fabricated such devices into an interlaced textile fiber architecture, thereby reducing integration difficulty and enhancing overall flexibility and conformability.[250] Recently, we also developed a bilayer hydrogel synaptic device asymmetrically doped with photothermal nanoparticles (Fig. 13(e)), capable of responding to both light and pressure.[251] In this system, ion migration is driven by the thermodiffusion effect under light and by the piezoionic effect under mechanical pressure. The distinct migration rate of cations and anions modulate the open-circuit voltage (ionic potential). Upon cessation of external stimuli, the slow ion backflow induces a gradual decay of the ionic potential, thereby mimicking the PSP memory (Fig. 13(f)).

4.1.2.4 Based on introducing heterogeneous interfaces. Heterogeneous interfaces can effectively regulate ion transport behavior, exhibiting pronounced ion selectivity and enabling the confinement of specific ions within designated regions. For

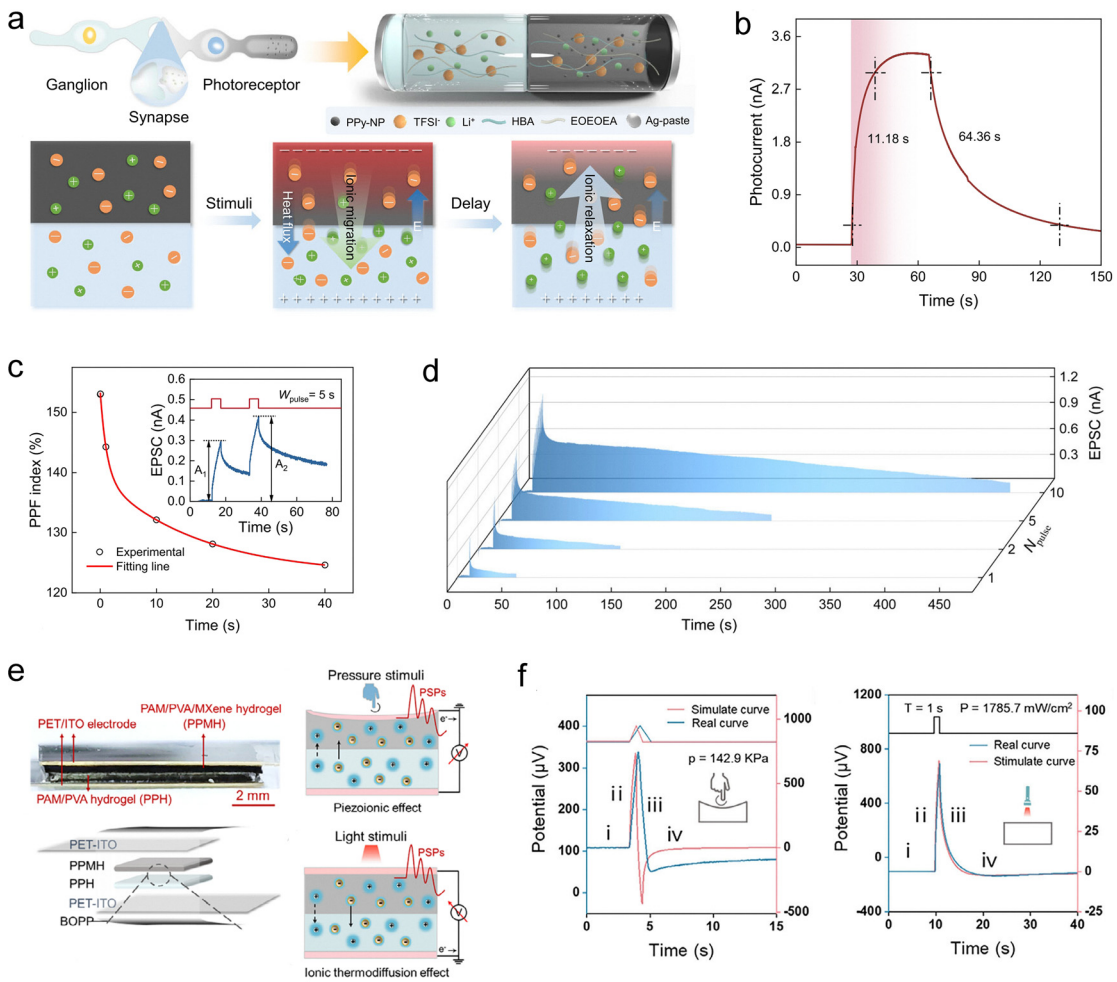

Fig. 13 (a) Schematic of a light-responsive ionic synaptic device with asymmetric doping of photothermal nanoparticles, along with the mechanism of ionic current relaxation. Light-pulse-induced EPSP (b), PPF (c), and LTP effects (d). Reproduced with permission from ref. 249. Copyright@2024, Springer Nature. (e) Schematic of a dual-responsive bilayer hydrogel synaptic device activated by both pressure and light stimuli, and the corresponding mechanism of ionic potential relaxation. (f) Stimulus-triggered ionic responses under pressure and light, mimicking PSP-like memory behavior. Reproduced with permission from ref. 251. Copyright@2025, Wiley-VCH.

example, Yossifon *et al.* developed an analog hydrogel synaptic memristor based on heterogeneous charge interfaces.[252] They constructed a multilayer structure of polyanionic hydrogel (P-gel)/neutral hydrogel (M-gel)/polycationic hydrogel (N-gel) within a microfluidic channel (Fig. 14(a)). Due to electrostatic repulsion at the interfaces, the P-gel end selectively permits cations to enter the M-gel, while the N-gel end selectively permits anions. Under a forward voltage, ion carriers

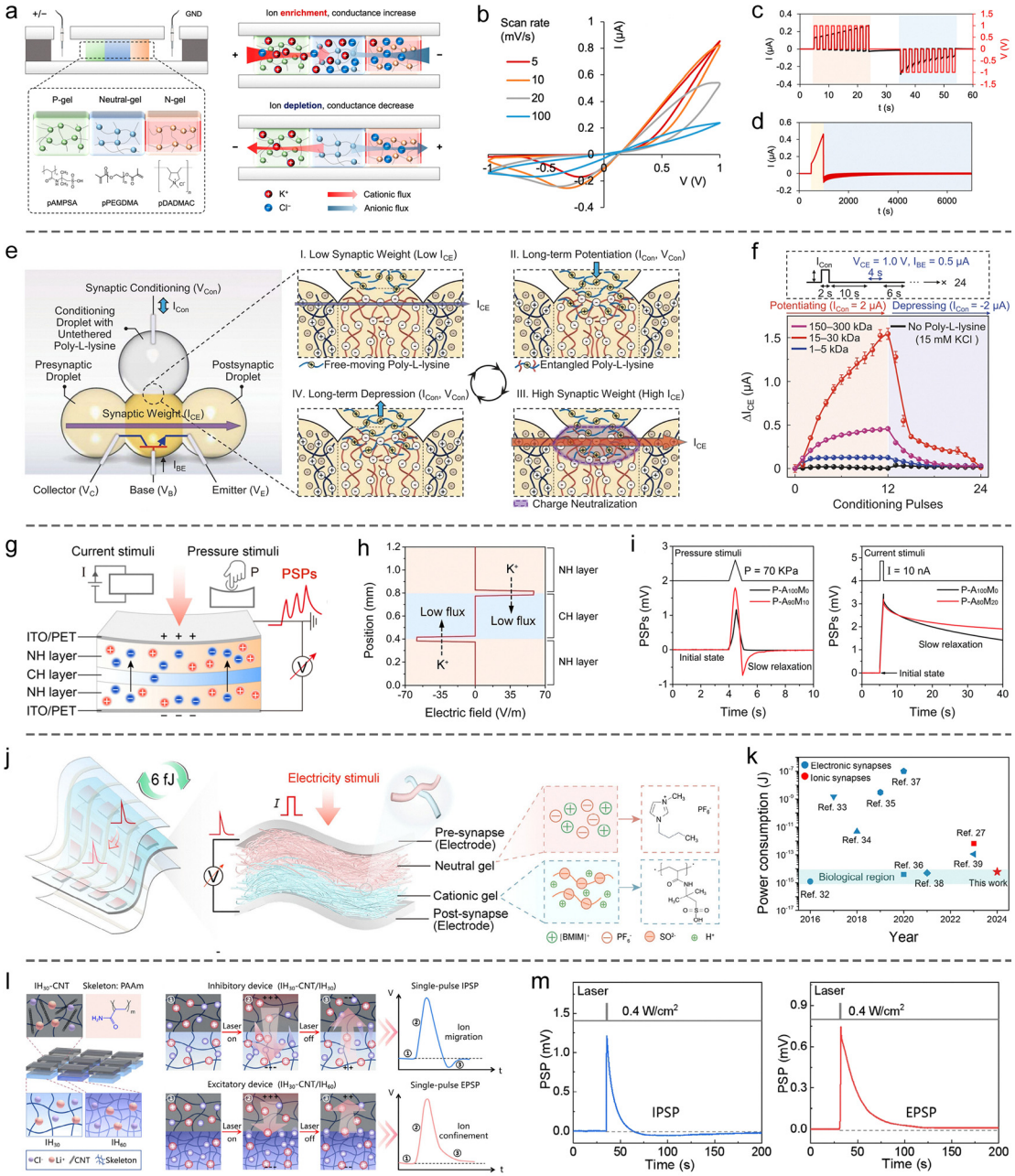

Fig. 14 SIC-based synaptic devices constructed by heterogeneous interface engineering. (a) Schematic illustration and memristive mechanism of a P-gel/N-gel/P-gel synaptic device. (b) Pinched hysteresis *I*–*V* curves demonstrating memristive behavior. (c) Emulation of synaptic plasticity, including PPF/PPD and LTP/LTD effects. (d) Memory retention test. Reproduced with permission from ref. 252. Copyright@2024, American Chemical Society. (e) Schematic representation of the structure and operating principle of a hydrogel synaptic transistor (npn type). (f) Bidirectional modulation of SWs in the device. Reproduced with permission from ref. 77. Copyright@2024, American Association for the Advancement of Science. (g) Schematic of a hydrogel-based synaptic device responsive to both pressure and electrical stimuli. (h) Electric field at the heterogeneous interface impedes cross-layer cation migration. (i) Voltage response signals triggered by pressure (left) and electrical stimuli (right), exhibiting PSP-like memory behaviors. Reproduced with permission from ref. 178. Copyright@2024, American Chemical Society. (j) Schematic of a nanofibrous ionogel synaptic device fabricated *via* electrospinning. (k) Demonstration of the device's low energy consumption advantage. Reproduced with permission from ref. 234. Copyright@2025, Wiley-VCH. (l) Schematic and working principle of a hydrogel synaptic device based on heterogeneous density interfaces. (m) Simulated IPSP (left) and EPSP (right) responses. Reproduced with permission from ref. 254. Copyright@2025, Wiley-VCH.

accumulate in the M-gel, increasing the device's conductivity. Conversely, under a reverse voltage, carrier depletion occurs, reducing the conductivity. Consequently, the conductivity of the device depends on the history of the applied voltages, as demonstrated by the typical pinched hysteresis loop observed in its *I–V* curves (Fig. 14(b)). Based on this mechanism, the conductivity (SWs) can be reversibly modulated by pulsed voltages of opposite polarities, achieving the simulation of PSP signalling patterns such as PPF/PPD and LTP/LTD (Fig. 14(c)). Furthermore, the incorporation of multiple heterogeneous interfaces effectively inhibits carrier backflow, allowing the device to achieve a maximum memory retention time of up to 4000 seconds (Fig. 14(d)).

Zhang *et al.* engineered a hydrogel synaptic transistor by incorporating dynamically tunable heterogeneous charge interfaces.[77] The device architecture comprised an npn-type ionic transistor, constructed using a p-type polyanionic hydrogel droplet positioned between two n-type polycationic hydrogel droplets (Fig. 14(e)). Above the n-type droplets, a regulatory hydrogel droplet containing freely dispersed, positively charged poly-L-lysine molecules was introduced. In the initial state, the heterogeneous charge interfaces within the npn heterojunction acted as barriers to anion transport, maintaining the device in a low-conductance state. Upon applying a forward regulatory current, poly-L-lysine molecules migrated from the regulatory droplet into the n-type hydrogel, weakening the charge interfaces, increasing anion flux, and thereby enhancing device conductance (Fig. 14(e)). Conversely, a reverse regulatory current extracted poly-L-lysine from the n-type hydrogel, reinforcing the charge interfaces, reducing anion flux, and decreasing conductance (Fig. 14(e)). This configuration enabled precise bidirectional modulation of SWs, demonstrating significant potential for in-memory computing applications (Fig. 14(f)). Notably, the proposed dropletronic platform offers a versatile paradigm for the micro/nano-fabrication and high-density integration of SIC-based devices.

In recent years, our research group has made notable contributions in this field. For instance, we developed a sandwich-structured device composed of neutral hydrogel, polycationic hydrogel, and neutral hydrogel to emulate synaptic functions (Fig. 14(g)).[178] The interfacial electric fields between the neutral polymer network and the polycationic polymer network within the device exhibit a pronounced ability to suppress cation migration across the layers (Fig. 14(h)). Consequently, following the migration of both cations and anions induced by pressure or electrical stimuli, the reflux of cations occurs at a slower rate, resulting in a relaxation behavior of the ionic potential (open-circuit voltage) at the device terminals (Fig. 14(i)), which effectively mimics the short-term memory characteristics of synapses. Based on this principle, repeated external stimuli can precisely modulate the ionic potential (SWs) of the device. Theoretical modeling revealed that the voltage response of the device to current stimulation is inversely proportional to its effective area.[178] Guided by this insight, we fabricated a bilayer synaptic device comprising a neutral ionogel and a polyanionic ionogel with a nanofibrous architecture *via* electrospinning (Fig. 14(j)).[234] The reduced effective area imparted by the fibrous structure enabled an ultralow single-event energy consumption of 6 fJ, comparable to that of biological synapses (Fig. 14(k)). Recently, Wu's team reported a similar study, in which synapse-like memory behavior was achieved by constructing a heterogeneous interface between neutral and positively charged ionogel networks.[253] The ionogel devices in this work exhibited excellent adhesion and self-healing capabilities, attributed to cation–π interactions. In addition, we engineered a heterogeneous density interface to realize hydrogel-based synaptic devices (Fig. 14(l)).[254] Our results show that the heterogeneous density interface selectively obstructs the migration of ions with larger hydrated radii across the interface and localize them within the high-density gel region. By tuning the density contrast between the upper and lower layers, we successfully constructed both excitatory and inhibitory synaptic devices, offering tunable synaptic behaviors (Fig. 14(m)).

4.1.3 Artificial neurons. To date, no complete artificial neuron device or circuit based on SICs has been realized. Such devices would enable the generation of action potentials and frequency-controllable signalling, comparable to mature electronic devices. While ionic artificial synapses have been extensively studied, the realization of ionic artificial neurons remains largely theoretical.[255] Nevertheless, considering the mechanisms of action potential generation and information transmission through controllable ion migration, SIC materials provide a unique physical and chemical basis for constructing artificial neurons.

In principle, SIC-based ionic memristors exhibiting threshold-switching behavior can be integrated with classical neuron models, such as the H–H or LIF models, to enable neuron-level signal integration, pulse generation, and frequency encoding. Although such devices have yet to be realized, the design strategies discussed in Section 3.3.5 of this review indicate that this challenge is achievable. Experimentally, despite the absence of standardized SIC neuron circuit platforms, existing studies demonstrate the potential of SIC devices to emulate neuronal dynamics. For instance, Madden *et al.* developed a piezoionic hydrogel device (Fig. 15(a)) in which ion species in a polyacrylamide hydrogel generate action potential-like ionic currents and voltages under mechanical force (Fig. 15(b)).[137] This behavior arises from hydrostatic pressure-driven asynchronous migration of cations and anions, known as the piezoionic effect.[165] Remarkably, the resulting ionic pulses can interface with mouse sciatic nerves to induce leg muscle contraction (Fig. 15(c)). Similarly, Xiao *et al.* reported a hydrogel-based artificial nerve fiber incorporating directionally aligned electronegative helical microfibers (Fig. 15(d)).[256] The combined piezoionic and nanoconfinement effects (Fig. 15(e)) substantially enhance action potential-like ionic pulses (Fig. 15(f)), which are also capable of interacting with animal nerves. Together, these studies underscore the promise of SICs for emulating neuronal function and for bio-interactive applications.

Additionally, Bayley *et al.* employed dropletronics to construct a biomimetic artificial nerve, achieving a complete

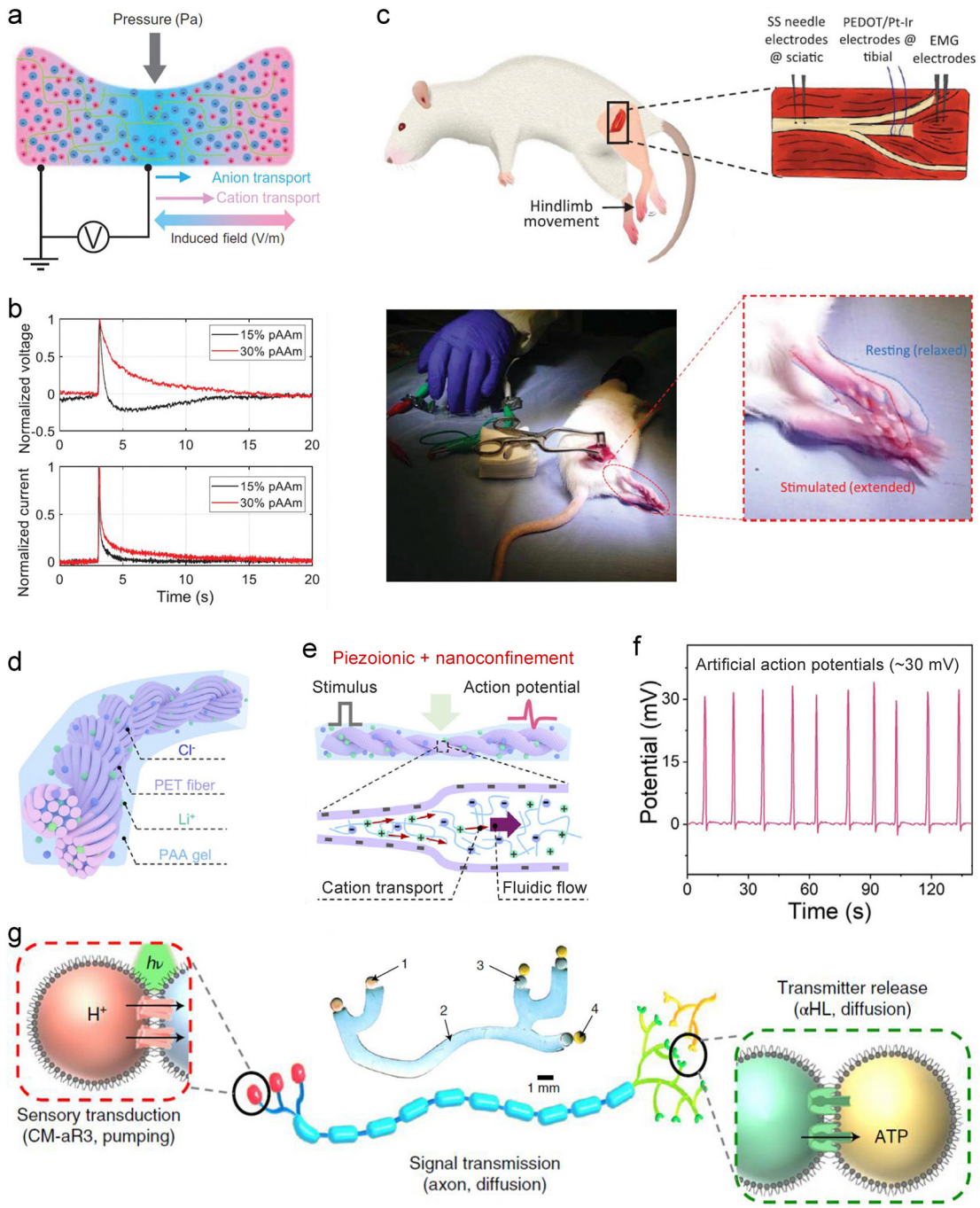

Fig. 15 SIC-based neuron devices. (a) A piezoionic hydrogel and its working mechanism, illustrating the piezoionic effect. (b) Ionic voltage and current responses under a pressure pulse, reproducing features of neuronal action potentials. (c) Interface with the mouse sciatic nerve, demonstrating induced leg muscle contraction. Reproduced with permission from ref. 137. Copyright@2022, American Association for the Advancement of Science. (d) A piezoionic hydrogel integrated with helical microfibers, functioning as an artificial nerve. (e) Schematic of synergistic amplification of piezoionic signals *via* piezoionic and nanoconfinement effects. (f) Generated piezoionic potential pulses reaching up to ~30 mV. Reproduced with permission from ref. 256. Copyright@2024, Elsevier. (g) Schematic and optical image (inset, top center) of a synthetic nerve assembled from microemulsion droplets and hydrogel fibers. Reproduced with permission from ref. 242. Copyright@2022, Springer Nature.

functional chain from physicochemical signal transduction to information propagation and neurotransmitter release (Fig. 15(g)).[242] The system consists of three modules: (1) a signal transduction module, comprising sensing droplets, hydrogel axons, and a light-responsive proton pump (Archaerhodopsin-3, aR3), which converts light into ionic currents along the axon; (2) a signal transmission module, formed by hydrogel fibers that convey ionic signals to the terminal, analogous to an axon; and (3) a neurotransmitter release module, composed of two synaptic droplets connected *via*

α-hemolysin (α-HL) pores, which release ATP in response to axonal signals. Furthermore, multi-channel spatiotemporal transmission and processing are achieved through nerve-bundle-like arrangements, providing a novel strategy for next-generation implants, soft machines and computing devices.

Overall, although SIC-based artificial neurons remain at the proof-of-concept stage, their unique advantages in material properties, biocompatibility, and interface design provide a solid foundation for constructing low-power, interactive, and adaptive brain-like systems. With continued advancements in SIC memristors, transistors, and dropletronics, SIC-based artificial neurons are expected to evolve from single-neuron behavior emulation to network-level cascades and neural circuit construction, thereby promoting human–machine integration, neural repair, and the development of soft intelligent devices.

4.2 Applications

4.2.1 Signal transmission. The hydrogel artificial axon developed by Suo *et al.* is an ideal tool for transmitting pulsed signals (Fig. 10(b)), and can be used in brain-like intelligent systems to connect pulse sources (such as signal generators, artificial neurons, sensors) to artificial synapses. For example, Suo *et al.* successfully used this axonal device to transmit music signals (electric pulse trains), effectively connecting a mobile phone and a loudspeaker (Fig. 16(a)).[169] Li *et al.* also verified that this type of axonal device can be used to transmit pulsed signals, and found that it works even at 300% stretch with essentially the same input and output signals.[258] Chen *et al.* constructed a neuromorphic tactile processing system by using such axonal devices to connect pressure sensors and synaptic transistors (Fig. 16(b)).[257] In this system, the pressure sensor, artificial axon and synaptic transistor mimic the receptor, axon and synapse of a biological sensory neuron, respectively. The pressure sensor converts pressure stimuli into electrical pulses, which are transmitted to the gate of the synaptic transistor *via* the hydrogel axonal device and further modulate the conductance (reflecting SW level) of the synaptic transistor. This study provides an important reference for employing such an artificial axon in constructing brain-like intelligent systems that utilize ions as charge carriers.

4.2.2 Information storage. One important function of the hippocampus in the brain is memory, which relies on the short-term potentiation and LTP of relevant synapses' SWs/PSPs.[28] The SW/PSP level reflects the strength of the memory. Short-term potentiation represents short-term memory, while LTP represents long-term memory. Similarly, artificial synapses can simulate this process, making them useful for information storage. For instance, a storage array (5 × 5) composed of 25 hydrogel synaptic devices has achieved image storage.[246] The SWs of each synaptic device in the array can be independently regulated. Thus, an image can be written by applying multiple pulsed stimuli to the devices corresponding to the image pixel points (to increase the SWs of the devices) (Fig. 17(a)). Depending on the memory behavior of the devices, the written image

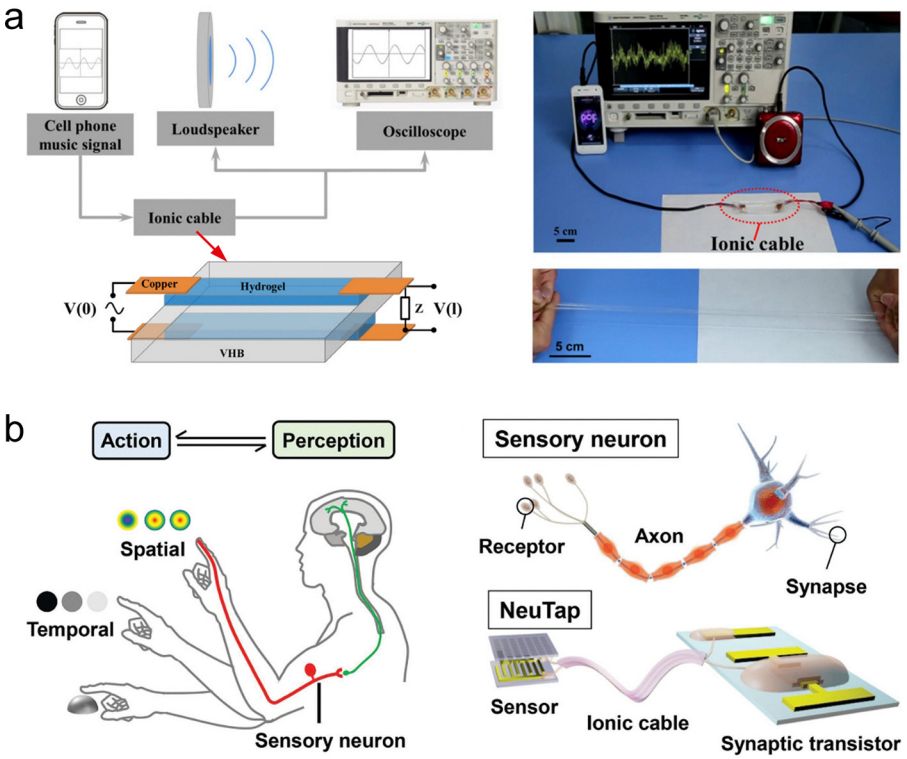

Fig. 16 Applications of the artificial axon developed by Suo *et al.* (a) Transmission of musical signals. Reproduced with permission from ref. 169. Copyright@2015, Elsevier. (b) Connection between a pressure sensor and a synaptic transistor. Reproduced with permission from ref. 257. Copyright@2018, Wiley-VCH.

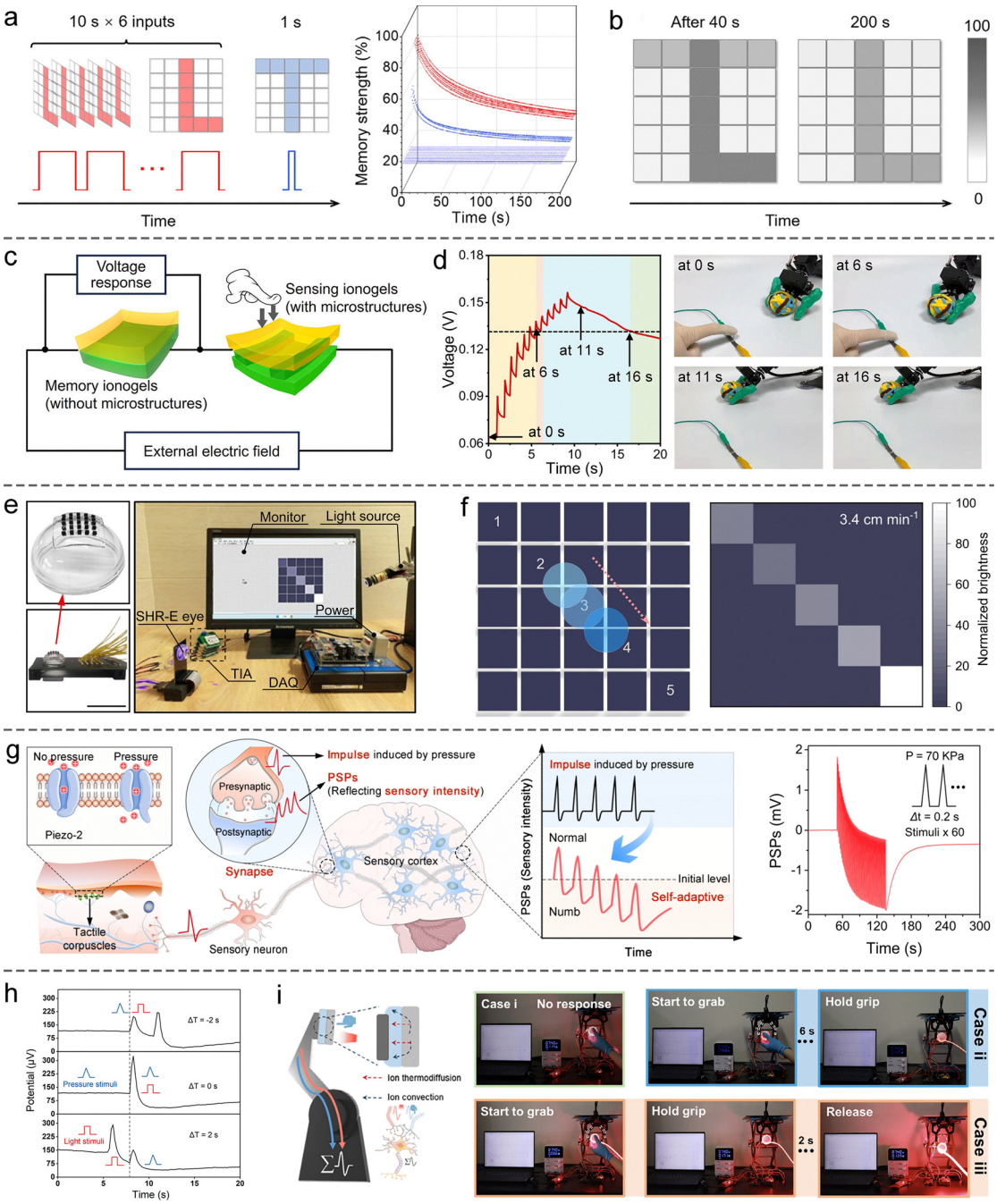

Fig. 17 SIC-based NIDs for information storage and machine perception. (a) Image-writing method on a hydrogel synaptic array and the corresponding real-time memory strength of each device. (b) Storage performance. Reproduced with permission from ref. 246. Copyright@2023, Elsevier. (c) Schematic of a fully ionogel-based ionic pressure-perception system, integrating both a pressure sensor and a synaptic device. (d) The left panel shows the voltage (*i.e.*, SWs) across the synaptic device in response to consecutive pressure pulses, while the right panel displays photographs of the robotic hand at selected time points. The hand grasps the ball when the SWs exceed a preset threshold and releases it when the SWs fall below the threshold. Reproduced with permission from ref. 253. Copyright@2025, Springer Nature. (e) An artificial retina based on ionic elastomer synaptic devices and its testing protocol. (f) Imaging performance. Reproduced with permission from ref. 249. Copyright@2024, Springer Nature. (g) A pressure-responsive hydrogel synaptic device for simulating self-adaptive tactile perception, illustrating the biological mechanism of skin adaptation (left) and the LTD effect emulated by this device (right). Reproduced with permission from ref. 178. Copyright@2024, American Chemical Society. (h) A hydrogel synaptic device capable of integrating pressure and light stimuli. (i) A robotic hand equipped with this device for intelligent grasping and hazard avoidance. Reproduced with permission from ref. 251. Copyright@2025, Wiley-VCH.

can be stored in the array for a long time (Fig. 17(b)). In recent years, many related applied studies have been reported, clearly highlighting the potential of SIC-based synaptic devices for information storage.[178,239,253,254]

4.2.3 Machine perception. The human perceptual system generally consists of receptors, afferent neurons (sensory neurons), and the sensory cortex.[259] External stimuli are initially transduced into ionic electrical signals by receptors, which are subsequently converted into nerve impulses by afferent neurons and relayed to the sensory cortex. There, SW/PSP at synapses is dynamically modulated by incoming impulses, enabling sensory perception. The magnitude of SW/PSP correlates with the intensity of the perceived stimuli. To replicate this perceptual process in intelligent robots, researchers typically integrate sensors, ring oscillators (optional, for converting DC signals into pulse signals to emulate afferent neurons), and artificial synapses to form an artificial sensory system.[260–263] In these designs, artificial synapses generally respond to electrical stimuli. Building on this concept, Wu *et al.* developed the first fully gel-based integrated ionic pressure-perception system.[253] The system combines an ionogel pressure sensor with an ionogel synaptic device, allowing temporal integration of pressure stimuli and mimicking the sensory mechanism of human skin (Fig. 17(c)). Importantly, it could allow intelligent control and adaptive modulation of robotic grasping, providing critical guidance for the development of smart soft robotics (Fig. 17(d)).

However, synaptic devices capable of directly responding to external physical stimuli, such as pressure, light, sound, or heat, would facilitate the development of highly integrated SIC-based intelligent sensory systems.[264] In recent years, numerous such SIC-based synaptic devices have been reported. For example, a 5 × 5 array of light-responsive ionic elastomer synaptic devices has been engineered to construct an artificial retina, imparting basic visual functionality to robotic platforms (Fig. 17(e)).[249] As a light spot traverses the array, the SW of the illuminated devices increases. However, due to relaxation dynamics, devices stimulated earlier exhibit lower SW than those stimulated later (Fig. 17(f)). This dynamic modulation enables not only image formation but also the real-time capture of the light spot's motion trajectory. Similarly, a 6 × 6 array of light-responsive hydrogel synaptic devices, integrated with a deep learning algorithm, has been demonstrated to directly impart mechanical systems with visual cognitive capabilities, allowing autonomous recognition of motion direction.[254]

Beyond visual perception, pressure-responsive SIC-based synaptic devices show great promise in emulating tactile perception. A representative example is a flexible ionic hydrogel synaptic device that exhibits PPD and LTD effects under applied pressure, thereby mimicking the self-adaptive tactile responses observed in human skin (Fig. 17(g)).[178] Moreover, the intrinsic multi-stimuli responsiveness of SIC materials offers a compelling strategy for constructing structurally simple, multimodal sensory fusion systems. For instance, a hydrogel synaptic device that simultaneously responds to both pressure and light stimuli can effectively integrate inputs across different sensory modalities (Fig. 17(h)).[251] When mounted on the fingertip of a robotic hand, such a device enables visual-tactile synergistic control, equipping the robotic platform with human-like capabilities for intelligent grasping and emergency avoidance (Fig. 17(i)).

4.2.4 Brain-like computing. Artificial synapses and neurons constitute the fundamental functional units of brain-inspired neuromorphic computing hardware. Artificial synapses can be categorized into volatile and non-volatile types, each serving distinct yet complementary roles. Volatile synaptic devices are typically employed for dynamic preprocessing of input signals, enabling functionalities such as temporal filtering,[265] noise suppression,[266] contrast enhancement,[267] transient memory,[268] and time-domain encoding.[269] These dynamic responses are critical for enhancing signal fidelity and selectivity in early sensory processing stages. Non-volatile synapses, on the other hand, are designed to emulate the learning and memory functions of biological synapses by providing multilevel, programmable conductance states with excellent retention stability.[270] Their ability to perform parallel processing and in-memory computation makes them ideal for constructing ANN and SNN hardware. In parallel, artificial neuron devices are engineered to replicate the integrate-and-fire behavior of biological neurons. These devices integrate input signals and generate output spikes once a threshold is reached, thereby encoding information into discrete temporal patterns.[26] The interplay between artificial synapses and neurons enables the implementation of fully hardware-based neuromorphic systems capable of low-power, parallel, and adaptive information processing.

SIC-based artificial synapses reported thus far are inherently volatile, with limited capability to maintain stable SWs over extended periods. Consequently, their primary utility lies in dynamic preprocessing of input signals. In one representative study, a hydrogel-based synaptic device was employed to temporally encode compressed images, thereby increasing the dimensionality and richness of the information content (Fig. 18(a)).[178] Remarkably, even when handwritten digit images were compressed to only ten dimensions, a fully connected neural network achieved a classification accuracy of up to 95%, substantially lowering computational complexity without compromising recognition performance (Fig. 18(b)). Additionally, a convolutional kernel comprising excitatory and inhibitory hydrogel synaptic devices was constructed to mimic the Mach band effect observed in biological visual systems (Fig. 18(c)), enabling edge enhancement and sharpening of image features (Fig. 18(d)).[254] This bioinspired preprocessing approach significantly improved edge definition and structural clarity in images (Fig. 18(d)), leading to enhanced classification accuracy in downstream tasks (Fig. 18(e)). Of particular note is a recent approach that exploits the electrolyte-sharing nature of ionic devices to emulate the ephaptic coupling effect observed in neural tissue, thereby achieving high-performance n-back working memory tasks.[234] In this system, multiple pairs of electrodes were patterned onto a single ionogel film, with each pair functioning as an individual synaptic node (Fig. 18(f)). Upon activation of a given synaptic node, local ionic activity generated electric fields that propagated through the shared electrolyte, modulating the SWs of adjacent nodes and thus enabling inter-synaptic coupling analogous to that in biological networks (Fig. 18(g)). This coupling mechanism greatly

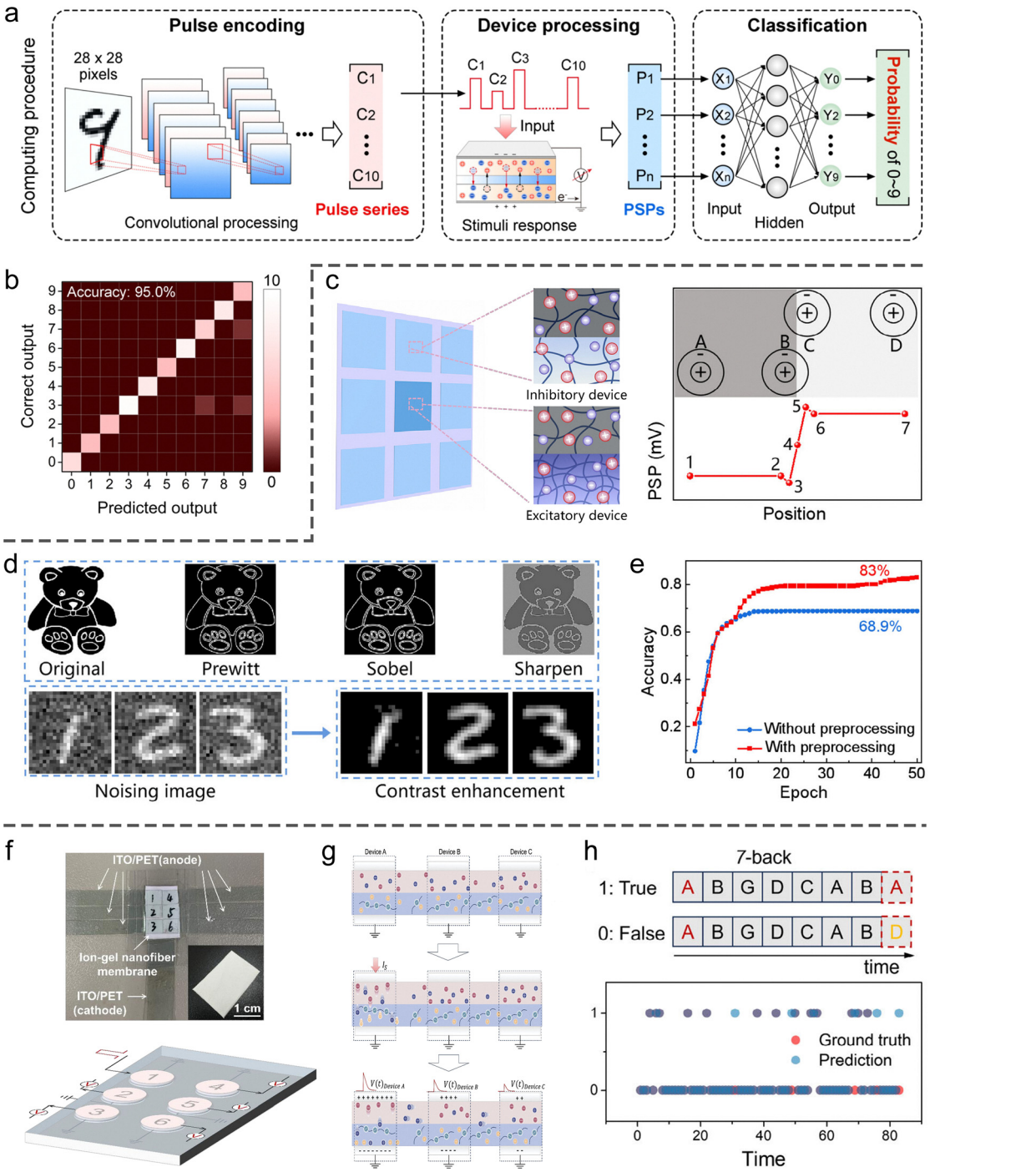

Fig. 18 SIC-based NIDs for brain-like computing. (a) Schematic of a hydrogel synaptic device used for processing compressed handwritten digit images. (b) Resulting classification accuracy. Reproduced with permission from ref. 178. Copyright@2024, American Chemical Society. (c) A bioinspired convolutional kernel composed of excitatory and inhibitory hydrogel synaptic devices (left), enabling simulation of the Mach band effect (right). (d) Image enhancement achieved using the convolutional kernel. (e) Improved recognition accuracy for preprocessed images. Reproduced with permission from ref. 254. Copyright@2025, Wiley-VCH. (f) An ionogel-based synaptic array for emulating the ephaptic coupling effect, with physical layout (top) and conceptual diagram (bottom). (g) Mechanism underlying inter-synaptic coupling *via* shared electrolyte fields. (h) Demonstrated performance in a 7-back working memory task. Reproduced with permission from ref. 234. Copyright@2025, Wiley-VCH.

enhanced temporal information integration, resulting in a marked improvement in n-back task performance (Fig. 18(h)).

Reservoir computing architectures typically consist of three layers. (1) An input layer encodes and distributes incoming data to the reservoir layer, which comprises a network of nonlinear, recurrently connected nodes. (2) A reservoir transforms the input into a high-dimensional state space that captures temporal features. (3) An output layer can be trained using linear or

logistic regression to map the reservoir states to the desired output.[271–273] Owing to their inherent memory properties, dropletronic memristors and memcapacitors are well-suited for handling complex temporal signals in the reservoir layer at significantly lower energy costs than traditional computing paradigms.[274] For instance, Maraj *et al.* used a voltage-dependent ion channel, monazomycin, embedded in the DIB to create a memristor with improved sensory adaptation, thereby amplifying small differences in temporal input signals.[275] The sensory adaptation resulted from the translocation of membrane-active monazomycin species to the opposite side of the membrane (the other droplet) under continuous voltage stimuli. In the modeling of a 5 × 5 digit classification task, they employed 5 independent dropletronic memristors in the reservoir layer. Each memristor received information from a distinct pixel row (Fig. 19(a)). By setting the translocation rate

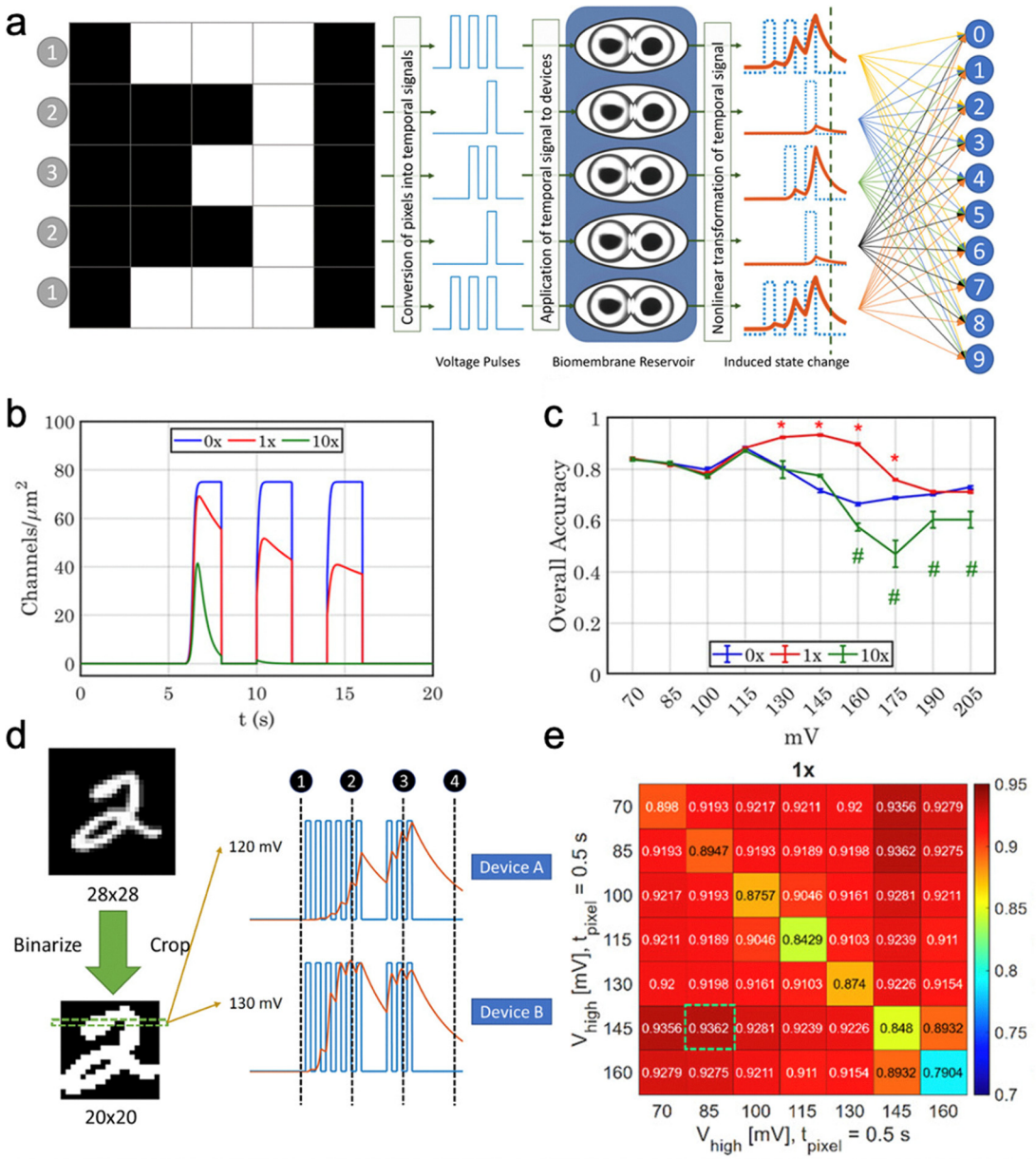

Fig. 19 Dropletronic devices used as the reservoir layer for neuromorphic computing. (a) By comparison with the conventional reservoir computing system, which consists of an input layer, a reservoir, and an output layer, droplet-based memristors can execute the reservoir function due to their memory effect. In a 5 × 5 digits classification task, 5 independent dropletronic memristors were included in the reservoir layer. (b) Difference in short-term plasticity between models with different translocation rate constants. The 1× group induced sensory adaptation with a moderate amount of inactivation of ion-conductive channels. The 10× group exhibited a greater degree of inactivation, resulting in a rapid return to baseline by the end of the second pulse. (c) The overall training and testing accuracies of the dropletronic memristor in a 5 × 5 digit classification task. (d) The handwritten digit classification task with the device-multiplexing setup. (e) The average accuracy heatmap (n = 20) of the model with the sensory adaptation. Reproduced with permission from ref. 275. Copyright@2023, Wiley-VCH.

constant from the conductive to inactivated channel state to the baseline values (1×), which was experimentally determined (Fig. 19(b)), their model adopted a slow activation for conductive ion channels in the reservoir layer, achieving a test accuracy of 90% (Fig. 19(c)). However, experimental results yielded only ~70% accuracy, suggesting that further optimization of input parameters and array assembly of droplet pairs will be required. They also simulated a classification task of the Modified National Institute of Standards and Technology handwritten digit dataset (Fig. 19(d)). Assuming that exploiting the history dependence of memristors is crucial for maximizing the performance of the reservoir layer, they adopted the device-multiplexing method.[276] Each input signal was sent to multiple devices, where voltage pulses with the same patterns but different amplitudes were sent to respective devices. With the sensory adaptation feature, their system achieved a peak testing accuracy of ~94% by using the device-multiplexing between voltage amplitudes of 85 and 145 mV (Fig. 19(e)).

5. Outlook and challenges

This review systematically summarizes recent advances in NIDs based on SICs (Table 1 summarizes key information on representative devices), with a particular focus on their biomimetic implementation of artificial axons, synapses, and neurons. We emphasize the ionic transport behaviors and structural design strategies of SIC materials, and analyze their application pathways for mimicking essential neural functionalities, including axonal signal propagation, synaptic plasticity, spike generation,

Table 1 Summary of key information on representative SIC-based NIDs

Device	Materials	Response type	Functionalities	Applications	Ref.
Artificial axon	Ionic hydrogel and elastomer (dielectric layer)	Electricity	Transmitting AC signals	Transmitting music	169
		Electricity	Transmitting pulse signals	Connecting sensor and synaptic device	257
		Electricity	Transmitting pulse signals	Connecting sensor and robotic hand	258
Artificial synapse	Dropletronic hydrogel	Electricity	Synaptic transistor (npn-type)	Simulation of reversible SW modulation	77
	Ionic elastomer	Electricity	Bipolar memristor	Neuromorphic computing	86
	Ionic hydrogel	Electricity, heat, and strain	EPSP/IPSP, PPF/PPD, SRDP	—	113
	Hydrogel p–n junction	Electricity	Rectification, EPSP/IPSP, PPF/PPD, LTP/LTD	Simulating hippocampal neural circuit	176
	Ionic hydrogel	Pressure and electricity	EPSP/IPSP, PPF/PPD, LTP/LTD, STDP	Tactile perception and neuromorphic computing	178
	Aqueous droplet	Electricity	Unipolar memristor	—	213
	Aqueous droplet	Electricity	Memory capacitor	—	214
	Ionogel	Electricity	EPSP/IPSP, PPF/PPD, LTP/LTD, SRDP, STDP	Reservoir computing and n-back task	234
	Ionic supramolecular hydrogel	Light and heat	EPSP, PPF, LTP	Machine perception and intelligent control	243 and 244
	Ionic organogel heterojunction	Electricity	Rectification, EPSP	—	245
	Asymmetric trimeric ionic hydrogel	Electricity	Rectification, IPSP, PPD	Multimodal memory and image storing	246
	Ionic elastomers	Electricity	EPSP/IPSP, PPF/PPD, LTP/LTD, SRDP	Simulating proprioception	247
	Ionic hydrogel	Electricity, chemical, and light	EPSP/IPSP, PPF/PPD, SRDP	Intelligent machine control	248
	Ionic elastomer	Light	EPSP, PPF, LTP	Artificial vision and motion tracking	249 and 250
	Ionic hydrogel	Pressure and light	EPSP, PPF, LTP	Tactile-visual fusion perception and machine control	251
	Ionic hydrogel	Electricity	Bipolar memristor	Simulation of reversible SW modulation	252
	Ionogel	Electricity	EPSP, PPF, LTP	Intelligent machine control	253
	Ionic hydrogel	Light	EPSP/IPSP, PPF/PPD, LTP/LTD, SRDP	Artificial vision and neuromorphic computing	254
	Aqueous droplet	Electricity	Unipolar memristor	Reservoir computing	275
Artificial neuron	Ionic hydrogel	Pressure	Piezoionic effect	Bionic mechanoreceptor for biointeraction	137 and 256
	Aqueous droplet and hydrogel	Light	Photochemical signal transduction and chemical signal transmission	Parallel information processing mimicking nerve bundles	242

sensory preprocessing (touch and vision), and short-term working memory. Notably, we outline several representative device engineering approaches rooted in the fundamental principles of ionic dynamics and control, providing valuable insights for future device development in this emerging field.

Benefiting from the inherent softness, bio-language homology, multi-stimuli responsiveness, rich designability, material diversity, and high biocompatibility of SIC materials, their devices offer distinctive advantages for constructing low-power, flexible, multimodal, and efficient human–machine interaction platforms and neuromorphic computing systems. However, despite rapid progress, the field remains in its infancy and faces critical technical bottlenecks that demand concerted efforts in the following directions (Fig. 20):

(1) Expansion of functional capabilities: most reported SIC-based synaptic devices exhibit volatile behavior, making them unsuitable for long-term weight retention, and thus limiting their role in learning and memory units within neuromorphic computing systems. Meanwhile, the development of hardware-level artificial neurons based on SICs with reliable spike-generation and time-domain encoding capabilities remains an unsolved challenge. Realizing SIC-based non-volatile synapses and functional neurons will be a crucial step toward constructing fully ionic brain-inspired chips.

(2) Enabling chemical responsiveness: current research predominantly focuses on SIC-based devices that respond to physical stimuli such as electrical, mechanical, optical, or thermal signals. However, devices with selective chemical recognition capabilities remain scarce. Future work could incorporate functional groups into the polymeric matrix of SICs to enable selective recognition and adaptive learning of specific ions or biomolecules, facilitating applications in physiological signal sensing, metabolic monitoring, and pathological diagnostics.

(3) Adaptation to complex environments and systems: while much attention has focused on the neuromorphic functionality of individual devices, their stability and durability under practical conditions remain largely unexplored. For real-world applications such as wearable electronics and human–machine interfaces, devices must reliably operate in humid, stretchable, and skin-contact environments, demanding advances in material formulation, structural design, and encapsulation strategies. Moreover, scalable integration architectures and packaging techniques are needed to achieve high-density, low-power, and extensible ionic neural networks. Dropletronic NIDs have shown considerable promise in these areas; however, current implementations predominantly rely on manual assembly, limiting their scalability and reproducibility. Future efforts should prioritize the development of scalable droplet-electronic networks to enhance computational complexity and processing speed. In this context, three-dimensional droplet fabrication platforms may offer an efficient and precise route to constructing large-scale dropletronic networks.[277] A further challenge is the instability caused by evaporation of aqueous droplets, which significantly constrains long-term device operation. Potential strategies to extend device lifetime include encapsulating droplets within an oil phase or integrating hydrogel scaffolds.

(4) Enhancing bio-interaction: SIC-based iontronic devices present significant potential for building safe and efficient bio-interaction systems. While previous studies have explored their interactions at the cellular,[78] tissue,[79,144] and animal

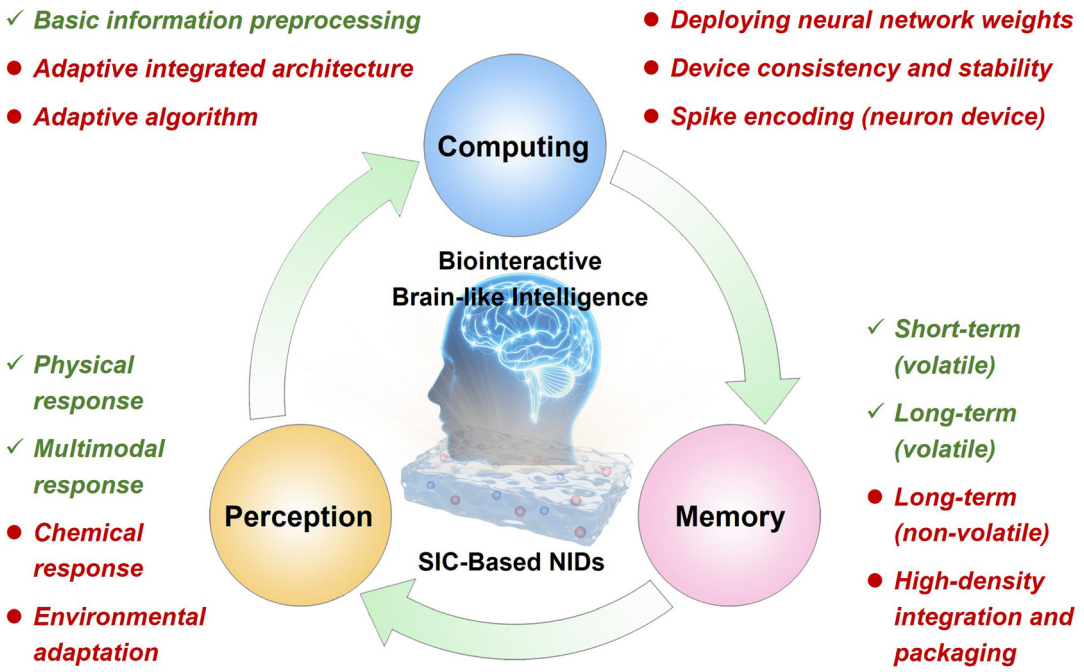

Fig. 20 Outlook and challenges. Achievements (in green font) and challenges (in red font) of SIC-based NIDs in advancing new-generation brain-like intelligence.

levels,[137,256] these have largely focused on unidirectional modulation of neural activity through ionic electrical signals, without achieving true bidirectional communication. Furthermore, these devices are mostly energy devices rather than neuromorphic systems, lacking adaptive regulation capabilities. Moving forward, interaction paradigms from electronic neuromorphic systems[278–280] could inform the development of SIC-based NIDs. Crucially, their bio-interactions should extend beyond electrical signalling to include material exchanges such as ions and signalling molecules, enabling more comprehensive and dynamic bio-device integration.

(5) Device-system-algorithm co-optimization: although SIC-based NIDs have shown promising results in image recognition, edge detection, and working memory tasks, challenges remain in terms of device uniformity, manufacturability, and system integrability. For example, the dropletronic platform proposed by Zhang *et al.* offers a promising solution to these issues.[78,79,212] Furthermore, the development of neuromorphic algorithms tailored to the dynamic characteristics of ionic devices will be critical for achieving effective coupling between device-level behaviors and network-level computing, ultimately enabling system-level co-optimization and intelligent evolution.

(6) Integration of ionic and electronic intelligence: ionic intelligent systems inherently offer bio-interactivity and excellent biocompatibility, with potential for stable operation in aqueous environments. However, their development remains immature, and their multifunctionality, computational capability, and operational stability still lag behind those of conventional electronic systems. Consequently, integrating ionic and electronic systems represents a promising development pathway, analogous to the established route of achieving compatibility between advanced neuromorphic systems and conventional complementary metal–oxide–semiconductor (CMOS) platforms. For instance, in bio-interfacing or *in vivo* applications, ionic devices can be placed in close contact with biological tissues to exploit their unique advantages, while electronic devices perform distal, complex signal processing to ensure robust system-level functionality. A key challenge in this approach is achieving efficient signal conversion at the ionic–electronic interface. To address this, ion- and molecule-tunable organic semiconductors may play a central role in establishing high-efficiency coupling, while high-precision, highly sensitive bioelectrodes can provide complementary solutions.

In summary, SIC-based NIDs are driving the evolution of neuromorphic systems from simple functional biomimicry toward integrated functional-mechanistic emulation. Continued progress in material design, interface modulation, micro/nanofabrication, dropletronics, and algorithm-device co-optimization will be critical to unlocking their full potential in next-generation applications such as flexible perception, human–machine interfaces, neural rehabilitation, and adaptive intelligent hardware. Looking ahead, SIC-based neuromorphic platforms are poised to enable closed-loop systems that seamlessly couple perception, computing, and storage, laying the groundwork for fully integrated, biointerfacing computing architectures (Fig. 20).

Author contributions

K. X., P. W., Y. Z., Y. L., and L. W. conceived the idea. L. W., Y. J., and H. Z. wrote the manuscript and performed the figure preparation.

Conflicts of interest

There are no conflicts of interest to declare.

Data availability

No primary research results, software or code have been included and no new data were generated or analyzed as part of this review.

Acknowledgements

This work was financially supported by the National Key Technologies R&D Program of China (2023YFC2415900), the Shenzhen Medical Research Fund (B2401005), the National Natural Science Foundation of China (22275079, 22402076, 22474053), the Guangdong Innovative and Entrepreneurial Research Team Program (2023ZT10C027), the Guangdong Basic and Applied Basic Research Foundation (2024A1515012600, 2025A1515011886), the Shenzhen Science and Technology Program (KQTD20221101093559017, JCYJ20230807093205011), the Guangdong Provincial Key Laboratory of Advanced Biomaterials (2022B1212010003), the High level of special funds (G03050K002), the Swiss National Science Foundation (10005601) from the École Polytechnique Fédérale de Lausanne (EPFL, BION) and the Starting Grants from Nanjing Tech University (NJTech).

References

1 C. Lopez, *Adv. Mater.*, 2023, **35**, 2208683.
2 D. Marković, A. Mizrahi, D. Querlioz and J. Grollier, *Nat. Rev. Phys.*, 2020, **2**, 499–510.
3 C. Mead, *Proc. IEEE*, 1990, **78**, 1629–1636.
4 G. Finocchio, J. A. C. Incorvia, J. S. Friedman, Q. Yang, A. Giordano, J. Grollier, H. Yang, F. Ciubotaru, A. Chumak, A. Naeemi, S. Cotofana, R. Tomasello, C. Panagopoulos, M. Carpentieri, P. Lin, G. Pan, J. J. Yang, A. Todri-Sanial, G. Boschetto, K. Makasheva, V. Sangwan, A. R. Trivedi, M. C. Hersam, K. Camsari, P. L. McMahon, S. Datta, B. Koiller, G. Aguilar, G. Temporão, D. Rodrigues, S. Sunada, K. Everschor-Sitte, K. Tatsumura, H. Goto, V. Puliafito, J. Akerman, H. Takesue, M. Di Ventra, Y. V. Pershin, S. Mukhopadhyay, K. Roy, I. Wang, W. Kang, Y. Zhu, B. K. Kaushik, J. Hasler, S. Ganguly, A. W. Ghosh, W. B. Levy, V. Roychowdhury and S. Bandyopadhyay, *Nano Futures*, 2024, **8**, 012001.

5 E. K. Boahen, H. Kweon, H. Oh, J. H. Kim, H. Lim and D. H. Kim, *Adv. Sci.*, 2025, **12**, 2409568.
6 D. Kudithipudi, C. Schuman, C. M. Vineyard, T. Pandit, C. Merkel, R. Kubendran, J. B. Aimone, G. Orchard, C. Mayr, R. Benosman, J. Hays, C. Young, C. Bartolozzi, A. Majumdar, S. G. Cardwell, M. Payvand, S. Buckley, S. Kulkarni, H. A. Gonzalez, G. Cauwenberghs, C. S. Thakur, A. Subramoney and S. Furber, *Nature*, 2025, **637**, 801–812.
7 D. R. Muir and S. Sheik, *Nat. Commun.*, 2025, **16**, 3586.
8 C. D. Schuman, T. E. Potok, R. M. Patton, J. D. Birdwell, M. E. Dean, G. S. Rose and J. S. Plank, *arXiv*, 2017, preprint, cs.NE, arXiv:abs/1705.06963, DOI: 10.48550/arXiv.1705.06963.
9 P. A. Merolla, J. V. Arthur, R. Alvarez-Icaza, A. S. Cassidy, J. Sawada, F. Akopyan, B. L. Jackson, N. Imam, C. Guo, Y. Nakamura, B. Brezzo, I. Vo, S. K. Esser, R. Appuswamy, B. Taba, A. Amir, M. D. Flickner, W. P. Risk, R. Manohar and D. S. Modha, *Science*, 2014, **345**, 668–673.
10 D. Mike, S. Narayan, L. Tsung Han, C. Gautham, C. Yongqiang, C. Sri Harsha and D. Georgios, *IEEE Micro*, 2018, **38**, 82–99.
11 J. Pei, L. Deng, S. Song, M. Zhao, Y. Zhang, S. Wu, G. Wang, Z. Zou, Z. Wu, W. He, F. Chen, N. Deng, S. Wu, Y. Wang, Y. Wu, Z. Yang, C. Ma, G. Li, W. Han, H. Li, H. Wu, R. Zhao, Y. Xie and L. Shi, *Nature*, 2019, **572**, 106–111.
12 A. Mehonic and A. J. Kenyon, *Nature*, 2022, **604**, 255–260.
13 J. W. Lee, J. Han, B. Kang, Y. J. Hong, S. Lee and I. Jeon, *Adv. Mater.*, 2025, **37**, 2413916.
14 Y. Liang, H. Li, H. Tang, C. Zhang, D. Men and D. Mayer, *Nano-Micro Lett.*, 2025, **17**, 198.
15 M. Zeng, Y. He, C. Zhang and Q. Wan, *Front. Neurosci.*, 2021, **15**, 690950.
16 J. Yu, Y. Wang, S. Qin, G. Gao, C. Xu, Z. Wang and Q. Sun, *Mater. Today*, 2022, **60**, 158–182.
17 Y. Sandamirskaya, M. Kaboli, J. Conradt and T. Celikel, *Sci. Rob.*, 2022, **7**, eabl8419.
18 Y. Lee, J. Y. Oh and T. W. Lee, *Adv. Mater. Technol.*, 2022, **7**, 2200193.
19 S. K. Khare, V. Blanes-Vidal, E. S. Nadimi and U. R. Acharya, *Inf. Fusion*, 2024, **102**, 102019.
20 Y. Wang, S. Liu, H. Wang, Y. Zhao and X. D. Zhang, *Microsyst. Nanoeng.*, 2022, **8**, 128.
21 E. Donati and G. Indiveri, *Prog. Biomed. Eng.*, 2023, **5**, 013002.
22 C. Bartolozzi, G. Indiveri and E. Donati, *Nat. Commun.*, 2022, **13**, 1024.
23 K. N. Kim, M. J. Sung, H. L. Park and T. W. Lee, *Adv. Electron. Mater.*, 2022, **8**, 2100935.
24 D. Rana, N. Babushkina, M. Gini, A. Flores Caceres, H. Li, V. Maybeck, V. Criscuolo, D. Mayer, M. Ienca, S. Musall, V. Rincon Montes, A. Offenhausser and F. Santoro, *Chem. Rev.*, 2025, **125**, 9092–9139.
25 C. Yang and Z. Suo, *Nat. Rev. Mater.*, 2018, **3**, 125–142.
26 J. K. Han, S. Y. Yun, S. W. Lee, Y. Man and Y. K. Choi, *Adv. Funct. Mater.*, 2022, **32**, 2204102.
27 Y. Wang, Z. Lv, L. Zhou, X. Chen, J. Chen, Y. Zhou, V. A. L. Roy and S.-T. Han, *J. Mater. Chem. C*, 2018, **6**, 1600–1617.
28 W. Huang, X. Xia, C. Zhu, P. Steichen, W. Quan, W. Mao, J. Yang, L. Chu and X. Li, *Nano-Micro Lett.*, 2021, **13**, 85.
29 B. Sun, Y. Chen, G. Zhou, Z. Cao, C. Yang, J. Du, X. Chen and J. Shao, *ACS Nano*, 2024, **18**, 14–27.
30 X. Liu, C. Sun, X. Ye, X. Zhu, C. Hu, H. Tan, S. He, M. Shao and R. W. Li, *Adv. Mater.*, 2024, **36**, e2311472.
31 K. Xiao, C. Wan, L. Jiang, X. Chen and M. Antonietti, *Adv. Mater.*, 2020, **32**, 2000218.
32 N. Aleksandr and D. Seth B., *Science*, 2023, **379**, 143–144.
33 J. Zhang, W. Liu, J. Dai and K. Xiao, *Adv. Sci.*, 2022, **9**, 2200534.
34 F. Yu and L. Q. Zhu, *Phys. Status Solidi RRL*, 2019, **13**, 1800674.
35 Y. G. Ro, S. Na, J. Kim, Y. Chang, S. Lee, M. S. Kwak, S. Jung and H. Ko, *ACS Nano*, 2025, **19**, 24425–24507.
36 Y. Hou and X. Hou, *Science*, 2022, **373**, 628–629.
37 Y. Hou, Y. Ling, Y. Wang, M. Wang, Y. Chen, X. Li and X. Hou, *J. Phys. Chem. Lett.*, 2023, **14**, 2891–2900.
38 L. Yu, X. Li, C. Luo, Z. Lei, Y. Wang, Y. Hou, M. Wang and X. Hou, *Nano Res.*, 2023, **17**, 503–514.
39 Z. Huang, T. Mei, X. Zhu and K. Xiao, *Chem. – Asian J.*, 2025, **20**, 202401170.
40 G. Xu, M. Zhang, T. Mei, W. Liu, L. Wang and K. Xiao, *ACS Nano*, 2024, **18**, 19423–19442.
41 T. Mei, W. Liu, G. Xu, Y. Chen, M. Wu, L. Wang and K. Xiao, *ACS Nano*, 2024, **18**, 4624–4650.
42 T. Xiong, C. Li, X. He, B. Xie, J. Zong, Y. Jiang, W. Ma, F. Wu, J. Fei, P. Yu and L. Mao, *Science*, 2023, **379**, 156–161.
43 P. Robin, T. Emmerich, A. Ismail, A. Nigues, Y. You, G. H. Nam, A. Keerthi, A. Siria, A. K. Geim, B. Radha and L. Bocquet, *Science*, 2023, **379**, 161–167.
44 T. Emmerich, Y. Teng, N. Ronceray, E. Lopriore, R. Chiesa, A. Chernev, V. Artemov, M. Di Ventra, A. Kis and A. Radenovic, *Nat. Electron.*, 2024, **7**, 271–278.
45 Y. Ling, L. Yu, Z. Guo, F. Bian, Y. Wang, X. Wang, Y. Hou and X. Hou, *J. Am. Chem. Soc.*, 2024, **146**, 14558–14565.
46 T. M. Kamsma, J. Kim, K. Kim, W. Q. Boon, C. Spitoni, J. Park and R. van Roij, *Proc. Natl. Acad. Sci. U. S. A.*, 2024, **121**, 2320242121.
47 X. Zhou, Y. Zong, Y. Wang, M. Sun, D. Shi, W. Wang, G. Du and Y. Xie, *Natl. Sci. Rev.*, 2024, **11**, nwad216.
48 K. Liu, Y. Wang, M. Sun, J. Lu, D. Shi and Y. Xie, *Nano Lett.*, 2025, **25**, 6530–6538.
49 P. Ramirez, V. Gómez, J. Cervera, S. Mafe and J. Bisquert, *J. Phys. Chem. Lett.*, 2023, **14**, 10930–10934.
50 Y. Xu, S. Yu, Z. Li, B. Kou, J. Pang, W. Zhao, H. Chen and J. Xu, *Proc. Natl. Acad. Sci. U. S. A.*, 2024, **121**, 2403143121.
51 A. Noy, Z. Li and S. B. Darling, *Nano Today*, 2023, **53**, 102043.
52 G. Xu, H. Cui, L. Wang, M. Zhang, W. Liu, T. Mei, B. Wu, C. Wan and K. Xiao, *ACS Appl. Mater. Interfaces*, 2025, **17**, 34659–34668.
53 P. Robin, N. Kavokine and L. Bocquet, *Science*, 2021, **373**, 687–691.
54 T. M. Kamsma, W. Q. Boon, T. ter Rele, C. Spitoni and R. van Roij, *Phys. Rev. Lett.*, 2023, **130**, 268401.

55 Y. Wang, B. Jian, Y. Ling, Z. Pan, F. Liu, Y. Hou, F. Huo and X. Hou, *Nano Lett.*, 2025, **25**, 2298–2306.
56 C. S. Law, J. Wang, K. Nielsch, A. D. Abell, J. Bisquert and A. Santos, *Appl. Phys. Rev*, 2025, **12**, 021309.
57 Z. Xu, *ACS Nano*, 2024, **18**, 9765–9772.
58 L. Bocquet, *Nat. Mater.*, 2020, **19**, 254–256.
59 W. Niu and X. Liu, *Macromol. Rapid Commun.*, 2022, **43**, 2200512.
60 C. Luo, Z. Huang, Z. H. Guo and K. Yue, *Chin. J. Chem.*, 2023, **41**, 835–860.
61 H. N. Li, C. Zhang, H. C. Yang, H. Q. Liang, Z. Wang and Z. K. Xu, *Mater. Horiz.*, 2024, **11**, 1152–1176.
62 H. Sheng, X. Wang, N. Kong, W. Xi, H. Yang, X. Wu, K. Wu, C. Li, J. Hu, J. Tang, J. Zhou, S. Duan, H. Wang and Z. Suo, *Extreme Mech. Lett.*, 2019, **30**, 100510.
63 H. Yuk, J. Wu and X. Zhao, *Nat. Rev. Mater.*, 2022, **7**, 935–952.
64 H. Yuk, B. Lu and X. Zhao, *Chem. Soc. Rev.*, 2019, **48**, 1642–1667.
65 J. Park, Y. Lee, S. Cho, A. Choe, J. Yeom, Y. G. Ro, J. Kim, D.-H. Kang, S. Lee and H. Ko, *Chem. Rev.*, 2024, **124**, 1464–1534.
66 M. Zhang, K. Hakobyan, C. Cheng and J. Xu, *Macromol. Chem. Phys.*, 2025, **226**, e00511.
67 X. Ye, Y. Chen, C. Lv, Y. Ying, J. Ping, J. Pan and L. Lan, *Mater. Horiz.*, 2025, **12**, 9537–9555.
68 H. R. Lee, C. C. Kim and J. Y. Sun, *Adv. Mater.*, 2018, **30**, 1704403.
69 X. Chen, X. Xia and C. Guo, *Adv. Funct. Mater.*, 2025, e12920, DOI: 10.1002/adfm.202512920.
70 Y. Li, N. Bai, Y. Chang, L. Zhiguang, J. Liu, X. Li, W. Yang, H. Niu, W. Wang, L. Wang, W. Zhu, D. Chen, T. Pan, C. Guo and G. Shen, *Chem. Soc. Rev.*, 2025, **54**, 4651–4700.
71 H. Tang, Y. Li, S. Liao, H. Liu, Y. Qiao and J. Zhou, *Adv. Healthcare Mater.*, 2024, **13**, e2400562.
72 M. Tu, T. Zhao, H. Guo, C. Zhang, M. Liu, Z. Zhang, B. Wang and H. Yu, *Luminescence*, 2025, **40**, e70148.
73 S. Chen, Z. Wu, C. Chu, Y. Ni, R. E. Neisiany and Z. You, *Adv. Sci.*, 2022, **9**, e2105146.
74 L. Y. Zhou, J. Fu and Y. He, *Adv. Funct. Mater.*, 2020, **30**, 2000187.
75 H. Liu, H. Zhang, W. Han, H. Lin, R. Li, J. Zhu and W. Huang, *Adv. Mater.*, 2021, **33**, 2004782.
76 H. Yoo, Y. H. Lee, M. G. Lee and J. Y. Sun, *Chem. Rev.*, 2025, **125**, 8956–9011.
77 Y. Zhang, C. M. J. Tan, C. N. Toepfer, X. Lu and H. Bayley, *Science*, 2024, **386**, 1024–1030.
78 Y. Zhang, J. Riexinger, X. Yang, E. Mikhailova, Y. Jin, L. Zhou and H. Bayley, *Nature*, 2023, **620**, 1001–1006.
79 Y. Zhang, T. Sun, X. Yang, L. Zhou, C. M. J. Tan, M. Lei and H. Bayley, *Nat. Chem. Eng.*, 2024, **1**, 691–701.
80 L. Fang, Y. Zhou and Q. Huang, *Adv. Mater.*, 2025, e2502140, DOI: 10.1002/adma.202502140.
81 M. Tepermeister, N. Bosnjak, J. Dai, X. Zhang, S. M. Kielar, Z. Wang, Z. Tian, J. Suntivich and M. N. Silberstein, *Front. Phys.*, 2022, **10**, 890845.
82 B. Lu, H. Yuk, S. Lin, N. Jian, K. Qu, J. Xu and X. Zhao, *Nat. Commun.*, 2019, **10**, 1043.
83 S. R. Jackson, G. W. Collins, R. L. Kingsford, P. W. Martin, J. N. Keller and C. G. Bischak, *J. Mater. Chem. C*, 2024, **12**, 9804–9813.
84 D. K. Tran, S. M. West, A. E. Stewart, W. Kaminsky and S. A. Jenekhe, *Adv. Funct. Mater.*, 2025, e10945, DOI: 10.1002/adfm.202510945.
85 S. Sun, Z. You, Y. Ji, Y. Li, Y. Feng, S. Liu, J. Cao, Y. Liu, Z. Yu and T. Wu, *J. Mater. Chem. C*, 2025, **13**, 19125–19148.
86 S. Zheng, Z. D. Zhang, X. Wang, X. Zou, Z. Liu, Q. Li, Y. N. Zhong, S. D. Wang and F. Yan, *Adv. Mater.*, 2025, e05312, DOI: 10.1002/adma.202505312.
87 F. Torricelli, D. Z. Adrahtas, Z. Bao, M. Berggren, F. Biscarini, A. Bonfiglio, C. A. Bortolotti, C. D. Frisbie, E. Macchia, G. G. Malliaras, I. McCulloch, M. Moser, T. Q. Nguyen, R. M. Owens, A. Salleo, A. Spanu and L. Torsi, *Nat. Rev. Methods Primers*, 2021, **1**, 66.
88 Y. Wang, S. Wustoni, J. Surgailis, Y. Zhong, A. Koklu and S. Inal, *Nat. Rev. Mater.*, 2024, **9**, 249–265.
89 D. Ohayon, V. Druet and S. Inal, *Chem. Soc. Rev.*, 2023, **52**, 1001–1023.
90 B. D. Paulsen, K. Tybrandt, E. Stavrinidou and J. Rivnay, *Nat. Mater.*, 2020, **19**, 13–26.
91 C. Zhao, J. Yang and W. Ma, *Nano-Micro Lett.*, 2024, **16**, 233.
92 N. A. Kukhta, A. Marks and C. K. Luscombe, *Chem. Rev.*, 2022, **122**, 4325–4355.
93 Y. Xiao, W. Sun, C. Gao, J. Jin, M. Siraj, P. Yan, F. Sun, X. Zhang, Q. Wang, W. Huang, C. Sheng and Y. F. Yu, *Nano Lett.*, 2024, **24**, 12515–12521.
94 L. Huang, D. Zhao, X. Yan, X. Liu, Q. Sun, H. Yang, X. Liu and H. Jia, *Adv. Electron. Mater.*, 2025, **11**, 2400474.
95 Z. Zhu, Y. Pang, Y. Li, Y. Gu, X. Wang, A. Yu, B. Liu, S. Liu, W. Huang and Q. Zhao, *ACS Nano*, 2025, **19**, 4084–4120.
96 Y. Tuchman, T. N. Mangoma, P. Gkoupidenis, V. D. B. Yoeri, R. A. John, N. Mathews, S. E. Shaheen, R. Daly, G. G. Malliaras and A. Salleo, *MRS Bull.*, 2020, **45**, 619–630.
97 S. G. Waxman, J. D. Kocsis and P. K. Stys, *The Axon: Structure, Function and Pathophysiology*, Oxford University Press, 1995.
98 S. Rama, M. Zbili and D. Debanne, *Curr. Opin. Neurobiol.*, 2018, **51**, 37–44.
99 R. C. M. Thomas and C. Südhof, *Neuron*, 2008, **60**, 469–476.
100 F. Cesca, P. Baldelli, F. Valtorta and F. Benfenati, *Prog. Neurobiol.*, 2010, **91**, 313–348.
101 T. J. Park, S. Deng, S. Manna, A. Islam, H. Yu, Y. Yuan, D. D. Fong, A. A. Chubykin, A. Sengupta, S. Sankaranarayanan and S. Ramanathan, *Adv. Mater.*, 2022, **35**, 2203352.
102 G. Neves, S. F. Cooke and T. V. P. Bliss, *Nat. Rev. Neurosci.*, 2008, **9**, 65–75.
103 R. K. Goyal and A. Chaudhury, *Auton. Neurosci.*, 2013, **176**, 11–31.
104 T. V. P. Bliss and G. L. Collingridge, *Nature*, 1993, **361**, 31–39.

105 D. Debanne and Y. Inglebert, *Curr. Opin. Neurobiol.*, 2023, **80**, 102707.
106 R. Rosenbaum, in *Encyclopedia of Computational Neuroscience*, ed. D. Jaeger and R. Jung, Springer New York, New York, NY, 2022, pp. 3103–3107, DOI: 10.1007/978-1-0716-1006-0_358.
107 D. M. Kullmann and K. P. Lamsa, *Nat. Rev. Neurosci.*, 2007, **8**, 687–699.
108 H. Chen, L. Xie, Y. Wang and H. Zhang, *Front. Comput. Neurosci.*, 2022, **16**, 804604.
109 S. Wang, L. Song, W. Chen, G. Wang, E. Hao, C. Li, Y. Hu, Y. Pan, A. Nathan, G. Hu and S. Gao, *Adv. Electron. Mater.*, 2022, **9**, 2200877.
110 Z. Zhang, X. Zhao, X. Zhang, X. Hou, X. Ma, S. Tang, Y. Zhang, G. Xu, Q. Liu and S. Long, *Nat. Commun.*, 2022, **13**, 6590.
111 K. Rabl, L. Cadetti and W. B. Thoreson, *J. Neurosci.*, 2006, **26**, 2555–2563.
112 S. Zhao, W. Ran, Z. Lou, L. Li, S. Poddar, L. Wang, Z. Fan and G. Shen, *Natl. Sci. Rev.*, 2022, **9**, nwac158.
113 X. Chen, L. Chen, J. Zhou, J. Wu, Z. Wang, L. Wei, S. Yuan and Q. Zhang, *Nano Lett.*, 2024, **24**, 10265–10274.
114 L. Wang, X. Wang, Y. Zhang, R. Li, T. Ma, K. Leng, Z. Chen, I. Abdelwahab and K. P. Loh, *Adv. Funct. Mater.*, 2020, **30**, 2004609.
115 H. M. Huang, R. Yang, Z. H. Tan, H. K. He, W. Zhou, J. Xiong and X. Guo, *Adv. Mater.*, 2019, **31**, 1803849.
116 J. C. Magee, *Nat. Rev. Neurosci.*, 2000, **1**, 181–190.
117 P. C. Harikesh, C. Y. Yang, H. Y. Wu, S. Zhang, M. J. Donahue, A. S. Caravaca, J. D. Huang, P. S. Olofsson, M. Berggren, D. Tu and S. Fabiano, *Nat. Mater.*, 2023, **22**, 242–248.
118 J. D. Nunes, M. Carvalho, D. Carneiro and J. S. Cardoso, *IEEE Access*, 2022, **10**, 60738–60764.
119 T. Wasserman and L. D. Wasserman, in *Therapy and the Neural Network Model*, ed. T. Wasserman and L. D. Wasserman, Springer International Publishing, Cham, 2019, pp. 27–43, DOI: 10.1007/978-3-030-26921-0_3.
120 J. G. Jefferys, *Physiol. Rev.*, 1995, **75**, 689–723.
121 P. Choi, N. H. Jalani and R. Datta, *J. Electrochem. Soc.*, 2005, **152**, A1548.
122 Y. Wang, Q. Li, H. Hong, S. Yang, R. Zhang, X. Wang, X. Jin, B. Xiong, S. Bai and C. Zhi, *Nat. Commun.*, 2023, **14**, 3890.
123 S. Wang and C. Zhi, *Next Energy*, 2025, **7**, 100293.
124 F. Liu, X. Du, Z. Zhang, X. Ma, F. Gao, X. Hao, L. Chang, Q. Wang, M. Liu and J. Luo, *Chem. Eng. Process.*, 2019, **143**, 107628.
125 G. Shao, S. Guo, R. Yu, N. Chen, M. Ye and X. Liu, *Acta Phys. Sin.*, 2020, **69**, 178801.
126 Q. Ren, K. Chen, H. Zhu, J. F. Zhang and Z. G. Qu, *Energy Convers. Manage.*, 2022, **251**, 115032.
127 M. S. Kilic, M. Z. Bazant and A. Ajdari, *Phys. Rev. E: Stat., Nonlinear, Soft Matter Phys.*, 2007, **75**, 021503.
128 K. Szyszkiewicz-Warzecha, G. Wilczek-Vera, A. Lewenstam, A. Gorska, J. Tarasiuk and R. Filipek, *Materials*, 2023, **16**, 1116.
129 J. Kamcev, D. R. Paul and B. D. Freeman, *Macromolecules*, 2015, **48**, 8011–8024.
130 A. Zhang, X. Yang, F. Yang, C. Zhang, Q. Zhang, G. Duan and S. Jiang, *Molecules*, 2023, **28**, 2042.
131 Y. Guo, Q. Yin and Z. Zhang, *J. Sci. Comput.*, 2024, **101**, 51.
132 B. Corry, S. Kuyucak and S.-H. Chung, *Biophys. J.*, 2003, **84**, 3594–3606.
133 S. K. Li, A.-H. Ghanem, K. D. Peck and W. I. Higuchi, *J. Pharm. Sci.*, 1997, **86**, 680–689.
134 A. Sawada, *Phys. Rev. E*, 2016, **93**, 052608.
135 G. Barbero and I. Lelidis, *J. Appl. Phys.*, 2014, **115**, 194101.
136 A. L. Alexe-Ionescu, G. Barbero and I. Lelidis, *J. Chem. Phys.*, 2014, **141**, 084505.
137 D. Yuta, D. Yao, P. Yael, N. N. Tan, S. S. Mirza, T. Yacine, L. W. N. Cliff, S. G. Ettore, T. M. N. Giao, C. Plesse, F. Vidal, C. A. Michal and J. D. W. Madden, *Science*, 2022, **376**, 502–507.
138 L. Jia, L. Li, Z. H. Guo, H. Sun, H. Huang, F. Sun, Z. L. Wang and X. Pu, *Adv. Mater.*, 2024, **36**, 2403830.
139 I. Lakatos and J. Lakatos-Szabó, *Colloids Surf., A*, 1998, **141**, 425–434.
140 H. Gudla, A. Hockmann, D. Brandell and J. Mindemark, *ACS Appl. Polym. Mater.*, 2025, **7**, 4716–4724.
141 D. Dong, W. Zhang, A. C. T. van Duin and D. Bedrov, *J. Phys. Chem. Lett.*, 2018, **9**, 825–829.
142 H. Yang and N. Wu, *Energy Sci. Eng.*, 2022, **10**, 1643–1671.
143 B. J. Morgan and P. A. Madden, *Phys. Rev. Lett.*, 2014, **112**, 145901.
144 W. Chen, L. Zhai, S. Zhang, Z. Zhao, Y. Hu, Y. Xiang, H. Liu, Z. Xu, L. Jiang and L. Wen, *Science*, 2023, **382**, 559–565.
145 Y. Hao, X. Zhang and L. Jiang, *Nanoscale Horiz.*, 2019, **4**, 1029–1036.
146 X. Zhang and L. Jiang, *Nano Res.*, 2019, **12**, 1219–1221.
147 L. Wen, X. Zhang, Y. Tian and L. Jiang, *Sci. China Mater.*, 2018, **61**, 1027–1032.
148 F. Wang, G. Xu, W. Shen, S. Park and Q. Li, *Sens. Actuators, A*, 2023, **363**, 114734.
149 B. Wang, P. Huang, B. Li, Z. Wu, Y. Xing and L. Liu, *Sens. Actuators, B*, 2025, **422**, 136649.
150 D. Morales, E. Palleau, M. D. Dickey and O. D. Velev, *Soft Matter*, 2014, **10**, 1337–1348.
151 T. Li, S. X. Li, W. Kong, C. Chen, E. Hitz, C. Jia, J. Dai, X. Zhang, R. Briber, Z. Siwy, M. Reed and L. Hu, *Sci. Adv.*, 2019, **5**, eaau4238.
152 K. Tybrandt, K. C. Larsson, A. Richter-Dahlfors and M. Berggren, *Proc. Natl. Acad. Sci. U. S. A.*, 2010, **107**, 9929–9932.
153 H. J. Kim, B. Chen, Z. Suo and R. C. Hayward, *Science*, 2020, **367**, 773–776.
154 S. M. Lim, H. Yoo, M. A. Oh, S. H. Han, H. R. Lee, T. D. Chung, Y. C. Joo and J. Y. Sun, *Proc. Natl. Acad. Sci. U. S. A.*, 2019, **116**, 13807–13815.
155 T. Yamamoto and M. Doi, *Nat. Commun.*, 2014, **5**, 4162.
156 O. J. Cayre, S. T. Chang and O. D. Velev, *J. Am. Chem. Soc.*, 2007, **129**, 10801–10806.

157 Y. He, S. Li, R. Chen, X. Liu, G. Omololu Odunmbaku, W. Fang, X. Lin, Z. G. Ou, Q. Gou, J. Wang, N. Aida Nadege Ouedraogo, J. Li, M. Li, C. Li, Y. Zheng, S. Chen, Y. Zhou and K. Sun, *Nano-Micro Lett.*, 2023, **15**, 101.
158 S. J. K. O'Neill, Z. Huang, X. Chen, R. L. Sala, J. A. McCune, G. G. Malliaras and O. A. Scherman, *Sci. Adv.*, 2024, **10**, eadn5142.
159 Y. Zhang, C. K. Jeong, J. Wang, X. Chen, K. H. Choi, L. Chen, W. Chen, Q. Zhang and Q. Wang, *Adv. Mater.*, 2021, **33**, 2103056.
160 W. Zhu, B. Wu, Z. Lei and P. Wu, *Adv. Mater.*, 2024, **36**, 2313127.
161 X. Wu, M. Ahmed, Y. Khan, M. E. Payne, J. Zhu, C. Lu, J. W. Evans and A. C. Arias, *Sci. Adv.*, 2020, **6**, eaba1062.
162 J. Wang, B. Wu, P. Wei, S. Sun and P. Wu, *Nat. Commun.*, 2022, **13**, 4411.
163 Z. Wang, N. Li, X. Yang, Z. Zhang, H. Zhang and X. Cui, *Microsyst. Nanoeng.*, 2024, **10**, 55.
164 C. Lu, X. Wang, Y. Shen, S. Xu, C. Huang, C. Wang, H. Xie, J. Wang, Q. Yong and F. Chu, *Adv. Funct. Mater.*, 2023, **34**, 2311502.
165 D. Ho, *ChemElectroChem*, 2024, **11**, 202300268.
166 S. Sun, M. Li, X. L. Shi and Z. G. Chen, *Adv. Energy Mater.*, 2023, **13**, 2203692.
167 H. Liu, X. Jin, Q. Xu, Y. Jin, X. Zhang and S. L. Lv, *ACS Appl. Mater. Interfaces*, 2025, **17**, 36943–36950.
168 H. Ma, K. Sun, Y. Cai, F. Li, L. Ma, Y. Qi, H. Sheng, L. Wu, K. Wang, J. Wang, Y. Fu, Y. Chai and W. Lan, *Angew. Chem., Int. Ed.*, 2025, **64**, 202420404.
169 C. Yang, B. Chen, J. J. Lu, J. H. Yang, J. Zhou, Y. M. Chen and Z. Suo, *Extreme Mech. Lett.*, 2015, **3**, 59–65.
170 S. Zhao, P. Tseng, J. Grasman, Y. Wang, W. Li, B. Napier, B. Yavuz, Y. Chen, L. Howell, J. Rincon, F. G. Omenetto and D. L. Kaplan, *Adv. Mater.*, 2018, **30**, 1800598.
171 W. Kong, C. Chen, G. Chen, C. Wang, D. Liu, S. Das, G. Chen, T. Li, J. Li, Y. Liu, Z. Li, B. C. Clifford and L. Hu, *Small*, 2021, **17**, 2008200.
172 W. Ren, H. Jing, S. Ding, J. Dan, Z. Xu, T. Guo, H. Wei, Y. Liu and Y. Liu, *Small*, 2024, **20**, 2404874.
173 H. Wang, C. N. Zhu, H. Zeng, X. Ji, T. Xie, X. Yan, Z. L. Wu and F. Huang, *Adv. Mater.*, 2019, **31**, 1807328.
174 T. Lei, Y. Wang, Y. Feng, X. Duan, Q. Zhang, A. Wan, Z. Xia, W. Shou and J. Fan, *J. Colloid Interface Sci.*, 2025, **678**, 726–741.
175 C. Li, A. Iscen, L. C. Palmer, G. C. Schatz and S. I. Stupp, *J. Am. Chem. Soc.*, 2020, **142**, 8447–8453.
176 S. H. Hana, S. I. Kima, M. A. Oha and T. D. Chung, *Proc. Natl. Acad. Sci. U. S. A.*, 2022, **120**, 2211442120.
177 J. Feng, K. Liu, M. Graf, D. Dumcenco, A. Kis, M. Di Ventra and A. Radenovic, *Nat. Mater.*, 2016, **15**, 850–855.
178 L. Wang, S. Wang, G. Xu, Y. Qu, H. Zhang, W. Liu, J. Dai, T. Wang, Z. Liu, Q. Liu and K. Xiao, *ACS Nano*, 2024, **18**, 29704–29714.
179 S. Dai, X. Liu, Y. Liu, Y. Xu, J. Zhang, Y. Wu, P. Cheng, L. Xiong and J. Huang, *Adv. Mater.*, 2023, **35**, e2300329.
180 J. Rivnay, S. Inal, A. Salleo, R. M. Owens, M. Berggren and G. G. Malliaras, *Nat. Rev. Mater.*, 2018, **3**, 17086.
181 S. Inal, G. G. Malliaras and J. Rivnay, *Nat. Commun.*, 2017, **8**, 1767.
182 D. Khodagholy, J. Rivnay, M. Sessolo, M. Gurfinkel, P. Leleux, L. H. Jimison, E. Stavrinidou, T. Herve, S. Sanaur, R. M. Owens and G. G. Malliaras, *Nat. Commun.*, 2013, **4**, 2133.
183 D. Khodagholy, T. Doublet, P. Quilichini, M. Gurfinkel, P. Leleux, A. Ghestem, E. Ismailova, T. Herve, S. Sanaur, C. Bernard and G. G. Malliaras, *Nat. Commun.*, 2013, **4**, 1575.
184 Y. van de Burgt, E. Lubberman, E. J. Fuller, S. T. Keene, G. C. Faria, S. Agarwal, M. J. Marinella, A. Alec Talin and A. Salleo, *Nat. Mater.*, 2017, **16**, 414–418.
185 S. T. Keene, C. Lubrano, S. Kazemzadeh, A. Melianas, Y. Tuchman, G. Polino, P. Scognamiglio, L. Cina, A. Salleo, Y. van de Burgt and F. Santoro, *Nat. Mater.*, 2020, **19**, 969–973.
186 C. Yan, L. Xiang, Y. Xiao, X. Zhang, Z. Jiang, B. Zhang, C. Li, S. Di and F. Zhang, *Nat. Commun.*, 2024, **15**, 10118.
187 P. Romele, M. Ghittorelli, Z. M. Kovacs-Vajna and F. Torricelli, *Nat. Commun.*, 2019, **10**, 3044.
188 J. Bisquert, B. Ilyassov and N. Tessler, *Adv. Sci.*, 2024, **11**, e2404182.
189 W. Kim, K. Lee, S. Choi, E. Park, G. Kim, J. Ha, Y. Kim, J. Jang, J. H. Oh, H. Kim, W. Jiang, J. Yoo, T. Kim, Y. Kim, K. N. Kim, J. Hong, A. Javey, D. W. Rha, T. W. Lee, K. Kang, G. Wang and C. Park, *Nat. Mater.*, 2025, **24**, 925–934.
190 A. Melianas, T. J. Quill, G. LeCroy, Y. Tuchman, H. V. Loo, S. T. Keene, A. Giovannitti, H. R. Lee, I. P. Maria, I. McCulloch and A. Salleo, *Sci. Adv.*, 2020, **6**, eabb2958.
191 E. Stein, O. Nahor, M. Stolov, V. Freger, I. M. Petruta, I. McCulloch and G. L. Frey, *Nat. Commun.*, 2022, **13**, 5548.
192 Y. Dai, S. Wai, P. Li, N. Shan, Z. Cao, Y. Li, Y. Wang, Y. Liu, W. Liu, K. Tang, Y. Liu, M. Hua, S. Li, N. Li, S. Chatterji, H. C. Fry, S. Lee, C. Zhang, M. Weires, S. Sutyak, J. Shi, C. Zhu, J. Xu, X. Gu, B. Tian and S. Wang, *Science*, 2024, **386**, 431–439.
193 H. Sun, J. Gerasimov, M. Berggren and S. Fabiano, *J. Mater. Chem. C*, 2018, **6**, 11778–11784.
194 C. Y. Yang, D. Tu, T. P. Ruoko, J. Y. Gerasimov, H. Y. Wu, P. C. Harikesh, M. Massetti, M. A. Stoeckel, R. Kroon, C. Müller, M. Berggren and S. Fabiano, *Adv. Electron. Mater.*, 2021, **8**, 2100907.
195 J. Ji, D. Gao, H. Y. Wu, M. Xiong, N. Stajkovic, C. Latte Bovio, C. Y. Yang, F. Santoro, D. Tu and S. Fabiano, *Nat. Commun.*, 2025, **16**, 4334.
196 H. Sun, M. Vagin, S. Wang, X. Crispin, R. Forchheimer, M. Berggren and S. Fabiano, *Adv. Mater.*, 2018, **30**, 1704916.
197 X. Liu, Y. Xiao, C. Yan, P. Du, F. Zhang and H. Xin, *ACS Appl. Mater. Interfaces*, 2025, **17**, 8072–8083.
198 I. P. Maria, S. Griggs, R. B. Rashid, B. D. Paulsen, J. Surgailis, K. Thorley, V. N. Le, G. T. Harrison, C. Combe, R. Hallani, A. Giovannitti, A. F. Paterson, S. Inal, J. Rivnay and I. McCulloch, *Chem. Mater.*, 2022, **34**, 8593–8602.

199 A. F. Paterson, A. Savva, S. Wustoni, L. Tsetseris, B. D. Paulsen, H. Faber, A. H. Emwas, X. Chen, G. Nikiforidis, T. C. Hidalgo, M. Moser, I. P. Maria, J. Rivnay, I. McCulloch, T. D. Anthopoulos and S. Inal, *Nat. Commun.*, 2020, **11**, 3004.
200 L. Ding, Z. D. Yu, X. Y. Wang, Z. F. Yao, Y. Lu, C. Y. Yang, J. Y. Wang and J. Pei, *Chem. Rev.*, 2023, **123**, 7421–7497.
201 X. Wang, Z. Zhang, P. Li, J. Xu, Y. Zheng, W. Sun, M. Xie, J. Wang, X. Pan, X. Lei, J. Wang, J. Chen, Y. Chen, S. J. Wang and T. Lei, *Adv. Mater.*, 2024, **36**, e2400287.
202 P. Li, W. Sun, J. Li, J.-P. Chen, X. Wang, Z. Mei, G. Jin, Y. Lei, R. Xin, M. Yang, J. Xu, X. Pan, C. Song, X.-Y. Deng, X. Lei, K. Liu, X. Wang, Y. Zheng, J. Zhu, S. Lv, Z. Zhang, X. Dai and T. Lei, *Science*, 2024, **384**, 528–590.
203 Z. Xu, Y. Ni, H. Han, H. Wei, L. Liu, S. Zhang, H. Huang and W. Xu, *Chin. Chem. Lett.*, 2023, **34**, 107292.
204 X. Wu, H. Tang, Z. Zhou, T. Salim, C. G. Tang, F. Huang and W. L. Leong, *Chem. Mater.*, 2024, **36**, 8639–8648.
205 C. Cea, G. D. Spyropoulos, P. Jastrzebska-Perfect, J. J. Ferrero, J. N. Gelinas and D. Khodagholy, *Nat. Mater.*, 2020, **19**, 679–686.
206 O. Parlak, S. T. Keene, A. Marais, V. F. Curto and A. Salleo, *Sci. Adv.*, 2018, **4**, eaar2904.
207 Y. Zhang, Y. Ma, L. Wang, C. Li, L. Wu, C. Zhong, B. Sun, Y. Chen and L. Jiang, *Small*, 2024, **20**, e2403629.
208 Y. J. Lee, Y. H. Kim and E. K. Lee, *Macromol. Rapid Commun.*, 2024, **45**, e2400165.
209 K. Xu, Z. Lu, Y. Zhou, Y. Zhang, L. Wang, D. Zhao, J. Chen, L.-W. Feng, Y. Cheng, L. Bai and W. Huang, *Sci. China Mater.*, 2025, **68**, 2910–2918.
210 S. Han, S. Yamamoto, A. G. Polyravas and G. G. Malliaras, *Adv. Mater.*, 2020, **32**, e2004790.
211 W. Xu, S. Y. Min, H. Hwang and T. W. Lee, *Sci. Adv.*, 2016, **2**, e1501326.
212 J. Liu, Y. Qing, L. Zhou, S. Chen, X. Li, Y. Zhang and H. Bayley, *Angew. Chem., Int. Ed.*, 2024, **63**, 202408665.
213 J. S. Najem, G. J. Taylor, R. J. Weiss, M. S. Hasan, G. Rose, C. D. Schuman, A. Belianinov, C. P. Collier and S. A. Sarles, *ACS Nano*, 2018, **12**, 4702–4711.
214 J. S. Najem, M. S. Hasan, R. S. Williams, R. J. Weiss, G. S. Rose, G. J. Taylor, S. A. Sarles and C. P. Collier, *Nat. Commun.*, 2019, **10**, 3239.
215 D. Bolmatov, J. Katsaras and C. Patrick Collier, *MRS Adv*, 2024, **9**, 565–573.
216 G. Paulo, K. Sun, G. Di Muccio, A. Gubbiotti, B. Morozzo della Rocca, J. Geng, G. Maglia, M. Chinappi and A. Giacomello, *Nat. Commun.*, 2023, **14**, 8390.
217 T. Ohno, T. Hasegawa, T. Tsuruoka, K. Terabe, J. K. Gimzewski and M. Aono, *Nat. Mater.*, 2011, **10**, 591–595.
218 Z. Wang, S. Joshi, S. E. Savel'ev, H. Jiang, R. Midya, P. Lin, M. Hu, N. Ge, J. P. Strachan, Z. Li, Q. Wu, M. Barnell, G. L. Li, H. L. Xin, R. S. Williams, Q. Xia and J. J. Yang, *Nat. Mater.*, 2017, **16**, 101–108.
219 P. Zhang, M. Xia, F. Zhuge, Y. Zhou, Z. Wang, B. Dong, Y. Fu, K. Yang, Y. Li, Y. He, R. H. Scheicher and X. S. Miao, *Nano Lett.*, 2019, **19**, 4279–4286.
220 D. Shi, W. Wang, Y. Liang, L. Duan, G. Du and Y. Xie, *Nano Lett.*, 2023, **23**, 11662–11668.
221 J. Moon, W. Ma, J. H. Shin, F. Cai, C. Du, S. H. Lee and W. D. Lu, *Nat. Electron.*, 2019, **2**, 480–487.
222 S. Pazos, K. Zhu, M. A. Villena, O. Alharbi, W. Zheng, Y. Shen, Y. Yuan, Y. Ping and M. Lanza, *Nature*, 2025, **640**, 69–76.
223 B. Xie, T. Xiong, G. Guo, C. Pan, W. Ma and P. Yu, *Proc. Natl. Acad. Sci. U. S. A.*, 2025, **122**, e2417040122.
224 Y. H. Jang, W. Kim, J. Kim, K. S. Woo, H. J. Lee, J. W. Jeon, S. K. Shim, J. Han and C. S. Hwang, *Nat. Commun.*, 2021, **12**, 5727.
225 R. A. John, F. Liu, N. A. Chien, M. R. Kulkarni, C. Zhu, Q. Fu, A. Basu, Z. Liu and N. Mathews, *Adv. Mater.*, 2018, **30**, e1800220.
226 R. Midya, Z. Wang, S. Asapu, X. Zhang, M. Rao, W. Song, Y. Zhuo, N. Upadhyay, Q. Xia and J. J. Yang, *Adv. Intell. Syst.*, 2019, **1**, 1900084.
227 T. Fu, X. Liu, H. Gao, J. E. Ward, X. Liu, B. Yin, Z. Wang, Y. Zhuo, D. J. F. Walker, J. Joshua Yang, J. Chen, D. R. Lovley and J. Yao, *Nat. Commun.*, 2020, **11**, 1861.
228 C. Mahata, G. Kim, H. So, M. Ismail, C. C. Hsu, S. Kim and S. Kim, *Adv. Funct. Mater.*, 2025, **35**, 2416862.
229 G. Milano, G. Pedretti, K. Montano, S. Ricci, S. Hashemkhani, L. Boarino, D. Ielmini and C. Ricciardi, *Nat. Mater.*, 2022, **21**, 195–202.
230 Y. Yamazaki and K. Kinoshita, *Adv. Sci.*, 2024, **11**, e2304804.
231 P. Gkoupidenis, N. Schaefer, B. Garlan and G. G. Malliaras, *Adv. Mater.*, 2015, **27**, 7176–7780.
232 D. Lee, M. Park, Y. Baek, B. Bae, J. Heo and K. Lee, *Nat. Commun.*, 2022, **13**, 5223.
233 M. R. Hossain, A. S. Mohamed, N. X. Armendarez, J. S. Najem and M. S. Hasan, *Adv. Intell. Syst.*, 2023, **5**, 2300346.
234 Y. Chen, J. Xia, Y. Qu, H. Zhang, T. Mei, X. Zhu, G. Xu, D. Li, L. Wang, Q. Liu and K. Xiao, *Adv. Mater.*, 2025, **37**, 2419013.
235 N. Ghenzi, T. W. Park, S. S. Kim, H. J. Kim, Y. H. Jang, K. S. Woo and C. S. Hwang, *Nanoscale Horiz.*, 2024, **9**, 427–437.
236 R. Song, P. Wang, H. Zeng, S. Zhang, N. Wu, Y. Liu, P. Zhang, G. Xue, J. Tong, B. Li, H. Ye, K. Liu, W. Wang and L. Wang, *Nano Lett.*, 2025, **25**, 5646–5655.
237 S. B. Laughlin, R. R. de Ruyter van Steveninck and J. C. Anderson, *Nat. Neurosci.*, 1998, **1**, 36–41.
238 G. J. Taylor, G. A. Venkatesan, C. P. Collier and S. A. Sarles, *Soft Matter*, 2015, **11**, 7592–7605.
239 H. Pei, H. Hu, Y. Dong, H. Zhu, C. Zhang, Y. Zhou, J. Huang, S. Shi, Z. Wang, X. Wu and W. Huang, *Adv. Funct. Mater.*, 2025, **35**, 2506431.
240 W. Zhao, F. Shao, F. Sun, Z. Su, S. Liu, T. Zhang, M. Zhu, Z. Liu and X. Zhou, *Adv. Mater.*, 2023, **35**, 2300876.
241 Q. Liang, Z. Shen, X. Sun, D. Yu, K. Liu, S. M. Mugo, W. Chen, D. Wang and Q. Zhang, *Adv. Mater.*, 2022, **35**, 2211159.

242 C. E. G. Hoskin, V. R. Schild, J. Vinals and H. Bayley, *Nat. Chem.*, 2022, **14**, 650–657.
243 H. Tian, C. Wang, Y. Chen, L. Zheng, H. Jing, L. Xu, X. Wang, Y. Liu and J. Hao, *Sci. Adv.*, 2023, **9**, eadd6950.
244 H. Tian, R. Zhou, L. Ke, K. Qian, Y. Liu and J. Hao, *Adv. Funct. Mater.*, 2025, **35**, 2505232.
245 F. Jiang, W. C. Poh, J. Chen, D. Gao, F. Jiang, X. Guo, J. Chen and P. S. Lee, *Nat. Commun.*, 2022, **13**, 6669.
246 Z. Lei and P. Wu, *Matter*, 2023, **6**, 429–444.
247 R. Qiu, J. Wang, Q. Ren, W. Huang, J. Zhu, D. Liu, X. Gao, W. Wang, Q. Liu and M. Zhang, *ACS Nano*, 2023, **17**, 12652–12662.
248 L. Chen, M. Ren, J. Zhou, X. Zhou, F. Liu, J. Di, P. Xue, C. Li, Q. Li, Y. Li, L. Wei and Q. Zhang, *Proc. Natl. Acad. Sci. U. S. A.*, 2024, **121**, e2407971121.
249 X. Luo, C. Chen, Z. He, M. Wang, K. Pan, X. Dong, Z. Li, B. Liu, Z. Zhang, Y. Wu, C. Ban, R. Chen, D. Zhang, K. Wang, Q. Wang, J. Li, G. Lu, J. Liu, Z. Liu and W. Huang, *Nat. Commun.*, 2024, **15**, 3086.
250 Z. Liu, J. Wu, M. Wang, K. Wang, Y. Zeng, X. Dong, K. Wang and J. Liu, *Adv. Funct. Mater.*, 2025, e10021, DOI: 10.1002/adfm.202510021.
251 J. Wu, L. Zhang, W. Chang, H. Zhang, W. Zhang, T. Mei, X. Zhu, L. Wang, M. Zhang and K. Xiao, *Adv. Funct. Mater.*, 2025, **35**, 2500048.
252 Z. Zhang, B. Sabbagh, Y. Chen and G. Yossifon, *ACS Nano*, 2024, **18**, 15025–15034.
253 N. Zhou, T. Cui, Z. Lei and P. Wu, *Nat. Commun.*, 2025, **16**, 4573.
254 H. Zhang, S. Wang, L. Wang, S. Li, H. Liu, X. Zhu, Y. Chen, G. Xu, M. Zhang, Q. Liu, R. Wang and K. Xiao, *Adv. Mater.*, 2025, **37**, 2500809.
255 M. Zhang, G. Xu, H. Zhang and K. Xiao, *ACS Nano*, 2025, **19**, 10589–10598.
256 J. Dai, Y. Xue, X. Chen, Z. Cao, L. Wang, J. Zhang, Y. Zhou, Y. Hu, W. Zhou, W. Tang, X.-Y. Kong, B. Tu, J. Liu and K. Xiao, *Device*, 2024, **2**, 100436.
257 C. Wan, G. Chen, Y. Fu, M. Wang, N. Matsuhisa, S. Pan, L. Pan, H. Yang, Q. Wan, L. Zhu and X. Chen, *Adv. Mater.*, 2018, **30**, 1801291.
258 C. Wang, Y. Liu, X. Qu, B. Shi, Q. Zheng, X. Lin, S. Chao, C. Wang, J. Zhou, Y. Sun, G. Mao and Z. Li, *Adv. Mater.*, 2022, **34**, 2105416.
259 Y. H. Jung, B. Park, J. U. Kim and T. I. Kim, *Adv. Mater.*, 2019, **31**, 1803637.
260 B. C. K. Tee, A. Chortos, A. Berndt, A. Kim Nguyen, A. Tom, A. McGuire, Z. Carter Lin, K. Tien, W. Gyu Bae, H. Wang, P. Mei, H. Hsiu Chou, B. Cui, K. Deisseroth, T. Nga Ng and Z. Bao, *Science*, 2015, **350**, 313–316.
261 Y. Lee, Y. O. Jin, W. Xu, O. Kim, T. Roy Kim, J. Kang, Y. Kim, D. Son, B.-H. T. Jeffery, J. P. Moon, Z. Bao and T.-W. Lee, *Sci. Adv.*, 2018, **4**, eaat7387.
262 J. Zhu, X. Zhang, R. Wang, M. Wang, P. Chen, L. Cheng, Z. Wu, Y. Wang, Q. Liu and M. Liu, *Adv. Mater.*, 2022, **34**, 2200481.
263 C. Wan, P. Cai, X. Guo, M. Wang, N. Matsuhisa, L. Yang, Z. Lv, Y. Luo, X. J. Loh and X. Chen, *Nat. Commun.*, 2020, **11**, 4602.
264 Y. R. Lee, T. Q. Trung, B. U. Hwang and N. E. Lee, *Nat. Commun.*, 2020, **11**, 2753.
265 E. S. Fortune and G. J. Rose, *Trends Neurosci.*, 2001, **24**, 381–385.
266 S. Jiang, L. Peng, Z. Hao, X. Du, J. Gu, J. Su, H. Guo, D. Gu, H. Zhang, Q. Wang, J. Qiu and Y. Li, *ACS Appl. Electron. Mater.*, 2023, **5**, 4915–4924.
267 P. Huang, B. Jiang, H. Chen, J. Xu, K. Wang, C. Zhu, X. Hu, D. Li, L. Zhen, F. Zhou, J. Qin and C. Xu, *Nat. Commun.*, 2023, **14**, 6736.
268 J. Chen, Z. Zhou, B. J. Kim, Y. Zhou, Z. Wang, T. Wan, J. Yan, J. Kang, J. H. Ahn and Y. Chai, *Nat. Nanotechnol.*, 2023, **18**, 882–888.
269 Y. Yang, H. Cui, S. Ke, M. Pei, K. Shi, C. Wan and Q. Wan, *Appl. Phys. Lett.*, 2023, **122**, 043508.
270 W. Haensch, A. Raghunathan, K. Roy, B. Chakrabarti, C. M. Phatak, C. Wang and S. Guha, *Adv. Mater.*, 2023, **35**, 2204944.
271 D. Verstraeten, B. Schrauwen, M. D'Haene and D. Stroobandt, *Neural Netw.*, 2007, **20**, 391–403.
272 M. Lukoševičius and H. Jaeger, *Comput. Sci. Rev.*, 2009, **3**, 127–149.
273 Y. Jeong, J. Lee, J. Moon, J. H. Shin and W. D. Lu, *Nano Lett.*, 2018, **18**, 4447–4453.
274 L. Alzubaidi, J. Zhang, A. J. Humaidi, A. Al-Dujaili, Y. Duan, O. Al-Shamma, J. Santamaria, M. A. Fadhel, M. Al-Amidie and L. Farhan, *J. Big Data*, 2021, **8**, 53.
275 J. J. Maraj, K. P. T. Haughn, D. J. Inman and S. A. Sarles, *Adv. Intell. Syst.*, 2023, **5**, 2300049.
276 L. Appeltant, M. C. Soriano, G. Van der Sande, J. Danckaert, S. Massar, J. Dambre, B. Schrauwen, C. R. Mirasso and I. Fischer, *Nat. Commun.*, 2011, **2**, 468.
277 G. Villar, A. D. Graham and H. Bayley, *Science*, 2013, **340**, 48–52.
278 W. Wang, Y. Jiang, D. Zhong, Z. Zhang, S. Choudhury, J.-C. Lai, H. Gong, S. Niu, X. Yan, Y. Zheng, C.-C. Shih, R. Ning, Q. Lin, D. Li, Y.-H. Kim, J. Kim, Y.-X. Wang, C. Zhao, C. Xu, X. Ji, Y. Nishio, H. Lyu, J. B.-H. Tok and Z. Bao, *Science*, 2023, **380**, 735–742.
279 Y. Kim, A. Chortos, W. Xu, Y. Liu, J. Y. Oh, D. Son, J. Kang, A. M. Foudeh, C. Zhu, Y. Lee, S. Niu, J. Liu, R. Pfattner, Z. Bao and T.-W. Lee, *Science*, 2018, **360**, 998–1003.
280 Y. Lee, Y. Liu, D. G. Seo, J. Y. Oh, Y. Kim, J. Li, J. Kang, J. Kim, J. Mun, A. M. Foudeh, Z. Bao and T. W. Lee, *Nat. Biomed. Eng.*, 2022, **7**, 511–519.